Recent and future vegetation change in the treeline region of Chukotka (NE Russia) inferred from field data, satellite data and modelling

Iuliia Shevtsova

Univ.-Diss.

zur Erlangung des akademischen Grades
"doctor rerum naturalium"
(Dr. rer. nat.)
in der Wissenschaftsdisziplin " Pflanzenökologie "

eingereicht an der
Mathematisch-Naturwissenschaftlichen Fakultät
Institut für Biochemie und Biologie
der Universität Potsdam
und
Alfred-Wegener-Institut, Helmholtz-Zentrum für Polar- und Meeresforschung

Ort und Tag der Disputation: Potsdam, 03.03.2022

Hauptbetreuerin: Prof. Dr. Ulrike Herzschuh
Zweiter Betreuer: Prof. Dr. Guido Grosse
Gutachter*innen: Prof. Dr. Howard Epstein, Prof. Dr. Birgit Kleinschmit

Online veröffentlicht auf dem
Publikationsserver der Universität Potsdam:
https://doi.org/10.25932/publishup-54845
https://nbn-resolving.org/urn:nbn:de:kobv:517-opus4-548452

Abstract

Vegetation change at high latitudes is one of the central issues nowadays with respect to ongoing climate changes and triggered potential feedback. At high latitude ecosystems, the expected changes include boreal treeline advance, compositional, phenological, physiological (plants), biomass (phytomass) and productivity changes. However, the rate and the extent of the changes under climate change are yet poorly understood and projections are necessary for effective adaptive strategies and forehanded minimisation of the possible negative feedbacks.

The vegetation itself and environmental conditions, which are playing a great role in its development and distribution are diverse throughout the Subarctic to the Arctic. Among the least investigated areas is central Chukotka in North-Eastern Siberia, Russia. Chukotka has mountainous terrain and a wide variety of vegetation types on the gradient from treeless tundra to northern taiga forests. The treeline there in contrast to subarctic North America and north-western and central Siberia is represented by a deciduous conifer, *Larix cajanderi* Mayr. The vegetation varies from prostrate lichen *Dryas octopetala* L. tundra to open graminoid (hummock and non-hummock) tundra to tall *Pinus pumila* (Pall.) Regel shrublands to sparse and dense larch forests.

Hence, this thesis presents investigations on recent compositional and above-ground biomass (AGB) changes, as well as potential future changes in AGB in central Chukotka. The aim is to assess how tundra-taiga vegetation develops under changing climate conditions particularly in Fareast Russia, central Chukotka. Therefore, three main research questions were considered:

1) What changes in vegetation composition have recently occurred in central Chukotka?
2) How have the above-ground biomass AGB rates and distribution changed in central Chukotka?
3) What are the spatial dynamics and rates of tree AGB change in the upcoming millennia in the northern tundra-taiga of central Chukotka?

Remote sensing provides information on the spatial and temporal variability of vegetation. I used Landsat satellite data together with field data (foliage projective cover and AGB) from two expeditions in 2016 and 2018 to Chukotka to upscale vegetation types and AGB for the study area. More specifically, I used Landsat spectral indices (Normalised Difference Vegetation Index (NDVI), Normalised Difference Water Index (NDWI) and Normalised Difference Snow Index (NDSI)) and constrained ordination (Redundancy analysis, RDA) for further k-means-based land-cover classification and general additive model (GAM)-based AGB maps for 2000/2001/2002 and 2016/2017. I also used Tandem-X DEM data for a topographical correction of the Landsat satellite data and to derive slope, aspect, and Topographical Wetness Index (TWI) data for forecasting AGB.

Firstly, in 2016, taxa-specific projective cover data were collected during a Russian-German expedition. I processed the field data and coupled them with Landsat spectral Indices in the RDA model

that was used for k-means classification. I could establish four meaningful land-cover classes: (1) larch closed-canopy forest, (2) forest tundra and shrub tundra, (3) graminoid tundra and (4) prostrate herb tundra and barren areas, and accordingly, I produced the land cover maps for 2000/2001/2002 and 2016/20017. Changes in land-cover classes between the beginning of the century (2000/2001/2002) and the present time (2016/2017) were estimated and interpreted as recent compositional changes in central Chukotka. The transition from graminoid tundra to forest tundra and shrub tundra was interpreted as shrubification and amounts to a 20% area increase in the tundra-taiga zone and 40% area increase in the northern taiga. Major contributors of shrubification are alder, dwarf birch and some species of the heather family. Land-cover change from the forest tundra and shrub tundra class to the larch closed-canopy forest class is interpreted as tree infilling and is notable in the northern taiga. We find almost no land-cover changes in the present treeless tundra.

Secondly, total AGB state and change were investigated for the same areas. In addition to the total vegetation AGB, I provided estimations for the different taxa present at the field sites. As an outcome, AGB in the study region of central Chukotka ranged from 0 kg m^{-2} at barren areas to 16 kg m^{-2} in closed-canopy forests with the larch trees contributing the highest. A comparison of changes in AGB within the investigated period from 2000 to 2016 shows that the greatest changes (up to 1.25 kg m^{-2} yr^{-1}) occurred in the northern taiga and in areas where land cover changed to larch closed-canopy forest. Our estimations indicate a general increase in total AGB throughout the investigated tundra-taiga and northern taiga, whereas the tundra showed no evidence of change in AGB within the 15 years from 2002 to 2017.

In the third manuscript, potential future AGB changes were estimated based on the results of simulations of the individual-based spatially explicit vegetation model LAVESI using different climate scenarios, depending on Representative Concentration Pathways (RCPs) RCP 2.6, RCP 4.5 and RCP 8.5 with or without cooling after 2300 CE. LAVESI-based AGB was simulated for the current state until 3000 CE for the northern tundra-taiga study area for larch species because we expect the most notable changes to occur will be associated with forest expansion in the treeline ecotone. The spatial distribution and current state of tree AGB was validated against AGB field data, AGB extracted from Landsat satellite data and a high spatial resolution image with distinctive trees visible. The simulation results are indicating differences in tree AGB dynamics plot wise, depending on the distance to the current treeline. The simulated tree AGB dynamics are in concordance with fundamental ecological (emigrational and successional) processes: tree stand formation in simulated results starts with seed dispersion, tree stand establishment, tree stand densification and episodic thinning. Our results suggest mostly densification of existing tree stands in the study region within the current century in the study region and a lagged forest expansion (up to 39% of total area in the RCP 8.5) under all considered climate scenarios without cooling in different local areas depending on the closeness to the current treeline. In scenarios with cooling air temperature after

2300 CE, forests stopped expanding at 2300 CE (up to 10%, RCP 8.5) and then gradually retreated to their pre-21st century position. The average tree AGB rates of increase are the strongest in the first 300 years of the 21st century. The rates depend on the RCP scenario, where the highest are as expected under RCP 8.5.

Overall, this interdisciplinary thesis shows a successful integration of field data, satellite data and modelling for tracking recent and predicting future vegetation changes in mountainous subarctic regions. The obtained results are unique for the focus area in central Chukotka and overall, for mountainous high latitude ecosystems.

Zusammenfassung

Die Veränderung der Vegetation in den hohen Breiten ist heutzutage eines der zentralen Themen im Hinblick auf den anhaltenden Klimawandel und hat potenziell auslösende Rückkopplungen. In den Ökosystemen der hohen Breiten umfassen die erwarteten Veränderungen das Fortschreiten der borealen Baumgrenze, sowie kompositorische, phänologische, physiologische, Biomassen- (Phytomasse) und Produktivitätsveränderungen. Die Geschwindigkeit und das Ausmaß der Veränderungen im Rahmen des Klimawandels sind jedoch noch wenig verstanden, und Projektionen sind für wirksame Anpassungsstrategien und eine vorausschauende Minimierung möglicher negativer Rückkopplungen erforderlich.

Die Vegetation selbst und die Umweltbedingungen, die bei ihrer Entwicklung und Verbreitung eine große Rolle spielen, sind in der gesamten Subarktis bis zur Arktis unterschiedlich. Zu den am wenigsten untersuchten Gebieten gehört Zentral-Tschukotka, in Nordost-Sibirien, Russland. Tschukotka hat gebirgiges Terrain und eine weite Bandbreite von Vegetationstypen entlang des Gradienten von der baumlosen Tundra bis zu den nördlichen Taiga-Wäldern. Die Baumgrenze dort wird im Gegensatz zum subarktischen Nordamerika sowie Nordwest- und Mittelsibirien durch eine laubabwerfende Nadelbaumart, *Larix cajanderi* Mayr, aufgebaut. Die Vegetation variiert von Tundra mit Flechten und *Dryas octopetala* L. über offene graminoide (Horstgras und nicht Horstgras) Tundra und hohe *Pinus pumila* (Pall.) Regel Strauchlandschaften zu lockeren Lärchenbeständen bis zu dichten Lärchenwäldern.

Somit werden in meiner Dissertation Untersuchungen zu den jüngsten Veränderungen der Vegetationszusammensetzung und der oberirdischen Biomasse (aus dem Englischen above-ground biomass, bzw. AGB), sowie zu potenziellen zukünftigen Veränderungen der AGB vorgestellt. Das Ziel meiner Arbeit ist es abzuschätzen, wie sich die Tundra-Taiga-Vegetation unter Klimawandel entwickelt, insbesondere in Fernost Russland, Zentral-Tschukotka. Daher wurden drei Hauptforschungsfragen berücksichtigt:

1) Welche Veränderungen in der Vegetationszusammensetzung sind in den letzten Jahrzehnten in Zentral-Tschukotka aufgetreten?

2) Wie haben sich die AGB-Raten und die Verteilung der oberirdischen Biomasse in Zentral-Tschukotka verändert?

3) Wie sind die räumlichen Dynamiken und Änderungsraten der Baum-AGB in dem kommenden Jahrtausend in der nördlichen Tundra-Taiga in Zentral-Tschukotka?

Fernerkundung liefert Informationen über die räumliche und zeitliche Vegetationsvariabilität. Ich habe Landsat-Satellitendaten zusammen mit Felddaten (Projektive Vegetationsbedeckung und AGB) von zwei Expeditionen in den Jahren 2016 und 2018 nach Tschukotka verwendet, um Vegetationstypen und AGB für das Untersuchungsgebiet räumlich abzubilden. Insbesondere habe ich die Landsat-Spektralindizes (Normalized Difference Vegetation Index (NDVI), Normalized Difference Water Index (NDWI) und Normalized Difference Snow Index (NDSI)) und eine Ordination mit Randbedingungen (Redundanzanalyse, RDA) verwendet, um eine Land-Klassifizierung mittels der k-means Methode zu entwickeln, und AGB-Karten mittels des General Additive Model (GAM) für 2000/2001/2002 und 2016/2017 zu erstellen. Außerdem verwendete ich Tandem-X-DEM-Daten, um die Landsat-Satellitendaten topografisch zu korrigieren und um die Hangneigung-, Hangaspekt- und TWI- (Topographical Wetness Index) Daten für die Vorhersage von AGB abzuleiten.

Auf einer russisch-deutschen Expedition im Jahr 2016 wurden Vegetationsdaten erhoben. Ich prozessierte die Felddaten zu taxaspezifischen-projektiven Vegetationsbedeckungsdaten. Ich habe die taxaspezifisch-projektive Vegetationsbedeckung mit Landsat-Spektralindizes im RDA-Modell gekoppelt, das für die k-means-Klassifizierung verwendet wurde.

Ich konnte vier repräsentative Landbedeckungsklassen einrichten: (1) Lärchen-Wald mit geschlossenem Blätterdach, (2) Waldtundra und Strauch-Tundra, (3) graminoide Tundra und (4) Kräutertundra und vegetationsarme Gebiete. Dementsprechend prozessierte ich dann die Landbedeckungskarten für 2000/2001/2002 und 2016/20017. Ich ermittelte die Änderungen der Landbedeckungsklassen zwischen dem Beginn des Jahrhunderts (2000/2001/2002) und der Gegenwart (2016/2017) und konnte sie als aktuelle Kompositionsänderungen in der Vegetation von Zentral-Tschukotka interpretieren. Die Transformation von der graminoiden Tundra zur Waldtundra oder zur Strauch-Tundra habe ich als Prozess der Strauchbildung interpretiert, die einer Flächenvergrößerung von 20% in der Tundra-Taiga Zone und einer Flächenvergrößerung von 40% in der nördlichen Taiga entspricht. Hauptakteure der Strauchung sind Erle, Zwergbirke und einige Arten der Heidekrautfamilie. Der Landbedeckungswechsel von der Waldtundra- und Strauch-Tundra-Klasse zur Klasse des Lärchen-Waldes mit geschlossenen Blätterdach wird als eine Verdichtung des Baumbestandes interpretiert und ist in der nördlichen Taiga bemerkenswert. In der heutigen baumlosen Tundra finden wir fast keine Landbedeckungsänderungen.

Im zweiten Projekt bestimmte ich den Gesamt-AGB-Zustand und die gesamte AGB-Veränderung für dieselben Regionen in Zentral-Chukotka. Zusätzlich zur gesamten AGB lieferte ich Schätzungen für die verschiedenen Taxa, die an den Feldstandorten vorhanden sind. Als Ergebnis lag

die AGB in der Untersuchungsregion von Zentral-Tschukotka zwischen 0 kg m^{-2} in vegetationsarmen Gebieten und 16 kg m^{-2} in den Wäldern mit geschlossenem Blätterdach mit dem größten Anteil von Lärchen. Ein Vergleich der Veränderungen der AGB im Untersuchungszeitraum von 2000 bis 2016 zeigt, dass die größten Veränderungen (bis zu 1,25 kg m^{-2} $Jahr^{-1}$) in der nördlichen Taiga und in den Gebieten auftraten, in denen sich die Landbedeckung hin zu einen Lärchenwald mit geschlossenen Blätterdach änderte. Unsere Schätzungen deuten auf einen allgemeinen Anstieg der gesamten AGB in der untersuchten Tundra-Taiga und der nördlichen Taiga hin. Im Gegensatz zeigte die Tundra innerhalb der 15 Jahre von 2002 bis 2017 keine Hinweise auf eine Veränderung der AGB.

Im dritten Projekt wurden potenzielle zukünftige Änderungen der oberirdischen Biomasse (AGB) basierend auf den Ergebnissen von Simulationen des individuell basierten räumlich expliziten Vegetationsmodells LAVESI unter Verwendung verschiedener Klimaszenarien, abhängig von RCP (Representative Concentration Pathways) 2.6, RCP 4.5 und RCP 8.5 (mit und ohne die Temperaturminderung nach den 2300 CE), geschätzt. Die LAVESI-basierte AGB wurde für den aktuellen Zustand bis 3000 CE für Lärchen-AGB simuliert, da wir davon ausgehen, dass die bemerkenswertesten Veränderungen im Baumgrenze-Ökoton mit einer Waldausdehnung zusammenhängen. Die räumliche Verteilung und der aktuelle Zustand der Baum-AGB wurden anhand von AGB-Felddaten, aus Landsat-Satellitendaten extrahierten AGB und einem Satellitenbild mit hoher räumlicher Auflösung und dadurch sichtbaren Einzelbäumen validiert. Die Simulationsergebnisse deuten auf Unterschiede in der Baum-AGB-Dynamik in Abhängigkeit von der Entfernung zur aktuellen Baumgrenze hin. Die simulierte Baum-AGB-Dynamik stimmt mit grundlegenden ökologischen (Auswanderungs- und Sukzessions-) Prozessen überein: die simulierte Baumbestandsentwicklung fängt mit Samenverbreitung an, Schaffung des Baumbestands, Baumbestand Verdichtung und episodische Verdünnung. Unsere Ergebnisse weisen auf eine Verdichtung des bestehenden Baumbestandes im Laufe dieses Jahrhunderts hin in der Untersuchungsregion, und auf eine zeitlich verzögerte Waldverbreitung (bis zu 39% der Fläche im RCP 8.5) unter allen betrachteten Klima-Szenarien ohne Abkühlung in verschiedenen lokalen Bereichen, abhängig von der Nähe zur heutigen Baumgrenze. In Szenarien mit Abkühlung nach 2300 CE beenden die Wälder ihre Ausbreitung um 2300 CE; bis zu 10%, RCP 8.5) um dann graduell zu ihrer vor-21. Jhd. Position zurückzuweichen.

Die gemittelten Änderungsraten der Baum AGB sind am höchsten in den ersten 300 Jahren des 21. Jahrhunderts. Die Änderungsraten hängen ab von dem RCP Szenarium, mit den höchsten Änderungsraten unter RCP 8.5, wie zu erwarten war. Insgesamt zeigt diese interdisziplinäre Arbeit eine erfolgreiche Integration von Felddaten, Satellitendaten und Modellen zur Verfolgung der aktuellen und vorhergesagten zukünftigen Vegetationsänderungen in subarktischen Gebirgsregionen. Die erzielten Ergebnisse sind einzigartig für den Schwerpunktbereich in Zentral-Tschukotka und insgesamt für Gebirgsregionen in den hohen Breiten.

Contents

Abbreviations

AGB	Above-Ground biomass
AVHRR	Advanced Very-High-Resolution Radiometer
AWI	Alfred-Wegener-Institut, Helmholtz-Zentrum für Polar- und Meeresforschung
CRU TS	Climate Research Unit gridded Time Series
DEM	Digital Elevation Model
ESA	European Space Agency
ETM	Enhanced Thematic Mapper
GAM	General Additive Model
IPCC	Intergovernmental Panel on Climate Change
LAVESI	*LArix* VEgetation SImulator
MODIS	Moderate Resolution Imaging Spectroradiometer
NDSI	Normalised Difference Snow Index
NDVI	Normalised Difference Vegetation Index
NDWI	Normalised Difference Water Index
NIR	Near Infrared
OLI	Operational Land Imager
RDA	Redundancy Analysis
RCP	Representative Concentration Pathway
SWIR	Short-wave Infrared
TDX	TanDEM-X
TWI	Topographical Wetness Index

Motivation

Recent climate change has already led to notable marine and terrestrial ecosystem changes, especially in the Arctic (Post et al., 2009; Walsh et al., 1996). In consequence of warming temperatures, lengthening of the growing season and permafrost degradation significant vegetation changes such as compositional and abundance changes (Myers-Smith et al., 2019; Myers-Smith et al., 2011; Frost et al., 2014; Frost & Epstein, 2013; Tape et al., 2006; Sturm et al., 2001), changes in above-ground biomass (Walker & Raynolds, 2018; Epstein et al., 2012; Hudson & Henry, 2009) and phenological changes (Mulder et al., 2017; Zeng & Jia, 2013; Wipf et al., 2006), etc. can be observed in arctic and subarctic terrestrial ecosystems. Nevertheless, high latitudes ecosystems are diverse in their environmental conditions (relief, wetness, distance from the ocean, anthropogenic activity, soils and active layer depth) and historical development. These parameters shaped the current high latitudes' ecosystems and recent climate-driven changes are proved to have substantial differences in the different areas of the Arctic and Subarctic. Guay et al (2014) show the strongest vegetation greening trends in Alaska and north-eastern Russia. Central Chukotka as part of north-eastern Russia is one of the least investigated areas in terms of vegetation and its changes in response to climate change. Recent records featured shrubification of southern Chukotka valleys (Frost & Epstein, 2013) and western Chukotka forest dynamics (Wieczorek et al., 2017; Berner et al., 2015; Berner et al., 2013; Berner et al., 2012; Blok et al., 2011), whereas central Chukotka is not described in any of the recent vegetation studies. The underestimated central Chukotka is a unique region for estimating recent and predicting future vegetation dynamics. There have been studies in the mountainous regions of the Arctic and Subarctic in Alaska (Dial et al., 2007; Berner et al., 2018; Berner et al., 2015; Shaver & Chapin, 1991, etc.), polar Ural (Devi et al., 2020), Sweden (Maslov et al., 2016; Michelsen et al., 2012; Wilson et al., 2009; Bokhorst et al., 2009; Graglia et al., 2001; Wallén, 1986), but all of them differ from each other by species composition and climate, what is leading to differences in character and rates of vegetation changes, happening in each of the regions. That is why it is worth investigating the understudied mountainous tundra-taiga region of central Chukotka, covering a gradient of vegetation types from *Dryas* and lichen-based communities up in the mountains via graminoid open tundra and tall shrublands to forest tundra and even dense taiga forests in the south of the region. The treeline in Siberia, unlike in North American, is represented by a deciduous conifer, namely the larch and unlike in most of the other Russian arctic regions in central Chukotka it is represented specifically by *Larix cajanderi*.

1 Introduction

1.1 Scientific background

1.1.1. Flora and common vegetation communities of the high latitudes

Vegetation in the northern high latitudes was first studied from a geobotanical point of view (e.g., Krasnoborov, 1988-2003; Egorova et al., 1991; Tolmatchev, 1960-1987; Karavaev, 1958) and provided a description of floristic composition and distribution of plant species in the high latitudes. The modern arctic vegetation is described by Walker et al (2005), covering the common vegetation types across the Arctic from cryptogram herb barrens to low-shrub tundra. The subarctic as an area between arctic tundra and boreal closed-canopy forests (e.g., Payette et al., 2001) and includes many arctic vegetation types as well as tree stands with different degrees of canopy closure, forming a treeline ecotone. The treeline position depends strongly on the air temperature and can be found not only in the high latitudes, but also at high elevations (alpine treeline, e.g., Danby & Hit, 2007). The treeline can be formed of different conifer species depending on the region. The Russian treeline ecotone is also called the tundra-taiga ecotone and is represented by *Larix* Mill. (Abaimov et al., 2010). In general, specific vegetation composition in the Arctic and subarctic is associated with regional climate, elevation, soil moisture (Billings et al., 1982), and historical development (Walker et al., 2005).

1.1.2 Vegetation and climate change in the high latitudes

Nowadays with the increasing importance of climate change and its consequences, more and more investigations on vegetation of high latitudes are done in this context. Experiments have shown potential vegetation changes in response to changing climate conditions. For instance, an increase in the deciduous shrub *Salix* and a decrease in the graminoid *Carex* was observed in response to warming (Carlson et al., 2018). Plot-based studies have shown enhanced tree and shrub growth in response to rising summer temperature and summer precipitation (Berner et al., 2013; Block et al., 2011), increases in shrub and graminoid species, and decreases in bare ground with an increase in the potential growing season length with warmer air and soil temperatures (Myers-Smith et al., 2019).

1.1.3 Remote sensing in vegetation studies of the Arctic and Subarctic

The increasing number and quality of remote-sensing products favours regional, circumpolar, and global scale investigations in addition to the local plot-based studies. Remote sensing enables us to study features on the Earth's surface by using reflected or emitted radiation (Campbell, 1944). For vegetation studies, the information is provided by spectral signatures, with the most valuable regions in the spectrum being green, red, near infrared (NIR), and shortwave infrared (SWIR-1).

Much of the spectral response in the visible part of the spectrum is controlled by the pigment chlorophyll, whose molecules absorb blue and red light and mostly reflect green light. Reflection in the NIR, however, is controlled by the spongy mesophyll tissue, from which the energy is scattered, which makes the internal structure of the living vegetation responsible for the magnitude of the NIR reflectance. In the mid infrared, water content in the plant controls the spectral response. With this, spectral remote sensing supports studying phenology, classification of vegetation of different communities or types (forest, open tundra etc.), distinguishing between different life forms (shrub, tree, grass etc.), studying plant diseases development, and assessing above-ground biomass (AGB) and net primary production amongst others.

Using remote sensing, vegetation of the high latitudes can be studied on the global, regional, and local scales. To measure vegetation changes, spectral vegetation indices are frequently used. One of the most common is the Normalised Difference Vegetation Index (NDVI). Its increase is interpreted as an increase in plant biomass, cover, and abundance (Myers-Smith et al., 2019).

1.1.4 Knowledge gaps in the current vegetation studies of the high latitudes

The need for local and regional vegetation studies arises from the fact that vegetation change is not uniform across the Arctic (Raynolds et al., 2006). It is also important to reinforce remote-sensing-based findings with field investigations.

Most of the vegetation studies, which include field-based estimations have been conducted in Alaska (Berner et al., 2015; Villarreal et al 2012; Walker et al., 2011; Lantz et al., 2010; Dial et al., 2007; Rupp et al., 2006; Shaver & Chapin, 1991), Scandinavia (Maslov et al., 2016; Wilson et al., 2009; Bokhorst et al., 2009; Graglia et al., 2001; Michelsen et al., 2012; Press et al., 1998; Wallén, 1986), fewer in Canada (Vankoughnett & Grogan, 2016; Walker et al., 2011; Hudson & Henry, 2009) and very few in the northern central Siberia (Yu et al 2011) and the Russian Far East, mostly near the research stations Chersky (Webb et al., 2017; Berner et al., 2015; Berner et al., 2013; Berner et al., 2012; Krestov et al., 2003) and Chokurdach (Blok et al., 2011). Although, analyses of Advanced Very-High-Resolution Radiometer (AVHRR) satellite data (Guay et al., 2014) showed strong greening in central Chukotka from 1982 to 2012, in terms of field investigations the region stayed largely unexplored.

Generally, many studies across the arctic and subarctic investigate total or partial AGB (Räsänen et al., 2018; Berner et al., 2018; Webb et al., 2017; Maslov et al., 2016; Vankoughnett & Grogan, 2016; Berner et al., 2014; Berner et al., 2012; Chen et al., 2009; Walker et al., 2003; Shaver & Chapin, 1991), but very few studies are done on the AGB change of the high-latitude ecosystems (Hudson & Henry, 2009). In central Chukotka there were neither studies on the state of AGB state, nor on AGB change conducted.

Predictions of future vegetation changes, especially AGB, are also rare among studies of high-latitude regions. Most of them are conducted on the global (Sitch et al., 2008; Bergengren et al., 2001; Bonan et al., 2003) or circumpolar scale (Druel et al., 2019; Zhang et al., 2013; Epstein et al., 2007), which leaves a knowledge gap in the accurate predictions for different regions, where potential vegetation changes could be quite different depending on the relief, species composition, soil development, and local climate etc.

1.2 Study region

The study region – central Chukotka – is in Far East Russia with a continental type of climate with average July temperatures of 13°C, average January temperatures of -30°C and an annual precipitation of 200 mm. The study region is in continuous permafrost. Active-layer thickness in late summer ranges from shallow depths of a few tens of centimetres to around one and a half metres, depending on the substrate, vegetation, topography, and elevation and on the latitude.

The investigated focus areas of this work represent tundra, tundra-taiga, and northern taiga (Figure 1).

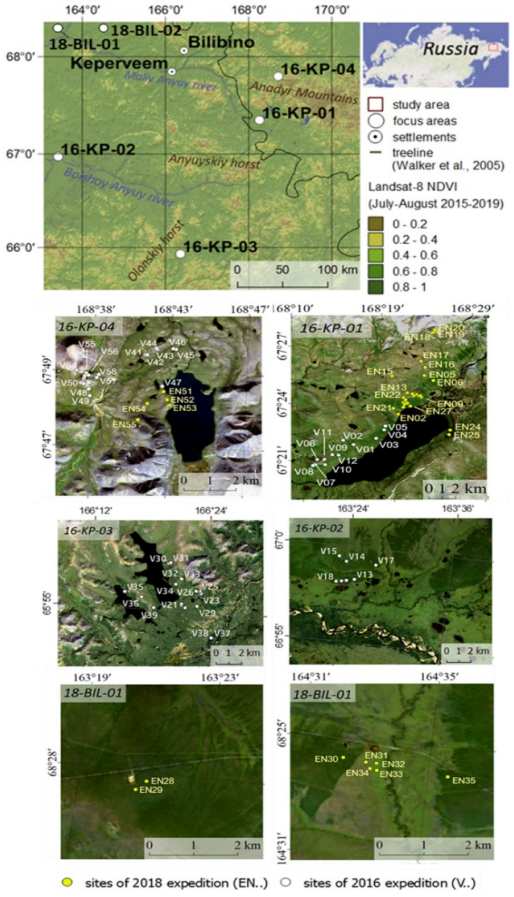

Figure 1. The study region in central Chukotka (Shevtsova et al., 2021). Overview of the study region and focus areas: tundra (16-KP-04), northern tundra–taiga (16-KP-01), southern tundra–taiga (16-KP-03), and northern taiga (16-KP-02), and two areas with supplementary AGB sampling: 18-BIL-01 and 18-BIL02 (tundra–taiga to northern taiga). Sample plot names of the 2016 expedition are V01-V58, sample plot names of the 2018 expedition are EN01-EN55.

All focus areas except 18-BIL-01 and 18-BIL-02 have mountainous relief with elevation up to 1500 m a.s.l. The treeline is represented by a deciduous conifer *Larix cajanderi*. The vegetation varies from prostrate lichen-*Dryas octopetala* L. tundra to open graminoid (hummock and non-hummock) tundra to tall *Pinus pumila* (Pall.) Regel scrublands to sparse and dense larch forests.

Direct anthropogenic influence in the region is very small. During the investigation period of this work covering the time from 2000 to 2017, in focus area 16-KP-01 a road construction took place, while the focus areas BIL-18-01 and BIL-18-02 are close to an operating highway.

1.3 Aims and objectives

Central Chukotka is a subarctic region that represents a mountainous tundra-taiga, where within about 200 km sparsely vegetated treeless tundra converts to forest tundra and even closed-canopy forests of the northern taiga. The species composition as well as climate in central Chukotka differs from other well-studied arctic and subarctic mountainous regions such as those in Alaska or the polar Urals. Global and circumpolar investigations show vegetation greening in Chukotka in recent years (Guay et al., 2014), but absence of field-based investigations leaves the reason for the greening unclear. Neither the spatial nor temporal development of vegetation, nor past nor potential future vegetation changes in central Chukotka specifically were previously investigated. Hence, the aim of this thesis is to investigate recent and potential future vegetation changes in this understudied tundra-taiga ecotone of central Chukotka.

Many studies involving observations and experiments support the hypotheses of shrubification (Myers-Smith et al., 2019; Myers-Smith et al., 2011; Sturm et al., 2005) and treeline advance (e.g., Gamache & Payette, 2005; Lloyd & Fastie, 2003) in response to climate change. Having these hypotheses in mind, and with field data on projective cover collected during the 2016 Russian-German expedition and the available long-term Landsat satellite data archive providing the possibility to trace vegetation change back in time, my first research question is: “what changes in vegetation composition occurred from 2000 to 2016 in central Chukotka?” To answer this question, I mapped land-cover in central Chukotka in its current state and back in 2000, using Landsat spectral indices, while coupling them with projective cover of different taxa from the field data. This enabled the investigation of compositional changes. Four representative areas of central Chukotka in northern taiga, southern and northern tundra-taiga, and treeless tundra were chosen for this research.

A second hypothesis, driving my investigations, considers the associations of greening and relating them to AGB increase (e.g., Myers-Smith et al., 2020). Above-ground carbon stocks are also an important parameter when investigating carbon cycling, which is gaining a lot of attention recently in high-latitude ecosystems (e.g., Ylänne et al., 2015; Campioli et al., 2009;

Sullivan et al., 2008). The research question that is asked is: “how have the AGB rates and distribution changed from 2000 to 2016 in central Chukotka?” To answer this question Landsat spectral data and field-based (2018 Russian-German expedition to Chukotka) estimations of above-ground biomass for different taxa were used.

The third hypothesis considered in this thesis, is that future climate conditions enhance forest expansion in the tundra and the treeline moving northward, causing an ecological zone shift (e.g., Greenwood & Jump, 2014). That is why my third research question is “what are the spatial dynamics and rates of tree AGB change in the upcoming millennia in the northern tundra-taiga from 2020 to 3000 CE?” To answer this question, I used my own AGB estimations for larch, enhanced the individual-based spatially explicit vegetation model LAVESI with topographical data and forced it with climate predictions to simulate the tree growth in the tundra-taiga ecotone in the central Chukotka mountainous region.

2 Materials and methods

All methods and data used in the study can be categorised into three major groups of objectives (see sections 4, 5, and 6 below): (1) the investigation of recent land-cover changes, interpreted as vegetation compositional changes, (2) the investigation of recent changes in total AGB, and (3) the simulation of potential future changes in tree AGB depending on the RCP (Representative Concentration Pathway) scenario (Fig. 2).

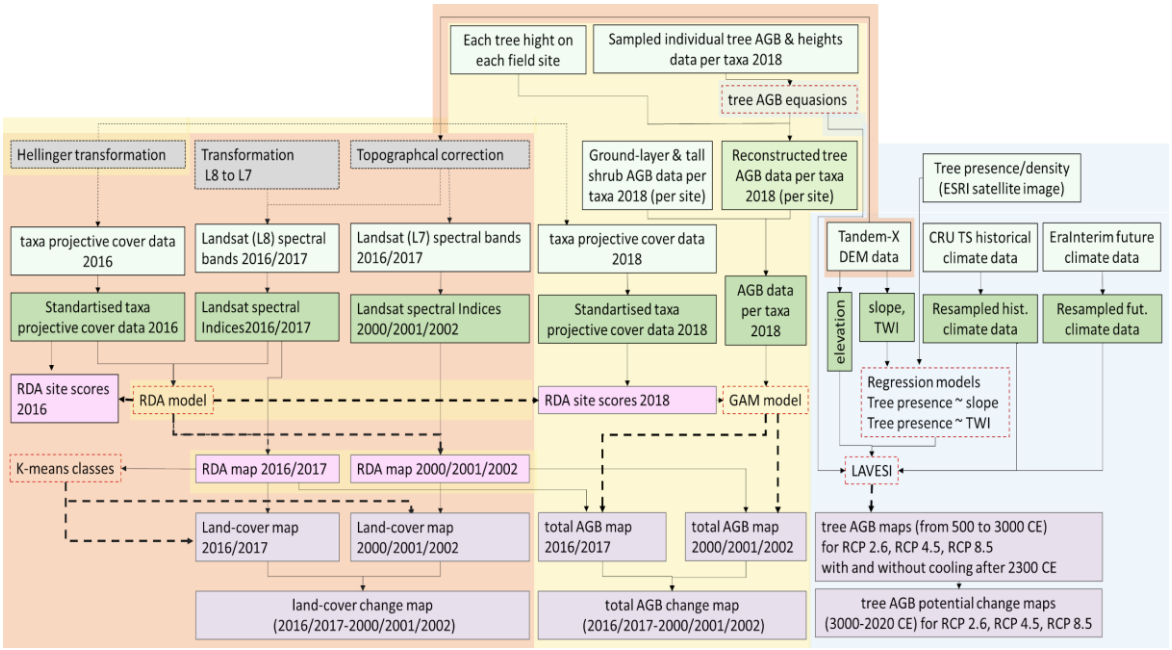

Figure 2. Overview of the methods and data used in the three manuscripts (Sections 4, 5 and 6). Background colour unites data and methods used for a part of the study: red – recent changes in-vegetation land-cover; yellow – recent changes in total above-ground biomass (AGB); blue – potential future changes in tree AGB. Fill colours and outlines of the boxes: grey box with dashed outline – transformations applied to the data; light green box – unprocessed data; dark green box – processed data ready to use in the model building; transparent box with red dashed outline – models, described by the name of the method used (redundancy analysis (RDA), k-means classification, general additive model (GAM), linear regression or LAVESI); pink box – intermediate results of modelling that were used in the next model (classification of GAM); violet box – results for the final analysis (state and change maps of land-cover, total AGB or simulated tree AGB). Dashed lines between boxes connect a model or transformation type and result or data (for easier visualisation). L7 and L8 stand for Landsat 7 ETM+ and Landsat 8 OLI satellite data accordingly.

Generally, all data consist of field samples and estimations (projective cover, AGB), as well as remote-sensing data (Landsat spectral indices (NDVI, NDWI, NDSI)), digital elevation model (DEM) data and climate data (historical Climate Research Unit gridded Time Series (CRU TS) and ECMWF Re-Analysis ERA-Interim future projections). The methods I used in this work were statistical modelling (RDA, GAM, linear regression), classification (k-means), and simulations using the individual-based spatially explicit model LAVESI. Transformations, which were applied to the data are standard Hellinger transformation (Legendre & Legendre, 2012) for the projective cover data, topographical correction for Landsat data, and my own development of a transformation to apply to the spectral bands of Landsat 8 to make them comparable with Landsat 7. The data and methods to develop the transformation, as well as validation methods are not shown on Fig. 2 but are described in detail in sections 4, 5, and 6.

Some data and methods of this thesis were subsequently developed for the different parts of it. Thus, the RDA model that was established for the land-cover investigations based on 2016 field data and Landsat spectral indices in the first manuscript, was also used to create RDA scores for the 2018 field data and to use the scores in the GAM model as predictors for total AGB estimated for the 2018 field sites in the second manuscript. Moreover, the established land-cover classification RDA maps were used together with the GAM model to upscale total AGB of the same study areas. DEM data were specifically used for derivation of elevation, slope, and TWI in the LAVESI-based simulation of the tree AGB project in the third manuscript, and they were also used to topographically correct the Landsat spectral bands in the very first steps of processing Landsat satellite data in the land-cover classification project. Equations for tree needle and tree wood AGB were established for the reconstruction of total tree AGB in the second manuscript focused on recent total AGB changes. These equations for the focus area 16-KP-01 in the tundra-taiga were also used in the LAVESI set-up for simulating tree AGB in this area in the third manuscript.

The field data were collected in 2018 specifically for this study, but remote-sensing data were rigorously chosen depending on the application. Thus, for the spatial upscaling in this study Landsat satellite data were chosen, Landsat collection 1 Level 2 imagery, processed by the United States Geological Survey (USGS) to surface reflectance with a 30-m spatial pixel ground resolution, provides the best available remote-sensing product covering long-time series at a landscape-scale spatial resolution. From the Landsat archive I extracted cloud-free acquisitions for the four focus areas, Landsat 7 ETM+ for an early (years 2000/2001/2002) time-slice and Landsat 8 OLI for a most recent time-slice in the years 2016/2017. However, Landsat satellite data only have acquisitions every 16 days and the investigated area is often heavily clouded. Thus, within the desired investigation period not many cloudless acquisitions were found. Absence of clouds and haze is extremely important for the application of our classification method because even thin clouds or close clouds strongly affect the quality of the data, making the atmospheric optical thickness thicker and affecting the values

of the spectral bands from which spectral indices will be calculated further on. This is why only acquisitions from earlier years (2000/2001 or 2002) and recent years (2016 or 2017) could be taken instead of all acquisitions in between 2000 and 2017. Instead of establishing a trend in vegetation changes, only two-time steps with the best available data spanning 15 or 16 years were analysed for land-cover and total AGB state and recent changes.

The choice of the statistical methods was guided by the simplicity and best possible variables explained by the predictors (RDA, linear and nonlinear (GAM) regression models). LAVESI is the individual-based spatially explicit *Larix* vegetation simulator specifically developed to simulate larch forest dynamics in the investigated area of the treeline ecotone by Stefan Kruse in my working group.

3 Thesis structure and author contributions

The thesis consists of (1) the general introduction, specifying the scientific background and motivation for the research and describing the study region, (2) methods overview, (3) three sections, highlighting three manuscripts (two published and one draft version in preparation), named accordingly (sections 4, 5 and 6) and (4) the synthesis. The following sections, which describe separate manuscripts, contain one published in the Journal Environmental Research Letters entitled "Strong shrub expansion in tundra-taiga, tree infilling in taiga and stable tundra in central Chukotka (north-eastern Siberia) between 2000 and 2017" (Shevtsova et al., 2020a), one manuscript published in the journal of Biogeosciences entitled "Recent above-ground biomass changes in central Chukotka (NE Siberia) combining field-sampling and remote sensing" (Shevtsova et al., 2021) and one manuscript entitled "Future spatially explicit tree above-ground biomass trajectories revealed for a mountainous treeline ecotone using the individual-based model LAVESI" submitted to the Journal Arctic, Antarctic, and Alpine Research.

3.1 Section 4 - Strong shrub expansion in tundra-taiga, tree infilling in taiga and stable tundra in central Chukotka (north-eastern Siberia) between 2000 and 2017

Authors: Iuliia Shevtsova (IS), Birgit Heim (BH), Stefan Kruse (SK), Julius Schröder (JS), Elena I. Troeva (ET), Luidmila A. Pestryakova (LP), Evgeniy S. Zakharov (EZ), Ulrike Herzschuh (UH)

Environ. Res. Lett. **15** 085006, 2020, https://doi.org/10.1088/1748-9326/ab9059

My first published manuscript presents land-cover changes, associated with compositional changes in central Chukotka for the 15 years until 2916/2017. IS, UH, BH and SK designed the study. JS made first attempts to implement the concept. LP, UH, SK and EZ planned, organised and coordinated the expedition for collecting field data. SK, JS, UH, LP and EZ have collected the field data, which were processed by IS (Shevtsova et al., 2019). ET has confirmed the botanical names of the sampled plants. BH advised the processing of remote sensing data. IS made a close-up analysis of Landsat satellite data, including searching available data, and making a justified choice of data to use, found after the first analyses that the inconsistencies between Landsat 7 and Landsat 8 sensors erroneously translated to vegetation change and optimized an own transformation between data from Landsat 7 and Landsat 8 sensors. IS also detected artefacts due to the mountainous terrain and applied a topographical correction to Landsat 7 and Landsat 8 sensor data. IS conducted a statistical analysis of field data on vegetation and remote sensing data for land-cover classification application, which included an explanatory analysis for vegetation cover data, application of RDA for linking vegetation cover data from the 2016 expedition and Landsat spectral Indices and the application of land-

cover classification methods (in this study the k-means method) and the change detection analyses. SK, UH and BH supervised the research activity and provided critical review during manuscript preparation.

3.2 Section 5 - Recent above-ground biomass changes in central Chukotka (NE Siberia) combining field-sampling and remote sensing

Authors: Iuliia Shevtsova (IS), Ulrike Herzschuh (UH), Birgit Heim (BH), Luise Schulte (LS), Simone Stünzi (SS), Luidmila A. Pestryakova (LP), Evgeniy S. Zakharov (EZ), and Stefan Kruse (SK)
Biogeosciences, 18, 3343–3366, 2021, https://doi.org/10.5194/bg-2020-416.

My second published manuscript present investigations of above-ground biomass state and change in central Chukotka for the past 15 years until 2016/2017. IS, UH and SK designed the study. SK, IS, UH, LS, SS, LP, EZ collected the field data. During the field expedition my (IS) responsibilities were to develop the concept for the biomass sampling and determination and the description of the ground layer vegetation cover on all the sites in the study areas 16-KP-01 and 18-BIL. SK and IS processed the field samples. Here I (IS) was responsible for drying and weighting of the AGB samples from all sites of areas 16-KP-01, 16-KP-04 and 18-BIL, processing the vegetation cover and AGB data from the 2018 expedition, processing of field notes on vegetation cover and ground-layer AGB and publishing the datasets in the PANGAEA data repository (Shevtsova et al., 2020b; Shevtsova et al., 2020c). BH advised the processing of remote sensing data. IS developed R code for processing all data used in the study, performed the formal analyses and visualisation, and prepared and edited the original manuscript. I (IS) comprehensively analysed the data on the sampled parts of individual tall shrubs and trees and developed specific allometric equations for tree AGB and finalising into a published dataset (Shevtsova et al., 2020d), analysed and upscaled the AGB data linking field estimations to the Landsat satellite data via the GAM method. SK, UH and BH supervised the research activity and provided critical review during manuscript preparation. UH, LP and SK were responsible for the management and coordination of the planning and execution of the expedition project.

3.3 Section 6 - Future spatially explicit tree above-ground biomass trajectories revealed for a mountainous treeline ecotone using the individual-based model LAVESI

Authors: Iuliia Shevtsova (IS), Ulrike Herzschuh (UH), Birgit Heim (BH), Luidmila A. Pestryakova (LP), Evgeniy S. Zakharov (EZ) and Stefan Kruse (SK)

Submitted to the Journal *Arctic, Antarctic, and Alpine Research* (in review).

In my third unpublished manuscript, I investigated potential future (for 980 years until 3000 CE) tree AGB rates and distribution. SK, UH and IS designed the study. SK developed the initial LAVESI model. Field data, used in the study was collected by SK. The expedition, during which the data was collected was planned, organised and coordinated by UH, LP, SK and EZ. IS processed the field data. IS undertook a comprehensive analysis of tree presence, density, distribution, depending on elevation, slope, aspect and TWI for the Lake Illerney region in the tundra-taiga ecotone, which included conducting a stratified random sampling of the digital elevation data, using the target object (trees) that are well visible features on ESRI satellite images by categories (tree presence). IS simulated tree AGB for this region for the future 980 years applying the LAVESI. SK, UH and BH supervised the research activity and provided critical review during manuscript preparation. The manuscript represents a draft, and a revision is planned before the submission.

4 Strong shrub expansion in tundra-taiga, tree infilling in taiga and stable tundra in central Chukotka (north-eastern Siberia) between 2000 and 2017

Iuliia Shevtsova[1,2,*], Birgit Heim[1], Stefan Kruse[1], Julius Schröder[1], Elena I. Troeva[3], Luidmila A. Pestryakova[4], Evgeniy S. Zakharov[3], Ulrike Herzschuh[1,2,5,*]

[1]Alfred Wegener Institute (AWI), Helmholtz Centre for Polar and Marine Research, Research Unit Potsdam, Germany

[2]Institute of Biochemistry and Biology, University of Potsdam, Karl-Liebknecht-Straße 24–25, 14476 Potsdam, Germany

[3]Institute for Biological problems of the Cryolithozone, Russian Academy of Sciences, Siberian branch, Yakutsk, Russia

[4] Institute of Natural Sciences, North-Eastern Federal University of Yakutsk, 677000 Yakutsk, Russia

[5] Institute of Environmental Sciences and Geography, University of Potsdam, Karl-Liebknecht-Straße 24–25, 14476 Potsdam, Germany

*Author e-mails:

iuliia.shevtsova@awi.de, ulrike.herzschuh@awi.de

Abstract

Vegetation is responding to climate change, which is especially prominent in the Arctic. Vegetation change is manifest in different ways and varies regionally, depending on the characteristics of the investigated area. Although vegetation in some Arctic areas has been thoroughly investigated, central Chukotka (NE Siberia) with its highly diverse vegetation, mountainous landscape and deciduous needle-leaf treeline remains poorly explored, despite showing strong greening in remote-sensing products. Here we quantify recent vegetation compositional changes in central Chukotka over 15 years between 2000/2001/2002 and 2016/2017. We numerically related field-derived information on foliage projective cover (percentage cover) of different plant taxa from 52 vegetation plots to remote-sensing derived (Landsat) spectral indices (Normalised Difference Vegetation Index (NDVI), Normalised Difference Water Index (NDWI) and Normalised Difference Snow Index (NDSI)) using constrained ordination. Clustering of ordination scores resulted in four land-cover classes: (1) larch closed-canopy forest, (2) forest tundra and shrub tundra, (3) graminoid tundra and (4) prostrate herb tundra and barren areas. We produced land-cover maps for early (2000, 2001 or 2002) and recent (2016 or 2017) time-slices for four focus regions along the tundra-taiga vegetation gradient. Transition from graminoid tundra to forest tundra and shrub tundra is interpreted as shrubification and amounts to 20% area increase in the tundra-taiga zone and 40% area increase in the northern taiga. Major contributors of shrubification are alder, dwarf birch and some species of the heather family. Land-cover change from the forest tundra and shrub tundra class to the larch closed-canopy forest class is interpreted as tree infilling and is notable in the northern taiga. We find almost no land-cover changes in the present treeless tundra.

1 Introduction

The Arctic is undergoing strong climate change, which is especially prominent in high latitudes (IPCC, 2019; Overland et al., 2014). Climate change is assumed to be the main driver of vegetation change in arctic and subarctic regions (Walker et al., 2006). Accordingly, drastic changes have been predicted with simulations, including an increase of graminoid, shrub and tree abundance and northward movement of vegetation transition ecotones (van der Kolk et al., 2016; Zhang et al., 2013). Indeed, remote-sensing data shows vegetation greening (e.g. Jia et al., 2003; Bunn & Goetz, 2006; Jia et al., 2009; Zeng et al., 2011). However, greening trends derived from spectral satellite data are complex (Myers-Smith et al., 2020) and only with the help of field-based approaches can aspects of vegetation change such as composition, structure and biomass be investigated as, for example, in many arctic vegetation studies (Forbes et al., 2010; Beck et al., 2011; Myers-Smith et al., 2011; Elmersdorf et al., 2012; Frost et al., 2013; Moffat et al., 2016). Regional-scale compositional vegetation-change analysis, thus, requires a direct combination of field-based measurements and remote-sensing data.

Studies from vast unexplored areas in eastern Eurasia are required as vegetation change varies regionally (Walker et al., 2017). Most of the published field data on the vegetation of arctic and subarctic regions are restricted to northern North America. Some land-cover investigation studies are available for north-western Siberia, southern and north-western Chukotka (Frost & Epstein, 2013), as well as eastern coastal Chukotka (Lin et al., 2012), whereas central Chukotka remains largely unexplored. Unlike the North American boreal treeline represented by evergreen conifers, the Siberian treeline is formed by larch – a deciduous conifer which characterises the seasonal forest's carbon cycling and better tolerates ice blasting, fire, and excessive heat or cold conditions (Givnish, 2002). Furthermore, larch forests typically have a low canopy cover, where understorey vegetation plays a greater role in the system's physical and biological properties (e.g., latent heat flux; Xue et al., 2011). In contrast to most tundra-taiga areas investigated in eastern Siberia, central Chukotka has mountainous terrain. The treeline here is restricted by a combination of elevational and latitudinal limits. Within only 140 km, treeless tundra turns via forest tundra into taiga, covering a large gradient of vegetation communities, which have a patchy pattern. Therefore, this unique vegetation of central Chukotka should be investigated at a regional scale, not as separate communities.

Commonly, broad-scale arctic vegetation changes are extracted from optical satellite missions' data. Analyses of Advanced Very-High-Resolution Radiometer (AVHRR) data (Guay, 2014) show that greening in central Chukotka from 1982 to 2012 is particularly strong. Therefore, further research into vegetation change in this region is needed. Increase in Normalised Difference Vegetation Index (NDVI) is commonly interpreted as an increase in plant biomass, cover and abundance (Myers-Smith et al., 2020). However, we aim to describe not only total cover change,

but which taxa play major roles in it. Normalised Difference Water Index (NDWI) and Normalised Difference Snow Index (NDSI) of winter/spring scenes may derive more composition-specific differences than NDVI alone, considering vegetation moisture content and differentiating dense from open forests, respectively. It is an advantage if the classification scheme of vegetation types is not solely based on remote-sensing derived indices, but directly involves field data to ensure association of land-cover change with vegetation composition. Such an approach, in contrast to others, allows the inference of vegetation compositional changes independent from expert knowledge of vegetation types in the classifying area. Furthermore, it connects, statistically, satellite spectral information of different vegetation types and field-based taxonomical composition of these types. A model built this way is suitable to apply to areas with a similar vegetation composition.

We aim to provide quantitative information on landscape-scale compositional vegetation changes in central Chukotka over 15 years starting in 2000. We built an ordination model coupling field-based foliage projective cover data with Landsat spectral indices and used the model scores to generate a land-cover classification. This allowed us to map vegetation types across four focus areas for two time slices and derive land-cover change from the difference maps. The results were used to answer i) what kind of changes in vegetation composition have happen within the investigated 15 years in central Chukotka and ii) what is the magnitude of these changes?

2 Materials and methods

In this study we used two sources of data: field foliage projective cover of selected taxa and Landsat satellite data. The foliage projective cover data were used to build a statistical model, which formed the basis of vegetation classes using Landsat Indices as an input. The general scheme of data processing is presented in Fig. 1.

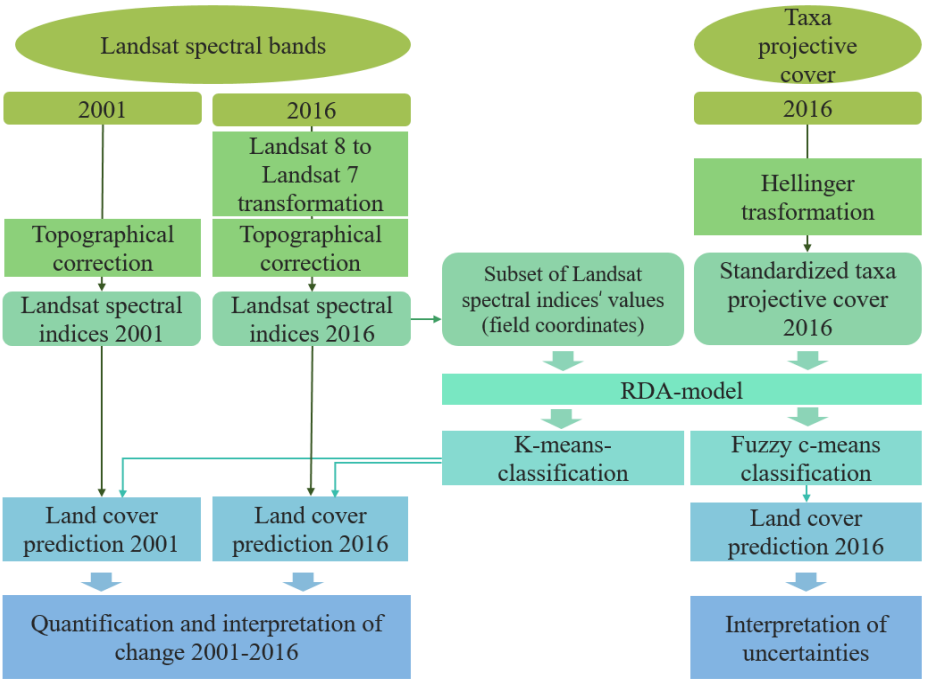

Figure 1. Scheme of the data and methods used in the study. Transformed and topographically corrected Landsat data and field data on projective cover were used in the ordination (redundancy analysis, RDA) model. The scores of the RDA model were used in the *k*-means and fuzzy *c*-means classification. Derived hard clusters were applied to Landsat images from 2000/2001/2002 and 2016/2017 to predict land-cover classes from remote-sensing data. From these land-cover maps we derived change maps.

2.1 Field data collection and processing

The study area is in central Chukotka, NE Siberia, Russia (Fig. 1). Large parts of the region are characterised by mountain complexes. Central Chukotka has a continental type of climate: cold winters with average January temperatures of -30°C, summers with average July temperature of +13°C, short growing seasons (100 days year^{-1}) and low precipitation (200 mm yr^{-1}; Menne et al., 2012).

Vegetation data were collected during the Russian-German expedition in summer 2016 (Kruse & Stoof-Leichsenring, 2016). Vegetation properties were investigated in four areas along a gradient (Fig. 2) from treeless mountainous tundra (16-KP-04,

Lake Rauchuagytgyn area), via the tundra–taiga transition (16-KP-01, Lake Ilirney area; 16-KP-03, Nutenvut lakes area) to the northern taiga (16-KP-02, Bolshoy Anyuy river area). In total, 57 sites were investigated (Shevtsova et al., 2019). The sites cover a large Landsat NDVI gradient (0.3–0.8) and differ in elevation (100–900 m a.s.l.), slope angle (0–54°) and aspect.

The 16-KP-04 focus area is in the Anadyr Mountains. It represents mostly mountainous terrain with elevation up to 1500 m a.s.l. and open tundra. The area around 16-KP-01 at Ilirney Lake, represents the tundra–taiga ecotone, which is characterised by diverse vegetation: open tundra, shrublands and forest tundra. The highest elevation is 1000 m a.s.l. 16-KP-03 is characterised mostly by open and forest tundra and mountainous areas (700–1000 m a.s.l) like 16-KP-01. 16-KP-02 belongs to the northern taiga biome with low mountains reaching an elevation of 300–500 m a.s.l. in the east. The river lowlands are covered by wetlands and uplands of forests and open land with visible fire scars.

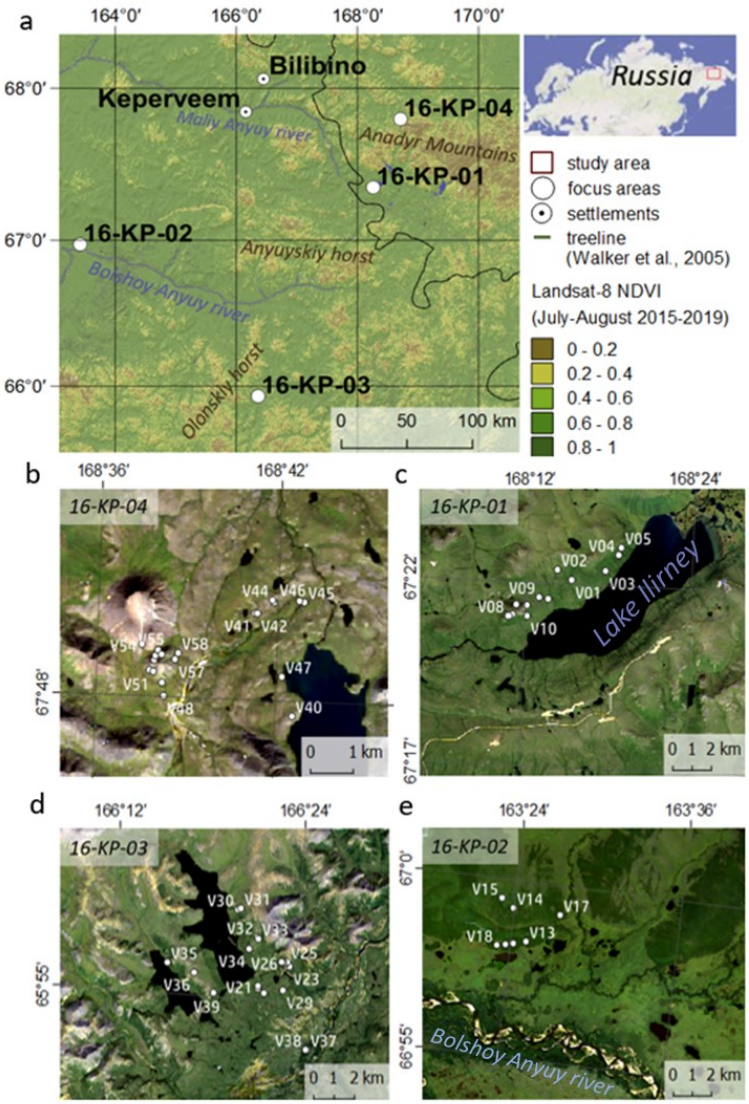

Figure 2. Chukotka district (Russia) and the sampling sites in the four focus areas: a) overview, b) 16-KP-04 (tundra, sites V40-58, total: 15 sites), c) 16-KP-01 (northern border of tundra–taiga transition, sites V1-V12, total: 12 sites), d) 16-KP-03 (southern border of tundra–taiga transition, sites V20-V39, total: 19 sites) and e) 16-KP-02 (northern taiga, sites V13-V19, total: 6 sites). Background (b–e): Landsat-8 quasi true Red Green Blue composites.

For every field site, a detailed description of the vegetation was made (Shevtsova et al., 2019). We used 52 sites (V01–V16, V18–V24, V26–V51, V54, V57–V58) from 57 investigated field-sites. Some sites were excluded due to their location in mountainous terrain being affected by shadows in the satellite images. During fieldwork we investigated vegetation in circular plots of 30m in diameter. Within each plot, we sampled five 2×2m subplots, with one subplot placed at the centre of the circle and the other four placed 7.5m away in each of the cardinal directions. Foliage projective cover

of tall (>100 cm) shrubs and trees was estimated for the entire plot, whereas foliage projective cover for all major taxa of the ground layer was estimated in each of the five 2×2m subplots and averaged for each plot. To accommodate the absence of the same species at compared sites and to standardise data, we applied the Hellinger transformation (Legendre & Legendre, 2012) to the foliage projective cover data.

2.2 Landsat data, pre-processing and spectral indices processing

Landsat collection 1 Level 2 imagery, processed by the United States Geological Survey (USGS) to surface reflectance with a 30-m spatial pixel ground resolution, provides the best available remote-sensing product covering long-time series at a landscape-scale spatial resolution. From the Landsat archive we extracted cloud-free acquisitions for the four focus areas from an early (years 2000/2001/2002) and late time-slice 2016/2017 (Appendix A, Table A1). We used only peak-summer acquisitions collected from mid-July to mid-August. We found only one cloudless or partly cloudless peak-summer acquisition from 2002 and one from 2017 for the 16-KP-04 area, one each from 2001 and 2016 for 16-KP-01 and 16-KP-03 and one from 2000 and 2016 for 16-KP-02. Apart from summer acquisitions, we selected cloudless snow-covered springtime acquisitions for the corresponding year and covering the same area as the peak-summer acquisitions.

Due to sensor problems on Landsat-7 since 2003 and the fact that Landsat-8 was launched in 2013 we needed to use both Landsat-7 and Landsat-8 data. To provide high consistency between the spectral bands of different Landsat missions, we applied the standard Landsat-7 to Landsat-8 transformation from Roy et al. (2016), but we still observed a sensor-related bias. Therefore, we empirically derived new transformation coefficients. We used concurrent Landsat-7 (12.08.2013 and 14.08.2013) to Landsat-8 (13.08.2013 and 15.08.2013) acquisitions and conducted random sampling of 500 000 points (only land, avoiding noisy shadowed areas) to build linear regression models for each spectral band we used in the processing:

$$L8ETM + like - GREEN\ surface\ reflectance\ =\ 1.03 * L8\ OLI - GREEN\ surface\ reflectance\ +\ 0.001$$

$$L8\ ETM + like - RED\ surface\ reflectance\ =\ 1.05 * L8\ OLI - RED\ surface\ reflectance\ +\ 0.0005$$

$$L8\ ETM \pm like - NIR\ surface\ reflectance\ =\ 0.91 * L8\ OLI - NIR\ surface\ reflectance - 0.009$$

$$L8\ ETM + like - SWIR1\ surface\ reflectance\ =\ 1.04 * L8\ OLI - SWIR1\ surface\ reflectance\ +\ 0.008$$

Where $ETM + -like$ is the transformed Landsat-8 OLI to Landsat-7 ETM+, $L8\ OLI$ is the original Landsat-8 OLI, $GREEN$ is the green, RED the red, NIR the near-infrared and $SWIR1$ the first short-wave infrared Landsat surface reflectance [0-1].

To the Landsat-7 and transformed Landsat-8 data we applied the topographical c-correction (Riano et al., 2003) to compensate for differences in solar illumination due to topography. We derived solar-geometry related parameters (solar zenith angle and solar azimuth angle) from the Landsat metadata. The slope and aspect angles of slopes were calculated from the ASTER Global Digital Elevation (GDEM, Tachikawa et. al., 2011) with the same spatial 30×30m pixel ground resolution as Landsat. Additionally, we masked clouds and water bodies in the Landsat spectral-band set using an optimised threshold in the NIR band. These pre-processed Landsat spectral bands were used to calculate Landsat spectral indices (Appendix C, Table C1) from summer acquisitions.

2.3 Redundancy analysis (RDA) and classification approaches

The length of the first detrended correspondence analysis axis is equal to 2.55 standard deviation units meaning the field data in our case is distributed on a short linear gradient rather than a unimodal distribution (Borcard et al., 2011). A suitable constrained ordination method for short gradients assuming linear species responses along the environmental gradients is redundancy analysis (RDA, Legendre & Legendre, 2012). Using RDA, we related foliage projective cover data to the Landsat spectral indices by extraction of pixel values using the field sites' coordinates. The best parameters for the RDA model were chosen according to stepwise selection and analysis of variance.

We built up the classification based on RDA scores using two clustering approaches: *k*-means (hard classification, Appendix D) and fuzzy *c*-means (soft classification; FCM; Bezdek, 1981; Appendix D). In both cases of clustering, compositionally similar data were arranged into groups according to similar behaviours of the explanatory Landsat data. In FCM classification we set a threshold of 0.6 and values exceeding this remained unclassified and were marked as uncertain (discussed in Appendix D). The optimal number of statistically significant clusters for *k*-means classification was chosen according to the gap statistics method (Tibshirani et al., 2001).

Based on hard classification we predicted cluster numbers for Landsat data from four focus areas for both early and late time slices. We obtained difference maps for each area reflecting changes in vegetation composition over the 15-year period. We interpreted the uncertainties that could appear in the land-cover classification in the study region using FCM results from 2016/2017. We validated the accuracy of the derived land-cover maps of 2016/2017 using field data from 2018 (Appendix E).

3 Results

3.1 General characteristics of the vegetation field data

We observed dense forests, formed by larch (*Larix cajanderi* Mayr) often with characteristic fire scars in the 16-KP-02 area (Shevtsova et al., 2019). Sparse forest tundra stands are common for the 16-KP-01 and 16-KP-03 areas. The sparse larch stands are commonly accompanied by low and dwarf shrubs: *Salix* spp., *Betula nana* L., *Ledum palustre* L., *Vaccinium* spp., *Empetrum nigrum* L. Elevational transitions between forest tundra and open tundra are often covered by patches of dwarf pine (*Pinus pumila* (Pall.) Regel). Open tundra on gentle slopes at lower elevations (540–700 m a.s.l) is graminoid rich and accompanied by dwarf *Salix* and *Vaccinium*. Intermediate elevations in mountain areas of 16-KP-01 (700–900 m a.s.l.) and 16-KP-03 (700–800 m a.s.l.) as well as lower elevations in 16-KP-04 (500–600 m a.s.l.) are dominated by *Dryas octopetala* L. accompanied by a selection of herbs (Poaceae, Fabacea, Astraceae etc.) and become barren at higher elevations. Mosses are common everywhere, having highest relative abundance in open tundra.

3.2 Relating field data to Landsat spectral indices in the RDA model

Landsat spectral indices NDVI, NDWI and NDSI together explained 33% of the variance in the field vegetation data. All three of them explain a significant unique portion of the variance (Table 1, Fig. 3). Adding further indices as explanatory variables to the RDA model did not improve the explained variance. Most of the variance (21%) of the field compositional data is explained by NDVI; NDWI and NDSI, explain around 7% and 5%, respectively. The Landsat spectral indices are distributed in the two RDA-axes space, where NDVI is negatively associated with the 1st RDA axis, NDWI positively with the 1st RDA axis and NDSI positively with the 2nd RDA axis. As axes 1 and 2 carry most information (29%) only these two RDA axes were retained for further analysis.

Table 1. Permutation test for the redundancy analysis (RDA) model with three indices as predictors: Normalised Difference Vegetation Index (NDVI), Normalised Difference Water Index (NDWI) and Normalised Difference Snow Index (NDSI) and their significance levels.

Index	Variance	F	*p*-value
NDVI	0.91	15.17	0.001
NDWI	0.03	5.13	0.001
NDSI	0.02	3.29	0.005
Residual	0.29		

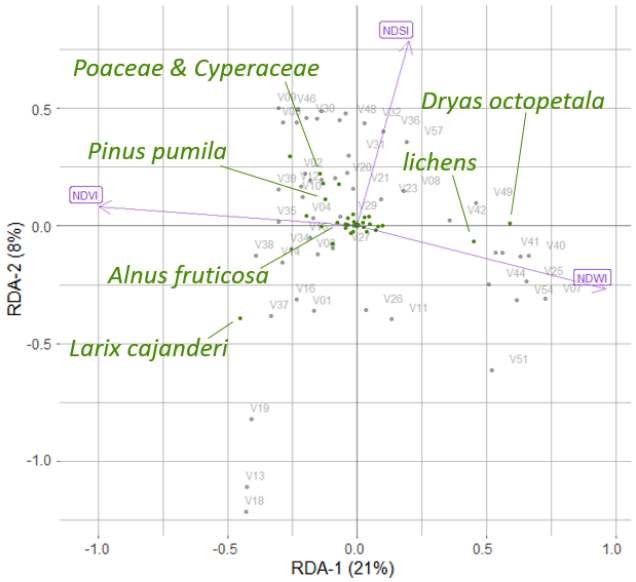

Figure 3. Redundancy analysis (RDA) model based on foliage projective cover data of the plot taxa and Landsat spectral indices (Normalised Difference Vegetation Index (NDVI), Normalised Difference Water Index (NDWI) and Normalised Difference Snow Index (NDSI)), where V01-V58 are the 52 vegetation field sites. The positions of the major taxa are shown.

3.3 Land-cover classification

The *k*-means classification (Fig. 4) yielded four reasonable land-cover classes named 1) larch closed-canopy forest, 2) forest tundra and shrub tundra, 3) graminoid tundra, 4) prostrate herb tundra and barren areas.

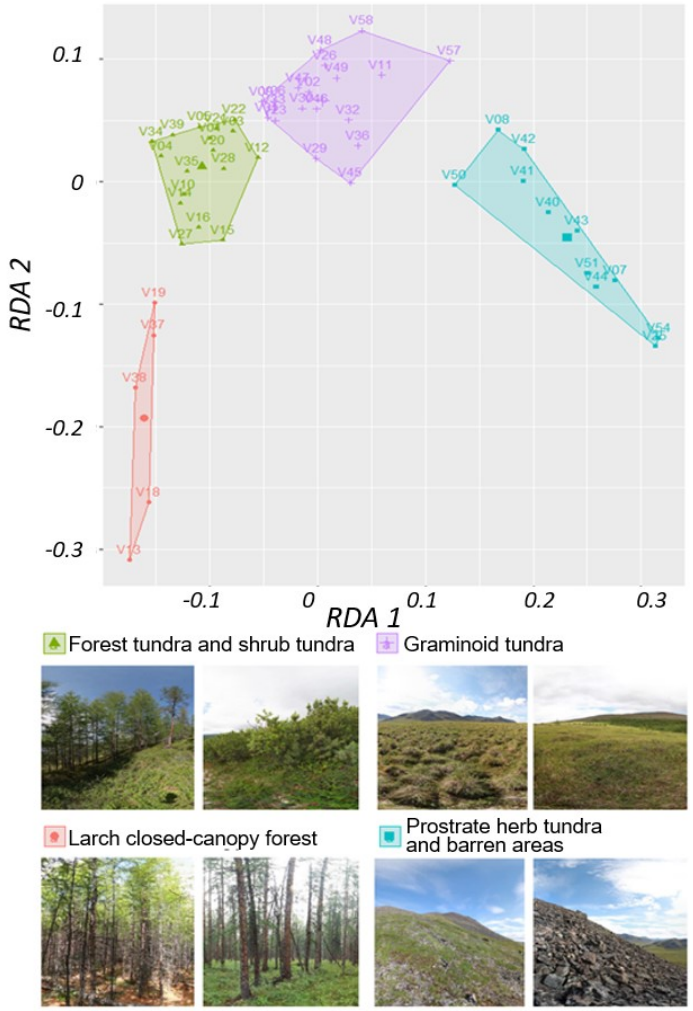

Figure 4. *K*-means classes based on two redundancy analysis (RDA) axes using Normalised Difference Vegetation Index (NDVI), Normalised Difference Water Index (NDWI) and Normalised Difference Snow Index (NDSI) as predictors. Images: extracts from 360x180 degree panoramic images, Stefan Kruse.

The larch closed-canopy forest is characterised by the highest NDVI values (0.75) and low NDSI (<0.6, Fig. 5). Despite the high biomass content, larch closed-canopy forests have generally poor biodiversity. The vegetation composition consists mostly of abundant *L. cajanderi* (20–70%) with moss or grass undergrowth (Fig. 6).

The forest tundra and shrub tundra class is characterised by higher NDVI values (0.68–0.78), but in contrast to larch closed-canopy forest has a higher NDSI (>0.6). In the landscape it represents dense *Alnus viridis* ssp. *fruticosa* (Rupr.) Nyman or *Pinus pumila* shrub communities and open *Larix cajanderi* forest (<20% cover) with relatively high dwarf birch (*Betula nana*) abundance (5–25%), with heathers (*Ledum palustre* L., *Vaccinium vitis-idaea* L., *V. uliginosum* L.) and a lichen–-moss ground layer.

The graminoid tundra is characterised by moderate to higher NDVI (0.5–0.68), higher NDWI than the first two classes and a higher NDSI (>0.6). This class represents hummock (*Eriophorum vaginatum* L.) and non-hummock (*Carex* spp.) graminoid tundra with moss prevailing in the ground layer.

The prostrate herb tundra and barren areas class is characterised by low NDVI (<0.5), very high NDWI (> –0.5) and higher NDSI (>0.6). Prostrate herb tundra is dominated by *Dryas octopetala* and lichens accompanied by some herbs (*Fabaceae, Orobanchaceae, Poaceae, Rosaceae, Saxifragaceae* etc.) and prostrate *Salix* spp. shrubs.

In the RDA model, larch closed-canopy forest is characterised by a combination of low axis-1 and axis-2 scores indicating high NDVI and low NDSI. NDSI increases along axis 2, indicating highly reflective surfaces covered by snow. High axis-2 scores in combination with low or moderate axis-1 scores indicate moderate to high NDVI, reflecting graminoid tundra or forest tundra and shrub tundra, respectively. The prostrate herb tundra and barren areas class is characterised by very high axis-1 scores originating from high NDWI and low NDVI caused by low biomass and dry barren land surface.

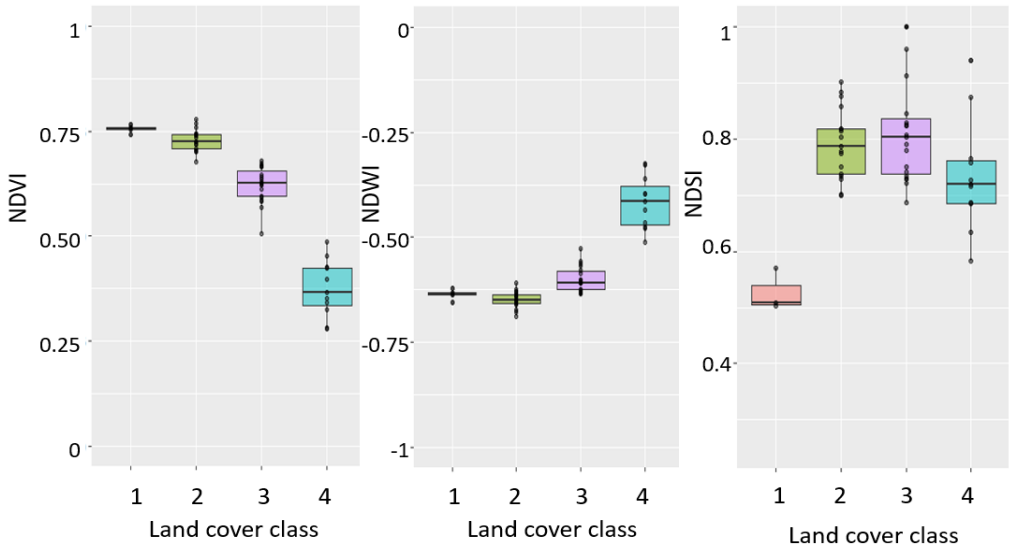

Figure 5. Value distribution of spectral Landsat indices (Normalised Difference Vegetation Index (NDVI), Normalised Difference Water Index (NDWI) and Normalised Difference Snow Index (NDSI)) by the four land cover classes: (1) larch closed-canopy forest, (2) forest tundra and shrub tundra, (3) graminoid tundra and (4) prostrate herb tundra and barren areas.

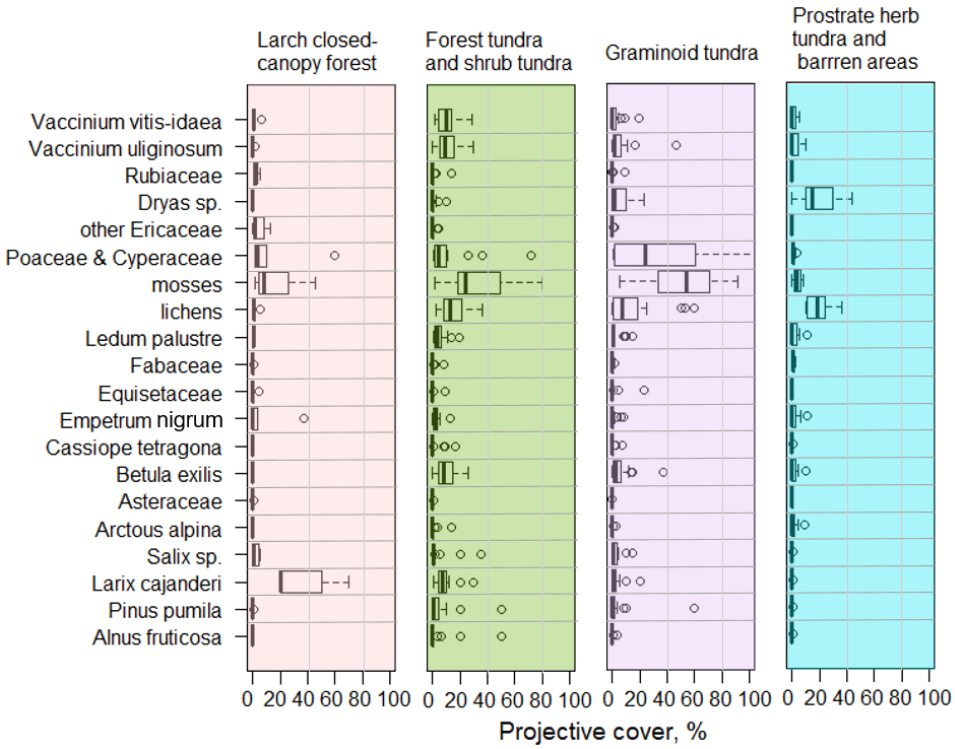

Figure 6. Foliage projective cover of the major taxa in four land-cover classes: larch closed-canopy forest, forest tundra and shrub tundra, graminoid tundra and prostrate herb tundra and barren areas.

The validation of land-cover maps showed 66% agreement between class numbers predicted for validation sites in tundra and tundra-taiga from projective cover and from Landsat Indices (Appendix E). The highest disagreement (19%) was obtained for prostrate herb tundra and barren areas that were misclassified as graminoid tundra when predicted from Landsat data.

3.4 Land-cover change between 2000 and 2017

Overall, the land cover in the treeless tundra (16-KP-04) has not significantly changed (<5%) from 2000 to 2017. In contrast, the forest tundra and shrub tundra class shows a major increase in area of up to 20–25% in the tundra–taiga (16-KP-01, 16-KP-03). Larch closed-canopy forest expanded significantly in the northern taiga (16-KP-02) accompanied by an increase of forest and shrub tundra at higher elevations.

The northernmost area (16-KP-04) is today dominated by prostrate herb tundra and barren areas (59% in 2017) and graminoid tundra (36% in 2017, Appendix F, Fig. F1). The change map (Fig. 7 a) between 2002 and 2017 indicates only a slight transition of graminoid tundra to forest and shrub tundra (4%).

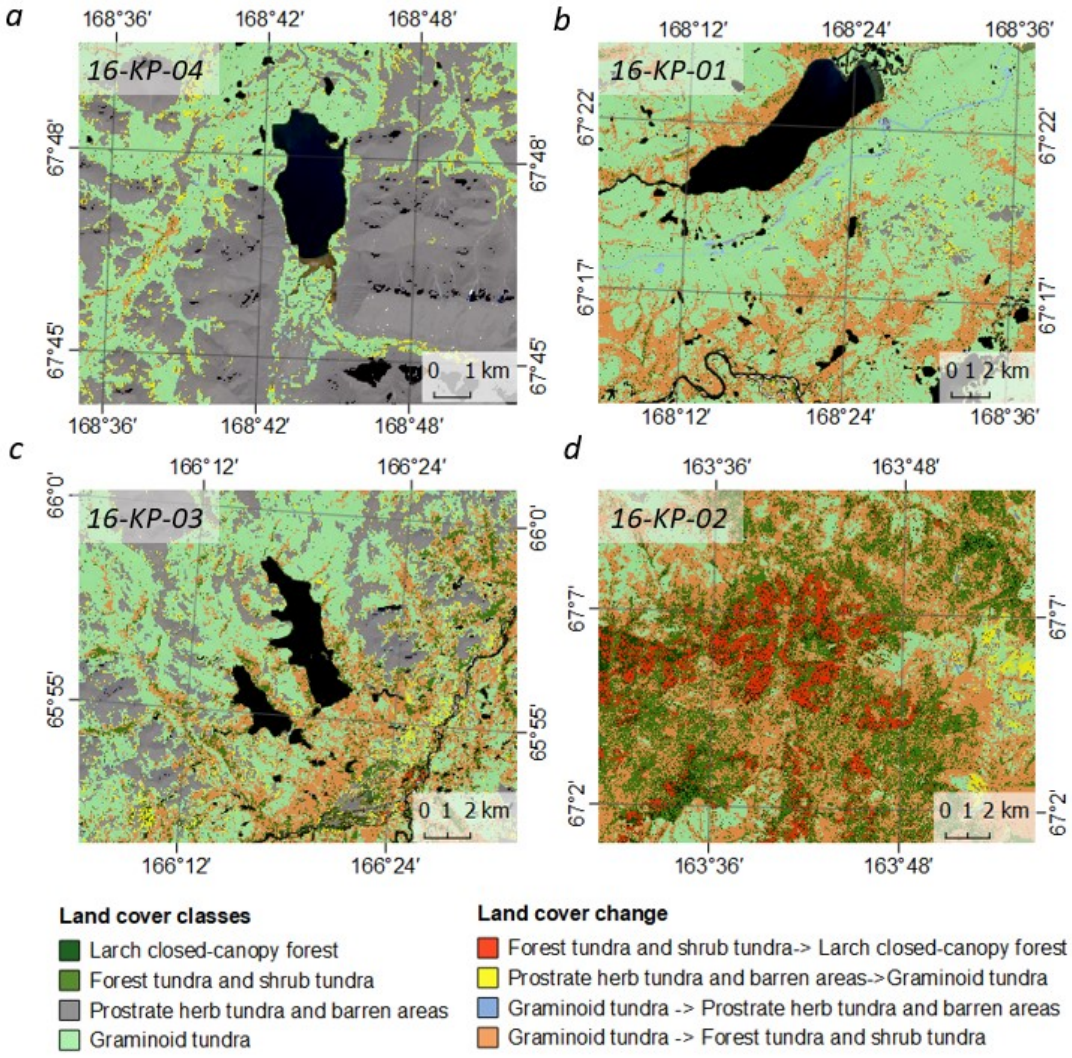

Figure 7. Colour-coded land-cover classes and colour-coded land-cover change: a) 16-KP-04 (treeless tundra), b) 16-KP-01 (tundra–taiga transition), c) 16-KP-03 (tundra–taiga transition) and d) 16-KP-02 (northern taiga).

In the typical tundra–taiga transition (16-KP-01), a large part of the area is represented by open and forest tundra: graminoid tundra occupies 92% of the area in 2001 and 68% of the area in 2016; forest tundra and shrub tundra occupies only 3% of the area in 2001, whereas by 2016 it covered 27% (Appendix F, Fig. F2). The change map of this area (Fig. 7 b) indicates the expansion of forest and shrub tundra by 21% replacing the graminoid tundra from 2001 to 2016. It occurs mostly in the drain valleys and gentle slopes around Lake Ilirney and smaller lakes. South of Lake Ilirney we observe a change from graminoid tundra to prostrate herb tundra and barren areas due to road construction.

The southernmost location (16-KP-03) represents the tundra–taiga transition as well. In contrast to 16-KP-01, it has more prostrate herb tundra and barren areas (34% in 2001 and 29% in 2016, Appendix F, Fig. F3). The change map (Fig. 7 c) shows a transition from graminoid tundra to forest tundra and shrub tundra of 19% between 2001 and 2016. Almost no change in the prostrate herb tundra

and barren areas is detected. The larch closed-canopy forest slightly expanded by 4% from 2001 to 2016.

The northern taiga 16-KP-02 area is covered by forest tundra and shrub tundra (39% in 2000 and 69% in 2016, Appendix F, Fig. F4) and larch closed-canopy forest (5% in 2000 and 13% in 2016). The change map (Fig. 7 d) from 2000 to 2016 indicates a 9% transition from forest tundra and shrub tundra to larch closed-canopy forest, as well as a 40% transition from graminoid tundra to forest tundra and shrub tundra.

4 Discussion

4.1 Dataset limitations and optimisation

Our approach yielded useful information on land-cover change despite facing several methodological challenges. We focussed on changes of major zonal vegetation types. Accordingly, azonal vegetation types were not investigated during fieldwork including polygonal tundra in lake depressions and floodplain vegetation, which are classified as graminoid tundra or forest and shrub tundra.

The vegetation survey plots were placed within an as homogenous as possible environment to represent broad land-cover classes and allow upscaling. However, heterogeneity in tundra and tundra–taiga landscapes is often higher than the spatial resolution of most of the remote-sensing products (Myers-Smith et al., 2011; Frost et al., 2014). Consequently, the spectral signal of a Landsat pixel with a spatial resolution of 30×30m is mixed if different vegetation types are present within the pixel. For instance, the spectral signal of a green forest canopy with low red reflectance due to photosynthetic pigment absorption and high multiple NIR scattering and thus high NDVI values can be mixed with the high red and low NIR reflectance of a lichen understorey reducing NDVI for the plot (Appendix G, Fig. G1). Also, *Pinus pumila* shrubland, a characteristic vegetation type in the investigated region, could hardly be distinguished by Landsat because it is usually found alongside sparse vegetation or bare ground and covers small patches of 25–800 m^2. For example, dense healthy green *P. pumila* patches occur in V23 (16-KP-03), but a large percentage of the cover in the site is of white-coloured lichen. This causes a significant decrease in NIR and an increase in red reflectance, which results in lower NDVI values for the 30×30m pixel (Appendix G, Fig. G2).

Landsat-derived NDVI and NDWI selected for building the RDA model are known for their potential to reflect vegetation-related properties. The combination of red and NIR spectral bands used for the NDVI calculation highlights plant biomass and its chlorophyll content (Boelman, 2003; Tucker, 1979). NDWI utilises green and NIR reflectance and reflects the water content (Lara, 2018). NDSI has been developed to indicate snow cover (Volovcin, 1976), although it has also been used for identifying dense forests without leaves, for example, in central Alaska (Hall et al., 1998).

In our data, spring-NDSI values of snow-covered landscapes helped to separate closed-canopy forests that are not covered by snow due to high standing wood from other vegetation types.

Our transformation coefficients allowed a high consistency between Landsat-7 and Landsat-8 spectral bands. A comparison of Landsat-7 data with Landsat-8 data without our transformation or with application of the standard transformation (Roy et al., 2016) resulted in inaccuracy due to sensor differences of the same strength as vegetation changes. We observe less variability in the spectral bands of Landsat-7 data than Landsat-8 data due to the much lower radiometric sensitivity of the Landsat-7 sensor (USGS, 2019a; 2019b).

We significantly corrected Landsat data for shadowed areas in our classification by combining two approaches. First, we used the standard way of avoiding topographic effects and variations in the sun illumination angle by employing normalised difference spectral indices instead of single spectral band values or single band ratios (Mróz & Sobieraj, 2004). Second, we applied topographical corrections (Riano et al., 2003), because in the mountainous parts of Chukotka, the quality of the spectral indices was still affected by steep slopes and very strong shadows, especially for the snow-covered acquisitions.

We validated the derived land-cover maps with new field data from the expedition in 2018 (Appendix E). 66% of validation sites were correctly assigned to one of the four land-cover classes. The highest misclassification, namely systematic overestimation, we found for prostrate herb tundra and barren areas over graminoid tundra. However, the derivation of relative changes compensates for the misclassification error.

4.2 Vegetation changes from 2000/2001/2002 to 2016/2017

4.2.1 Tree infilling with no evidence of substantial treeline advance

The expansion of the sole tree species *Larix cajanderi* is attributed to a change from forest tundra and shrub tundra to larch closed-canopy forest. The most prominent results are obtained for the northern taiga area (16-KP-02). The larch closed-canopy forest increase resulted in an absolute *L. cajanderi* cover increase from 2000 to 2016 of about 5% (or an area of 15.8 km^2) with respect to its abundance in each of the accounted land-cover classes (Appendix H, Tables H1, H2). The spatial pattern of larch expansion derived from the land-cover classes' differences suggests tree infilling behaviour rather than treeline advance since the larch closed-canopy forest only significantly increased in the northern taiga where it was previously present at the landscape scale. Contrarily, we found no evidence of significant larch forest advance in the tundra–taiga ecotone.

We compared the increase of larch tree cover in our study region to other Siberian subarctic regions where the treeline is formed by *Larix* spp. (Fig. 8). Both areas of the tundra-taiga ecotone (16-KP-01 and 16-KP-03) have similar increases to north-western Siberia as explored by Frost & Epstein (2013).

Increase of larch cover in northern taiga (16-KP-02) is twice as high as in the tundra-taiga ecotone. Despite these similarities, one needs to be careful in such comparisons since tree cover is increasing nonlinearly and one needs to consider the period of investigation (Frost & Epstein: 1965–2009; this study: 2000–2017) and the different spatial resolutions of the studies.

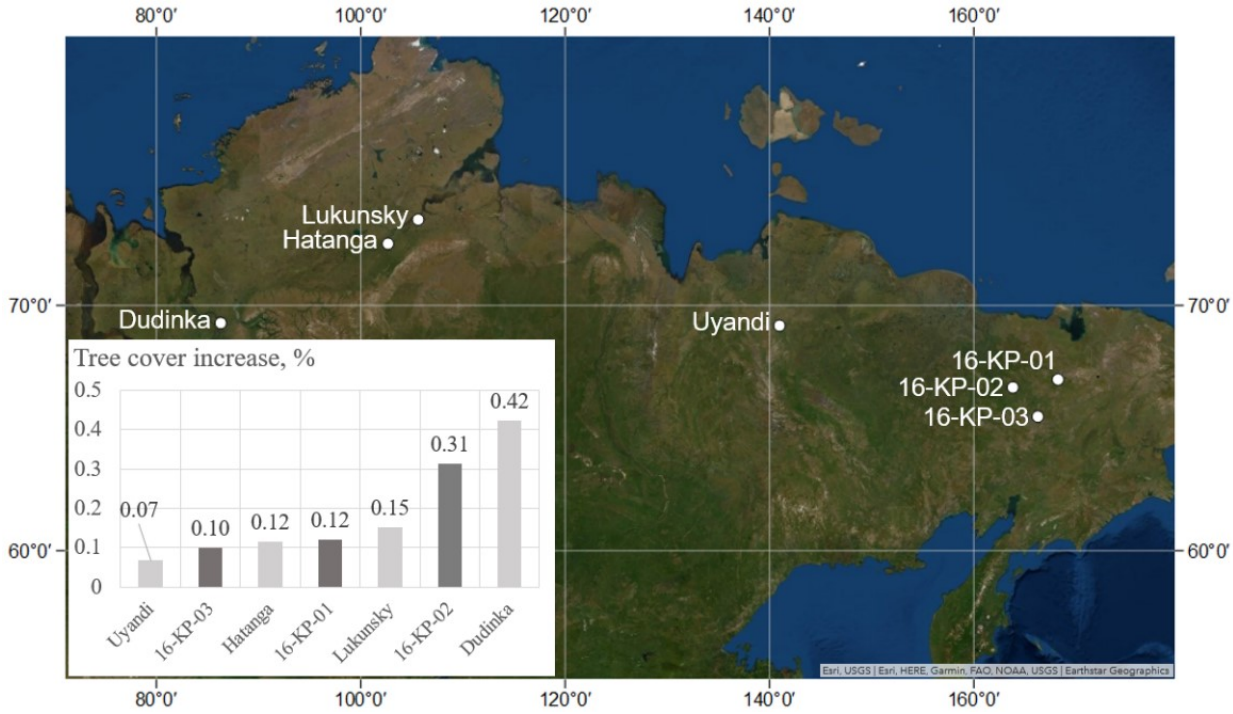

Figure 8. Larch tree cover increase, recalculated as average per year: for our study areas (16-KP-01 (northern treeline border), 16-KP-02 (northern taiga), 16-KP-03 (southern treeline border)) and the study areas of Frost & Epstein (2013; Uyandi, Hatanga, Lukunsky, Dudinka). Background map Esri, USGS | Esri, HERE, Garmin, FAO, NOAA, USGS | Earthstar Geographics.

It is likely the ecological niche of *L. cajanderi* will shift further north with recent warming. However, larch migration to the north might be limited by seed dispersal and reproduction rates (Wieczorek et al., 2017a). Our inferences of strong infilling in southern areas and a simultaneously slow treeline advance in northern areas is in accordance with simulation results of an individual-based larch model (Kruse et al., 2019a). Climate-driven infilling might be overestimated in areas recently heavily impacted by fires. However, we selected a region in the northern taiga area with no fire dynamics within the investigated period.

4.2.2 Shrub expansion and graminoid decline

Throughout the explored region forest tundra and shrub tundra increased in area from 13% in the early time-slice to 32% in the late time-slice (Appendix H, Table H1). This increase in vegetation biomass is also captured by the significant greening trend between 2002 and 2008 observed in our study area, interpreted as an increase in growing season NDVI (MODIS and AVHRR, in Guay et al., 2014) and increase in peak-summer MODIS NDVI from 2000 to 2018 (Appendix B).

We interpret the areal increase as expansion of the forest tundra and shrub tundra into areas formerly covered by graminoid tundra. The forest and shrub tundra class has an average shrub cover of 60%, which is much higher than the shrub cover in all other vegetation classes (Fig. 9). The main taxa contributing to shrubification are deciduous dwarf shrubs *Vaccinium vitis-idaea*, *Betula nana* (strong contribution only in tundra–taiga), *Ledum palustre* and *V. uliginosum* (tundra–taiga, northern taiga), *Empetrum nigrum* (stronger contribution in northern taiga, less strong in tundra–taiga), *Cassiope tetragona* and *Salix* spp. (minor contribution in both tundra–taiga and northern taiga) and *Alnus viridis* ssp. *fruticosa* (strong contribution only in tundra–taiga, Fig. 10).

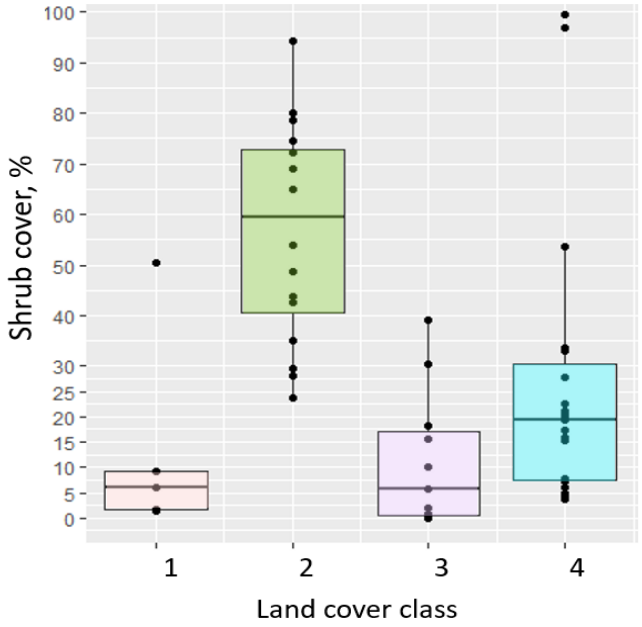

Figure 9. Foliage projective cover of the shrub portion in each of the four land-cover classes: (1) larch closed-canopy forest, (2) forest tundra and shrub tundra, (3) graminoid tundra and (4) prostrate herb tundra and barren areas. Shrubs (high, low and dwarf) include: *Alnus viridis* ssp. *fruticosa, Pinus pumila, Betula nana, Salix* spp., *Vaccinium vitis-idaea, V. uliginosum, Ledum palustre, Rosa* sp. and *Rhododendron adamsii.*

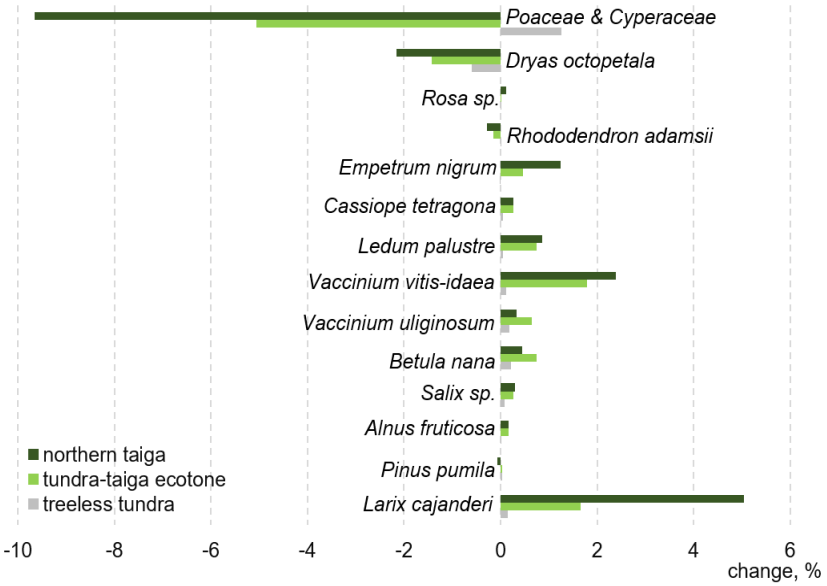

Figure 10. Average absolute foliage projective cover change (for the study period) in the northern taiga, tundra–taiga ecotone and treeless tundra areas for selected taxa based on their foliage projective cover contributions in each land-cover class.

The shrubification goes along with a significant decrease in the graminoid tundra class from an average of 60% in 2001 to 41% in 2016 throughout the explored region (Appendix H, Table H1). Dominant taxa of the graminoid tundra are Poaceae and Cyperaceae, which form 37% of the cover of this class, much higher than for other classes.

Myers-Smith et al. (2011) describe how shrub expansion in the tundra–taiga ecotone in recent years can be related to various environmental drivers including climate (earlier snowmelt alongside higher temperatures), natural disturbances (permafrost degradation, fire) and anthropogenic impact. Many studies report tall (mostly *Alnus*, rarely *Pinus pumila*), low and dwarf (*Salix*, *Betula*) shrub expansion all over the arctic region (Myers-Smith et al., 2011; Frost et al., 2014; Frost & Epstein, 2013; Tape et al., 2006; Sturm et al., 2001). Most of these studies investigate different and/or longer time periods or focus on local-scale changes (floodplains, river slopes etc.). The rates of shrubification in the central Chukotka mountainous area appear to be much lower than in the other studied circum-Arctic regions that represent lowland landscapes. We suspect that most of the shrubification in the tundra-taiga transition area in Chukotka could be related to climate changes, because anthropogenic impact is low except in the 16-KP-01 region, where road construction along Lake Ilirney is indicated as a decrease in vegetation cover (Fig.7).

Trends in the annual mean air temperature suggests an increase of 0.25–1°C per decade (1979–2009 years trend) in our study area, as well as a decrease in snow cover duration (1–2 days per decade, 1979–2009 years trend; Liston & Hiemstra, 2011). The increase in air temperature has caused

warming of permafrost in recent years (Biskaborn et al., 2019), which may also support a deepening of the active layer and thus can benefit plants with long root systems. According to Fyodorov-Davydov (2008), active-layer thickness significantly increased in eastern Siberia (Northern Yakutia)) from 1999 to 2006 by about 35–70 cm in typical tundra, 7 cm in the tundra–taiga ecotone and 13 cm in the northern taiga.

Despite modern climate conditions in the tundra–taiga ecotone being favourable for both shrub and forest expansion, at first, fast reproduction rates allow low and dwarf shrubs to rapidly colonise the area. These areas will be subsequently replaced by generally slower expanding forests (cf. Kharuk et al.; 2006; Montesano et al.; 2016; Wieczorek et al., 2017b; Kruse et al., 2019).

Overall, our findings of shrub expansion and decline of graminoid cover agree with modelling results. For example, a simulation experiment by Carlson et al. (2018) for the subarctic claims an increase in the abundance of deciduous shrubby *Salix* and a decline of the graminoid *Carex* under a warming treatment.

4.2.3 Stable treeless tundra

In contrast to the fast-changing northern taiga and tundra–taiga ecotone we observed a much slower change in the tundra. Even though there is only 40 km between 16-KP-01 (tundra–taiga) and 16-KP-04 (tundra), the tundra area stayed stable during the explored 15 years. However, we could detect shrub cover increase in river valleys that suggests favourable environmental conditions for shrub growth (nutrient availability, moisture, soil development, active layer depth, shelter against harsh wind). Valley shrubification is common for many arctic regions (e.g., Frost & Epstein, 2013; Naito & Cairns, 2014), but the rates of changes are much lower in Chukotkian tundra (16-KP-04).

Similarly, stable tundra, where shrub cover is represented by *Salix glauca, Betula nana* and *Vaccinium uliginosum,* has been reported for Disko Island in west Greenland (Callaghan et al., 2011). There have been few studies of Siberian tundra and many of these focus on areas of expected strong shrubification and treeline advance. Vegetation turnover might still be occurring but is hidden within our broad vegetation classes.

The circum-Arctic NDVI change supports our findings of weak greening in the Northern Chukotka tundra region, which contrasts greatly to the strong tundra greening trend on the North Slope in Alaska (Epstein et al., 2018).

Conclusions

We presented a land-cover classification and land-cover change over 15-years in the recent past from four areas of central Chukotka (eastern Siberia, Russia) ranging from northern taiga to treeless tundra. In our approach, foliage projective cover from vegetation plots is statistically related to Landsat spectral indices. The derived model was then used for classification of Landsat images which enabled us to detect 15-year changes in land-cover classes and interpret the magnitude and major taxonomical contributors of vegetation change.

Our analyses yielded that the class larch closed-canopy forest significantly increased only in the northern taiga where it was previously present at the landscape scale. Contrarily, we found no evidence of significant larch forest advance in the tundra–taiga ecotone. This led us to the conclusion that tree infilling behaviour rather than treeline advance characterises the study area.

We observed a strong increase of the forest tundra and shrub tundra class in northern taiga and tundra-taiga. Major contributors of shrubification are alder, dwarf birch and some species of the heather family. It is concomitant with a decrease in graminoid tundra which is consistent with a previous warming treatment experiment (Carlson et al., 2018).

We found that treeless tundra stayed rather stable within the investigated period, which contrasts with the strong tundra greening on the North Slope in Alaska (Epstein et al., 2018), but is similar to Disko Island in west Greenland (Callaghan et al., 2011).

Absolute rates of vegetation change across circum-Arctic studies are only partly comparable because of differences in methodological approaches and analysed time spans and would require a harmonised circum-Arctic approach in the future that numerically links field and remote-sensing data.

Acknowledgements

This study has been supported by the German Federal Ministry of Education and Research (BMBF), which enabled the Russian-German research programme “Kohlenstoff im Permafrost KoPf” (grant no. 03F0764A), by the Initiative and Networking Fund of the Helmholtz Association and by the ERC consolidator grant Glacial Legacy of Ulrike Herzschuh (grant no. 772852). Birgit Heim acknowledges funding by the Helmholtz Association Climate Initiative REKLIM. We thank our Russian and German colleagues from the joint German-Russian expedition “Keperveem 2016” for support in the field. Special thanks to Lena Popova for providing technical support with Landsat data preparation.

Data availability statement

The data that support the findings of this study are openly available via the following link https://doi.pangaea.de/10.1594/PANGAEA.908570 and cited in the references as Shevtsova et al. (2019).

References

ACIA 2005 Arctic Climate Impact Assessment. ACIA Overview report *Cambridge University Press* 1020 pp.

Beck P S A, Horning N, Goetz S J, Loranty M M and Tape K D 2011 Shrub cover on the North Slope of Alaska: a circa 2000 baseline map *Arctic, Antarctic, and Alpine Research* **43** 355–63 https://doi.org/10.1657/1938-4246-43.3.355

Bezdek J C 1981 Models for Pattern Recognition *Pattern Recognition with Fuzzy Objective Function Algorithms* 1–13 doi: 10.1007/978-1-4757-0450-1

Biskaborn, B K, Smith, S L, Noetzli, J et al 2019 Permafrost is warming at a global scale *Nature Commun*ications **10** 264 doi: 10.1038/s41467-018-08240-4

Boelman N T, Stieglitz M, Rueth H M, Sommerkorn M, Griffin K L, Shaver G R and Gamon J A 2003 Response of NDVI, biomass, and ecosystem gas exchange to long-term warming and fertilization in wet sedge tundra *Oecologia* **135** 414–21 doi: 10.1007/s00442-003-1198-3

Box J E, Colgan W E, Christensen T R, Schmidt N M, Lund M, Parmentier F-J W, Brown R, Bhatt U S, Euskirchen E S, Romanovsky V E, Walsh J E, Overland J E, Wang M, Corell R W, Meier W N, Wouters B, Mernild S, Mård J, Pawlak J and Olsen M S 2019 Key indicators of Arctic climate change: 1971–2017 *Environmental Research Letters* **14** 045010 doi: 10.1088/1748-9326/aafc1b

Bunn A G and Goetz S J 2006 Trends in satellite-observed circumpolar photosynthetic activity from 1982 to 2003: the influence of seasonality, cover type, and vegetation density *Earth Interactions* **10** 1–19 doi: 10.1175/EI190.1

Callaghan T V, Christensen, T R and Jantze, E J 2011 Plant and Vegetation Dynamics on Disko Island, West Greenland: Snapshots Separated by Over 40 Years *Ambio* **40** 624 doi: 10.1007/s13280-011-0169-x

Carlson L G, Beard K H, Adler P B 2018 Direct effects of warming increase woody plant abundance in a subarctic wetland *Ecology and Evolution* **8**(5) 2868-2879 doi: 10.1002/ece3.3902

Elmendorf S C, Henry G H R, Hollister R D et al. 2012 Plot-scale evidence of tundra vegetation change and links to recent summer warming *Nature Climate Change* **2** 453–7 doi: 10.1038/nclimate1465

Epstein H, Bhatt U, Raynolds M, Walker D, Forbes B C, Horstkotte T, Macias-Fauria M, Martin A, Phoenix G, Bjerke J, Tømmervik H, Fauchald P, Vickers H, Myneni R and Dickerson C 2018 Tundra Greenness *Arctic Report Card 2018* URL: https://www.arctic.noaa.gov/Report-Card

Forbes B C, Fauria M M and Zetterberg P 2010 Russian Arctic warming and 'greening' are closely tracked by tundra shrub willows *Global Change Biology* **16** 1542–54 doi: 10.1111/j.1365-2486.2009.02047.x

Frost G V, Epstein H E, Walker D A, Matyshak G and Ermokhina K 2013 Patterned-ground facilitates shrub expansion in Low Arctic tundra *Environmental Research Letters* **8** 015035 doi: 10.1088/1748-9326/8/1/015035

Frost G V and Epstein H E 2013 Tall shrub and tree expansion in Siberian low Arctic ecotones since the 1960s *Global Change Biology* **20** 1264–77 doi: 10.1111/gcb.12406

Frost G V, Epstein H E and Walker D A 2014 Regional and landscape-scale variability of Landsat-observed vegetation dynamics in northwest Siberian tundra *Environmental Research Letters* **9** 025004 doi: 10.1088/1748-9326/9/2/025004

Fyodorov-Davydov D, Kholodov A, Ostroumov V, Kraev G, Sorokovikov V, Davydov S and Merekalova A 2008 Seasonal Thaw of Soils in the North Yakutian Ecosystems, in *9th International conference on permafrost proceedings* vol 1, edited by D L Kane and K M Hinkel (Institute of Northern Engineering, University of Alaska Fairbanks) 481–486

Givnish TJ 2002 Adaptive significance of evergreen vs. deciduous leaves: solving the triple paradox *Silva Fennica* **36**(3) 703–743 doi: 10.14214/sf.535

Guay K C, Beck P S A, Berner L T, Goetz S J, Baccini A and Buermann W 2014 Vegetation productivity patterns at high northern latitudes: a multi-sensor satellite data assessment *Global Change Biology* **20** 3147–58 doi: 10.1111/gcb.12647

Jia G J, Epstein H E and Walker D A 2003 Greening of arctic Alaska 1981–2001 *Geophysical Research Letters* **30** 2067 doi: 10.1029/2003GL018268

Jia G J, Epstein H E and Walker D A 2009 Vegetation greening in the Canadian Arctic related to decadal warming *Journal of Environmental Monitoring* **11** 2231 doi: 10.1039/B911677J

Kharuk V I, Ranson, K J, Im S T and Naurzbaev M M 2006 Forest-tundra larch forests and climatic trends *Russian Journal of Ecology* **37** 291–298 doi: 10.1134/S1067413606050018

Kolk H-J V D, Heijmans M M P D, Huissteden J V, Pullens J W M and Berendse F 2016 Potential Arctic tundra vegetation shifts in response to changing temperature, precipitation and permafrost thaw *Biogeosciences* **13** 6229–45 doi: 10.5194/bg-13-6229-2016

Kruse S and Stoof-Leichsenring K R 2016 *Keperveem* - Past and present vegetation dynamics at the most eastern extension of the Siberian boreal treeline, in Russian-German Cooperation: Expeditions to Siberia in 2016, edited by P. P. Overduin, F. Blender, D. Y. Bolshiyanov, M. N. Grigoriev, A. Morgenstern and H. Meyer (Bremerhaven: Alfred-Wegener-Institut, Helmholtz-Zentrum für Polar- und Meeresforschung) doi:10.2312/BzPM_0709_2017

Kruse S, Gerdes A, Kath N J, Epp L S, Stoof-Leichsenring, K R, Pestryakova L A and Herzschuh U 2019a Dispersal distances and migration rates at the arctic treeline in Siberia – a genetic and simulation-based study *Biogeosciences* **16**, 1211-1224 doi: 10.5194/bg-16-1211-2019

Kruse S, Bolshiyanov D, Grigoriev M N, Morgenstern A, Pestryakova, L, Tsibizov L and Udke, A 2019b Russian-German Cooperation: Expeditions to Siberia in 2018 *Reports on Polar and Marine Research [Berichte Zur Polar-Und Meeresforschung]* **734** doi: 10.2312/BzPM_0734_2019

Lantz T C, Gergel S E and Henry G H R 2010 Response of green alder (*Alnus viridis* subsp. *fruticosa*) patch dynamics and plant community composition to fire and regional temperature in north-western Canada *Journal of Biogeography* **37**(8) 1597–1610 doi:10.1111/j.1365-2699.2010.02317.x

Lara M J, Nitze I, Grosse G and Mcguire A D 2018 Tundra landform and vegetation productivity trend maps for the Arctic Coastal Plain of northern Alaska *Scientific Data* **5** 180058 doi: 10.1038/sdata.2018.58

Legendre P and Legendre L 2012 *Numerical ecology,* 3rd English edition (Amsterdam: Elsevier)

Lin D H, Johnson D R, Andresen C and Tweedie C E 2012 *Environmental Research Letters* **7** 025502 doi: 10.1088/1748-9326/7/2/025502

Liston G E and Hiemstra CA 2011 The Changing Cryosphere: Pan-Arctic Snow Trends (1979–2009) *Climate* **24** 5691–5712 doi: 10.1175/JCLI-D-11-00081.1

Martínez I, Wiegand T, Camarero J J, Batllori E and Gutiérrez E 2011 Disentangling the formation of contrasting tree-line physiognomies combining model selection and Bayesian parameterization for simulation models *The American Naturalist* **177**(5) E136–E152 doi:10.1086/659623

Menne M J, Durre I, Korzeniewski B, McNeal S, Thomas K, Yin X, Anthony S, Ray R, Vose R S,.Gleason B E and Houston T G 2012 *Global Historical Climatology Network - Daily (GHCN-Daily), Version 3 NOAA National Climatic Data Center* doi:10.7289/V5D21VHZ

Moffat N D, Lantz T C, Fraser R H and Olthof I 2016 Recent Vegetation Change (1980–2013) in the Tundra Ecosystems of the Tuktoyaktuk Coastlands, NWT, Canada *Arctic, Antarctic, and Alpine Research* **48** 581–97 doi: 10.1657/AAAR0015-063

Montesano, PM, Sun, G, Dubayah, RO and Ranson, K J 2016 Spaceborne potential for examining taiga–tundra ecotone form and vulnerability *Biogeosciences* **13** 3847–3861 doi: 10.5194/bg-13-3847-2016

Mróz M and Sobieraj A 2004 Comparison of several vegetation indices calculated on the basis of a seasonal SPOT XS time series, and their suitability for land cover and agricultural crop identification *Technical Sciences* **7**

Myers-Smith I H, Forbes B C, Wilmking M et al. 2011 Shrub expansion in tundra ecosystems: dynamics, impacts and research priorities. *Environmental Research Letters* **6** 045509 doi: 10.1088/1748-9326/6/4/045509

Myers-Smith I H, Kerby J T, Phoenix G K et al. 2020 Complexity revealed in the greening of the Arctic *Nature Climate Change* **10** 106–117 doi: 10.1038/s41558-019-0688-1

Naito A T and Cairns D M 2014 Patterns of shrub expansion in Alaskan arctic river corridors suggest phase transition *Ecology and Evolution* **5** 87–101 doi: 10.1002/ece3.1341

Overland J E, Wang M, Walsh J E, Stroeve J S 2014 Future arctic climate changes: Adaptation and mitigation time scales *Earths Future* **2** 68–74 doi: 10.1002/2013EF000162

Riano D, Chuvieco E, Salas J and Aguado I 2003 Assessment of different topographic corrections in Landsat-TM data for mapping vegetation types (2003) *IEEE Transactions on Geoscience and Remote Sensing* **41** 1056–61 doi: 10.1109/TGRS.2003.811693

Roy D P, Kovalskyy V, Zhang H K, Vermote E F, Yan L, Kumar S S and Egorov A 2016 Characterization of Landsat-7 to Landsat-8 reflective wavelength and normalized difference vegetation index continuity *Remote Sensing of Environment* **185** 57–70 doi: 10.1016/j.rse.2015.12.024

Shevtsova I, Herzschuh U, Heim B, Kruse S, Schröder J, Troeva, E I, Pestryakova, L A and Zakharov E S 2019 Foliage projective cover of 57 vegetation sites of central Chukotka from 2016 Alfred Wegener Institute - Research Unit Potsdam PANGAEA https://doi.pangaea.de/10.1594/PANGAEA.908570

Sturm M, Racine C H and Tape K D 2001 Increasing shrub abundance in the Arctic *Nature* **411** 546–7 doi: 10.1038/35079180

Tape K, Sturm M and Racine C 2006 The evidence for shrub expansion in Northern Alaska and the Pan-Arctic *Global Change Biology* **12** 686–702 doi: 10.1111/j.1365-2486.2006.01128.x

Tachikawa T, Hato M, Kaku M and Iwasaki A 2011 Characteristics of ASTER GDEM version 2 *2011 IEEE International Geoscience and Remote Sensing Symposium* (Vancouver, BC) 3657–3660

doi: 10.1109/IGARSS.2011.6050017

Tibshirani R, Walther G and Hastie T 2001 Estimating the number of clusters in a data set via the gap statistic *Journal of the Royal Statistical Society: Series B (Statistical Methodology)* **63** 411–23 doi: 10.1111/1467-9868.00293

Tucker C J 1979 Red and photographic infrared linear combinations for monitoring vegetation *Remote Sensing of Environment* **8** 127–50 doi:10.1016/0034-4257(79)90013-0

United States Geological Survey USGS 2019a Landsat 4-7 surface reflectance (LEDAPS) product guide: version 2.0 accessed at https://prd-wret.s3.us-west-2.amazonaws.com/assets/palladium/production/atoms/files/LSDS-1370_L4-7_SurfaceReflectance-LEDAPS_ProductGuide-v2.pdf

United States Geological Survey USGS 2019b Landsat 8 surface reflectance code (LASRC) product guide: version 2.0 accessed at https://prd-wret.s3-us-west-2.amazonaws.com/assets/palladium/production/atoms/files/LSDS-1368_L8_SurfaceReflectanceCode-LASRC_ProductGuide-v2.pdf

Valovcin F R 1976 *Snow/cloud discrimination* (Hanscom AFB, MA: Meteorology Division, Air Force Geophysics)

Walker M D, Wahren C H, Hollister R D et al. 2006 Plant community responses to experimental warming across the tundra biome *Proceedings of the National Academy of Sciences* **103** 1342–6 doi: 10.1073/pnas.0503198103

Walker M D, Daniëls F JA, Matveyeva N V et al. 2017 Circumpolar Arctic Vegetation Classification *Phytocoenologia* **48** (2) 181-201 doi: 10.1127/phyto/2017/0192

Wieczorek M, Kolmogorov A, Kruse S, Jacobsen I, Nitze I, Nikolaev A, Heinrich I, Pestryakova L and Herzschuh U 2017a Disturbance-effects on treeline larch-stands in the lower Kolyma River area (NE Siberia) *Silva Fennica* **51**(3) 1666 doi: 10.14214/sf.1666

Wieczorek, M, Kruse, S, Epp L S, Kolmogorov A, Nikolaev A N, Heinrich I, Jeltsch, F, Pestryakova, L A, Zibulski, R and Herzschuh U 2017b Dissimilar responses of larch stands in northern Siberia to increasing temperatures- a field and simulation based study *Ecology* **98** 2343–2355 doi 10.1002/ecy.1887

Xue B L, Kumagai T, Iida S, Nakai T, Matsumoto K, Komatsu H, et al. 2011 Influences of canopy structure and physiological traits on flux partitioning between understory and overstory in an eastern Siberian boreal larch forest *Ecological Modelling Elsevier* B.V **222**: 1479–1490 doi: 10.1016/j.ecolmodel.2011.01.021

Zeng H, Jia G and Epstein H 2011 Recent changes in phenology over the northern high latitudes detected from multi-satellite data Environmental Research Letters **6** 045508 https://doi.org/10.1088/1748-9326/6/4/045508

Zhang W, Miller P, Smith B, Wania R, Koenigk T and Döscher, R 2013 Tundra shrubification and tree-line advance amplify arctic climate warming: Results from an individual-based dynamic vegetation model *Environmental Research Letters* **8** 034023 doi: 10.1088/1748-9326/8/3/034023

Appendix A. Detailed description of Landsat acquisitions

Here we describe in detail the Landsat data used for retrieving the Normalised Difference Vegetation Index (NDVI), Normalised Difference Water Index (NDWI) and Normalised Difference Snow Index (NDSI). NDVI and NDWI were retrieved from peak-summer acquisitions and NDSI from snow-covered acquisitions. The pixel size of each Landsat image is 30×30m. Before indices calculation the Landsat data was topographically corrected. The subsets that we used for land-cover classification were cloud free and cloud-shadow free. Additionally, we masked all water bodies. Latdsat-8 data were transformed to Landsat-7-like (see section 1.2 Landsat data, pre-processing and spectral indices processing).

Table A1. Dates and short description of Landsat data used for retrieving spectral indices and further land-cover classification.

Focus area	Landsat acquisition			Short description (season/ Landsat mission/ spatial resolution)
	year	Month	day	
16-KP-01	2001	7	30	peak-summer, Landsat-7, 30 m
	2001	3	24	snow-covered, Landsat-7, 30 m
	2016	7	31	peak-summer, Landsat-8, 30 m
	2016	3	16	snow-covered, Landsat-8, 30 m
16-KP-02	2000	8	8	peak-summer, Landsat-7, 30 m
	2001	3	22	snow-covered, Landsat-7, 30 m
	2016	8	12	peak-summer, Landsat-8, 30 m
	2016	3	5	snow-covered, Landsat-8, 30 m
16-KP-03	2001	7	30	peak-summer, Landsat-7, 30 m
	2001	3	24	snow-covered, Landsat-7, 30 m
	2016	7	31	peak-summer, Landsat-8, 30 m
	2016	3	16	snow-covered, Landsat-8, 30 m
16-KP-04	2002	8	9	peak-summer, Landsat-7, 30 m
	2001	3	24	snow-covered, Landsat-7, 30 m
	2017	8	10	peak-summer, Landsat-8, 30 m
	2016	3	16	snow-covered, Landsat-8, 30 m

Appendix B. MODIS NDVI time series from 2000 to 2018

The Landsat archive had very few cloud-free peak-summer acquisitions for our study area between 2000 and 2018, so we could not calculate a consistent trend over the full period. Therefore, we selected the two most distant time steps with available data. We analysed continuous land-cover change using MODIS NDVI data. We used 16-day MODIS MOD13Q1 NDVI time-series data averaged for the period from July 12th to August 11th, with a spatial resolution of 250 m, calculated as mean NDVI value from the areal extent of each of the four Landsat subsets of the focus areas for every year from 2000 to 2018. As we see in the Fig. B1 the MODIS peak-summer NDVI time series do show an overall increase from 2000 to 2018. In general, regardless of extreme years such as low NDVI in 2013, the selected years of 2000, 2001, 2002, as well as 2016 and 2017 are representative years for vegetation change.

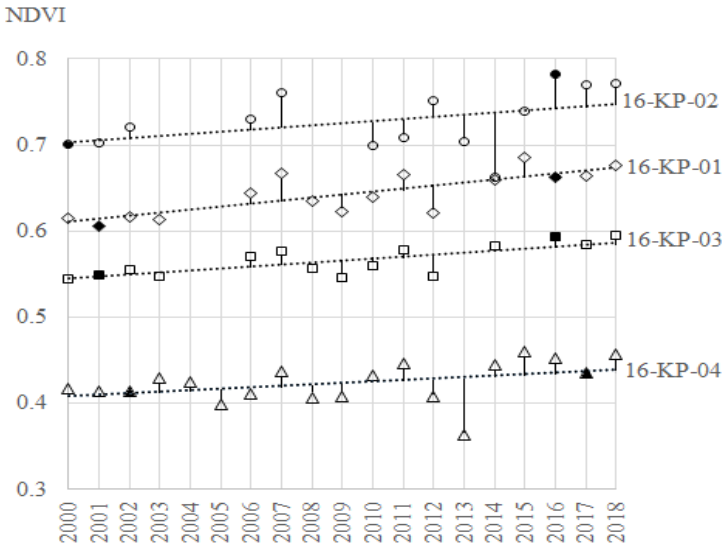

Figure B1. The selected years (black-filled symbols) used in vegetation change analysis are representative for the general vegetation trend indicated by peak-summer 16-days MODIS MOD13Q1 NDVI time-series.

Appendix C. Landsat Indices values for each analysed vegetation site

The Landsat spectral Indices which were calculated from acquisitions in summer:

Normalised Difference Vegetation Index, $NDVI = (NIR - RED)/(NIR + RED)$,

Normalised Difference Water Index, $NDWI = (GREEN - NIR)/(GREEN + NIR)$,

and from acquisitions in March:

Normalised Difference Snow Index, $NDSI = (GREEN - SWIR1)/(GREEN + SWIR1)$.

Table C1. Indices used in the model-building at each site. (NDVI: Normalised Difference Vegetation Index, NDWI: Normalised Difference Water Index, NDSI: Normalised Difference Snow Index)

Site \ Index	NDVI	NDWI	NDSI	Site \ Index	NDVI	NDWI	NDSI
V01	0.72	-0.64	0.88	V42	0.43	-0.48	0.69
V02	0.64	-0.60	0.91	V43	0.37	-0.41	0.73
V03	0.70	-0.63	0.90	V44	0.34	-0.40	0.58
V04	0.77	-0.67	0.81	V45	0.59	-0.56	0.74
V05	0.74	-0.66	0.88	V46	0.63	-0.61	0.73
V06	0.67	-0.61	1.00	V47	0.65	-0.63	0.69
V07	0.33	-0.36	0.87	V48	0.63	-0.63	0.74
V08	0.45	-0.48	0.94	V49	0.61	-0.61	0.73
V09	0.68	-0.63	0.82	V50	0.49	-0.51	0.63
V10	0.74	-0.66	0.70	V51	0.35	-0.40	0.69
V11	0.57	-0.56	1.00	V54	0.28	-0.33	0.76
V12	0.68	-0.63	0.73	V57	0.51	-0.53	0.96
V13	0.75	-0.63	-0.06	V58	0.59	-0.60	0.80
V14	0.75	-0.64	0.86	V29	0.62	-0.59	0.79
V15	0.70	-0.61	0.80	V30	0.64	-0.61	0.85
V16	0.73	-0.64	0.70	V31	0.67	-0.62	0.83
V18	0.74	-0.62	0.14	V32	0.60	-0.58	0.81
V19	0.76	-0.65	0.51	V33	0.67	-0.63	0.75
V20	0.72	-0.65	0.77	V34	0.78	-0.69	0.78
V21	0.72	-0.66	0.73	V35	0.74	-0.65	0.82
V22	0.70	-0.65	0.75	V36	0.58	-0.57	0.78
V23	0.66	-0.63	0.72	V37	0.76	-0.64	0.57
V25	0.28	-0.33	0.72	V38	0.77	-0.64	0.50
V26	0.62	-0.61	0.83	V39	0.76	-0.68	0.79
V27	0.74	-0.63	0.82	V40	0.40	-0.43	0.77
V28	0.71	-0.64	0.74	V41	0.42	-0.46	0.72

Appendix D. Fuzzy *c*-means classification for interpretation of uncertainties for land-cover mapping

Fuzzy *c*-means (FCM) classification results with a threshold set to 0.6 (Fig. D1) gave six sites (10%) out of the 52 field sites that remained unclassified and fell into the uncertainty class. These are the sites with the most mixed vegetation. The majority of the field data (90%) is strongly associated with one of the four land-cover classes. The classes are similar to *k*-means results (Appendix F) but given as probabilities.

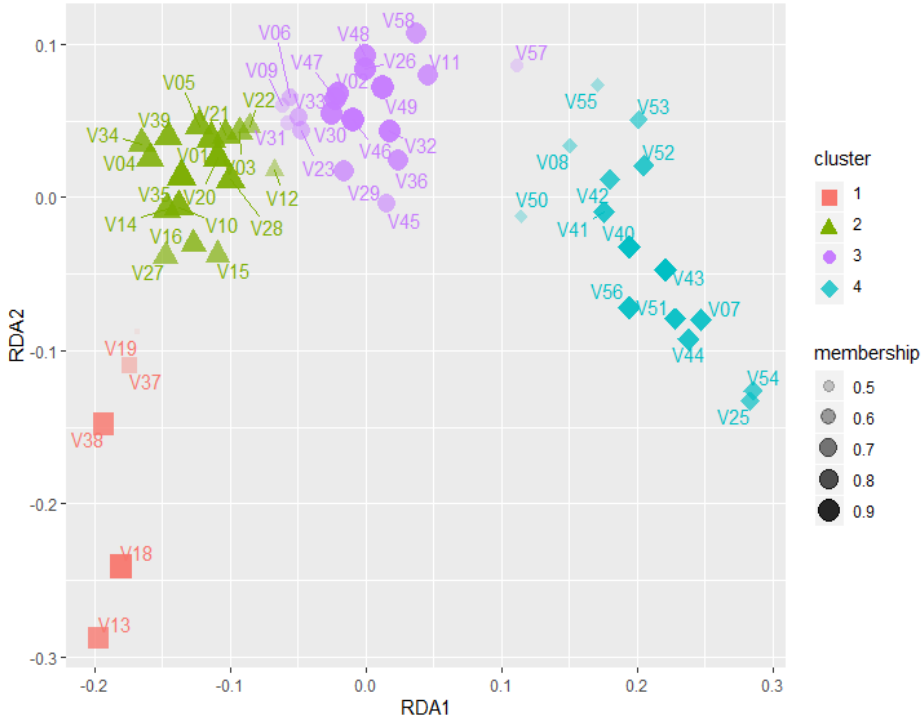

Figure D1. Results of FCM classification on 2 RDA-axes using NDVI, NDWI and NDSI as predictors. Cluster description (represented by different colours): (1) larch closed-canopy forest, (2) forest tundra and shrub tundra, (3) graminoid tundra and (4) prostrate herb tundra and barren areas. Membership is presented as the proportion of a site that belongs to a certain class.

The mapped FCM classification is useful to understand which portion of the land surface does not belong to one of the four classes defined by hard *k*-means classification but instead stays unclassified. About 30% of the land surface in the study area remains unclassified by FCM: these are (1) types not represented by field data (high mountains, wetlands) and (2) transitional open-forest tundra zones.

In the mountainous parts, uncertainties mostly occur in high-elevation areas with extreme values of spectral reflectance (16-KP-04, 16-KP-03, Fig. D2). These land surfaces fall outside the established classes because no field data were sampled there. In the *k*-means classification (Appendix F) these areas are included in the prostrate herb tundra and barren areas class.

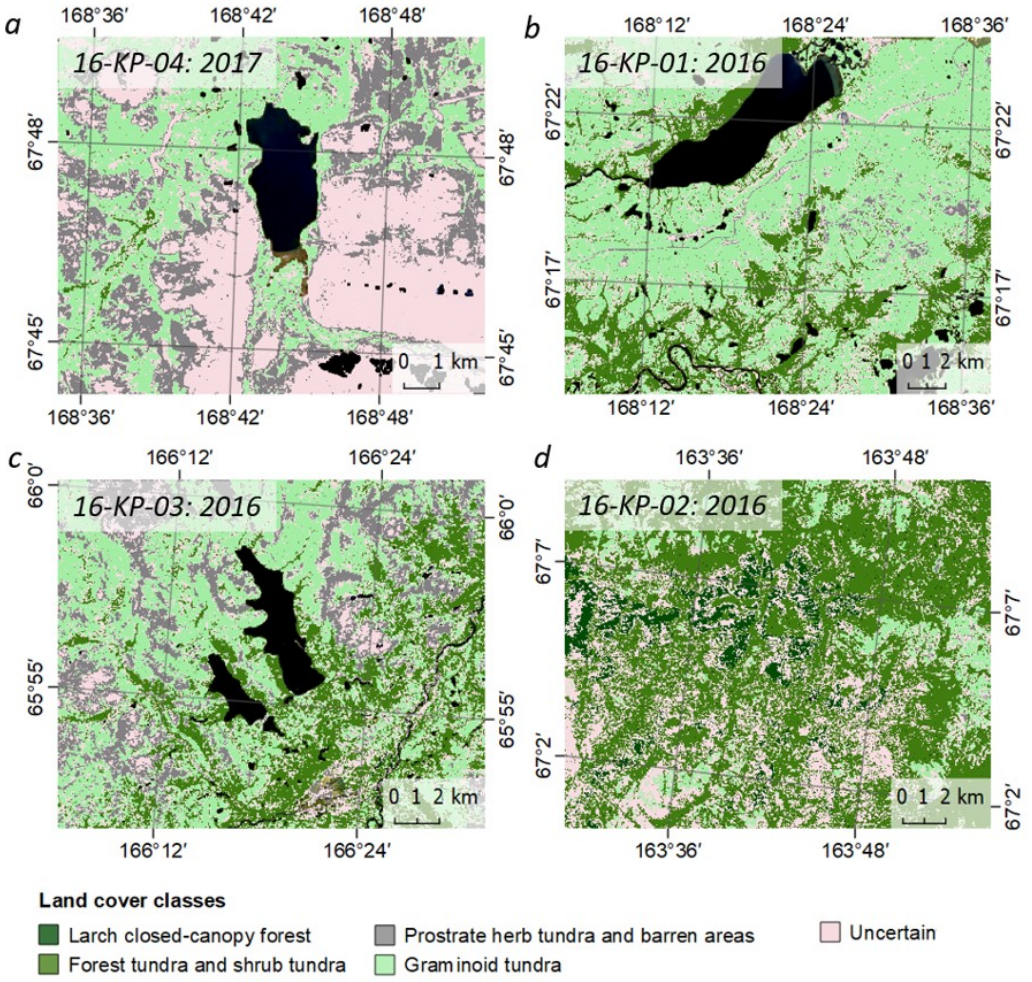

Figure D2. Colour-coded land-cover classes from *c*-means classification with a threshold of 0.6 and uncertainty for which membership for each class was lower than 0.6: a) 16-KP-04, 2017, uncertain is 44%; b) 16-KP-01, 2016, uncertain is 20%; c) 16-KP-03, 2016, uncertain is 24%; d) 16-KP-02, 2016, uncertain is 42%.

Transition areas between grass-dominant and shrub-dominant vegetation types as well as between open and forest tundra are responsible for much of the uncertainty (16-KP-01, 16-KP-03, Fig. D2). In the *k*-means results these areas are represented by both graminoid tundra and forest and shrub tundra.

In the northern taiga (16-KP-02, Fig. D2) more area was classified as uncertain: mostly formerly burnt areas and wetlands. Pioneer vegetation that occupied the burned areas in the first decades comprises highly abandant foliar *Alnus viridis* shrubs (Lantz, 2010) and dense green understorey which are difficult to separate from other vegetation groups using remote-sensing information as it just captures high-biomass green vegetation. These areas belong to larch closed-canopy forest or forest tundra and shrub tundra in the *k*-means classification. Wetlands are characteristic of river floodplains and were not surveyed in the field and therefore fall mostly under uncertain. They are mostly represented as forest tundra and shrub tundra with some patches of larch closed-canopy forest in the *k*-means classification.

Appendix E. Validation of land-cover maps

We validated the derived land-cover maps with new field data from the expedition "Chukotka 2018" (Kruse et al., 2019b), that revisited the regions 16-KP-01 (tundra-taiga transition, 27 sites) and 16-KP-04 (tundra, 5 sites). In 2018, we did not collect field data from northern taiga, so it was not possible to validate closed-canopy forest class with this approach. We used almost the same sampling scheme during both expeditions in 2016 and 2018. Tree and tall-shrub (>100cm) cover was estimated the same way. The difference was only in the placement of the 2×2m subplots for low-shrub and ground vegetation estimation. We used a 15 m-radius at each plot but in 2018, rather than systematic placement of the subplots in the cardinal directions and the centre, we placed three subplots into each of the differentiated three major vegetation classes (e.g. lichen-dominant communities, low-shrub tundra communities with *Vaccinium* spp. dominance etc.). We estimated foliage projective cover for the ground layer taxa and averaged, first, across vegetation pattern and, second, across the whole 15-m radius circular plot using the estimated proportions of vegetation classes within it. With this, we can ensure the direct comparison between the foliage projective cover data from both expeditions.

Table E1. Number of sites predicted into four land-cover classes using two different origins of RDA-scores: foliage projective cover (columns) and Landsat spectral Indices (rows).

		Class predicted from foliage projective cover data			
		Larch closed-canopy forest	Forest tundra and shrub tundra	Graminoid tundra	Prostrate herb tundra and barren areas
Class predicted from Landsat spectral Indices	Larch closed-canopy forest	0	0	0	0
	Forest tundra and shrub tundra	2	7	1	0
	Graminoid tundra	0	2	13	6
	Prostrate herb tundra and barren areas	0	0	0	1

To validate the land-cover maps, we projected the new field data from 2018, as well as corresponding Landsat spectral indices data, into the ordination space we previously created. Predicted classes were similar for the majority of 21 plots (66%, Table E1). Two sites were misclassified as larch closed-canopy forest in the foliage projective cover data due to high larch cover (up to 20%), whereas they were correctly classified into the class forest tundra and shrub tundra by Landsat spectral data. Only three plots were differently classified as graminoid tundra or forest tundra and shrub tundra and vice versa. These are characterised by mixed typical vegetation, which can hardly be distinguished by the applied classifiers. While the predicted vegetation class based on the foliage projective cover data was correctly assigned to prostate and herb tundra: the Landsat spectral indices misclassified the majority (6 of 7) of open tundra communities dominated by *Dryas octopetala* and *Cassiope tertragona* into graminoid tundra.

Therefore, one needs to interpret changes between these two classes with caution. However, we did not find big changes between graminoid tundra and prostrate herb tundra in tundra-taiga or tundra zones. In addition, considering systematic overestimation of graminoid tundra in both compared years compensates for the errors of misclassification.

Appendix F. *K*-means classification results

The results of *k*-means classification for our four focus areas giving four dominant land-cover classes at two time slices (ordered from treeless tundra via tundra–taiga transition to northern taiga zone: Fig. F1, F2, F3, F4)

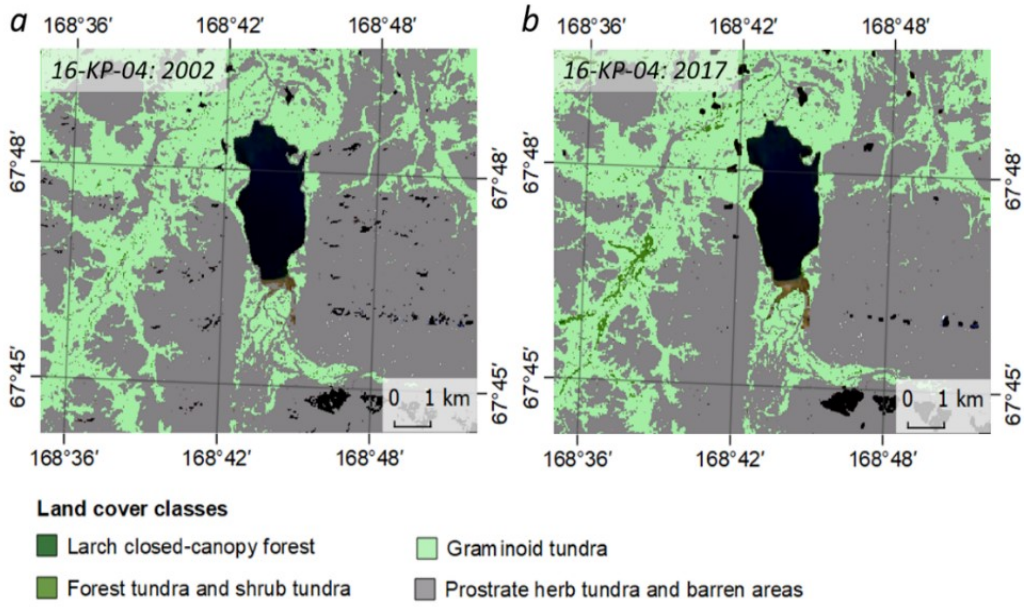

Figure F1. Colour-coded land-cover classes of 16-KP-04 (treeless tundra): a) for 2002, where dominant classes are prostrate herb tundra and barren areas (63%) and graminoid tundra (36%); b) for 2017, where dominant classes are also prostrate herb tundra and barren areas (59%) and graminoid tundra (39%). The forest tundra and shrub tundra class appears here at a very low proportion (1%).

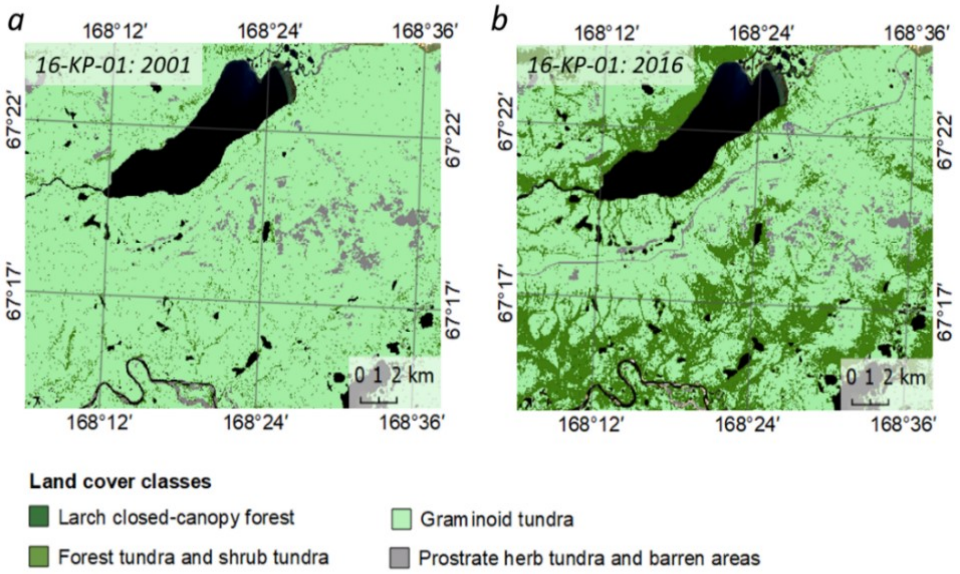

Figure F2. Colour-coded land-cover classes of 16-KP-01 (northern border of tundra–taiga ecotone): a) for 2001, where the dominant class is graminoid tundra (92%), while prostrate herb tundra and barren areas occurred in the hilly areas (5%) and forest tundra and shrub tundra is sparsely distributed in the valleys and gentle slopes (3%); b) for 2016, where the dominant classes are graminoid tundra (69%) and forest tundra and shrub tundra (27%) distributed in the valleys and gentle slopes. The prostrate herb tundra and barren areas class (3%) is still found in the hilly areas but now also includes road construction.

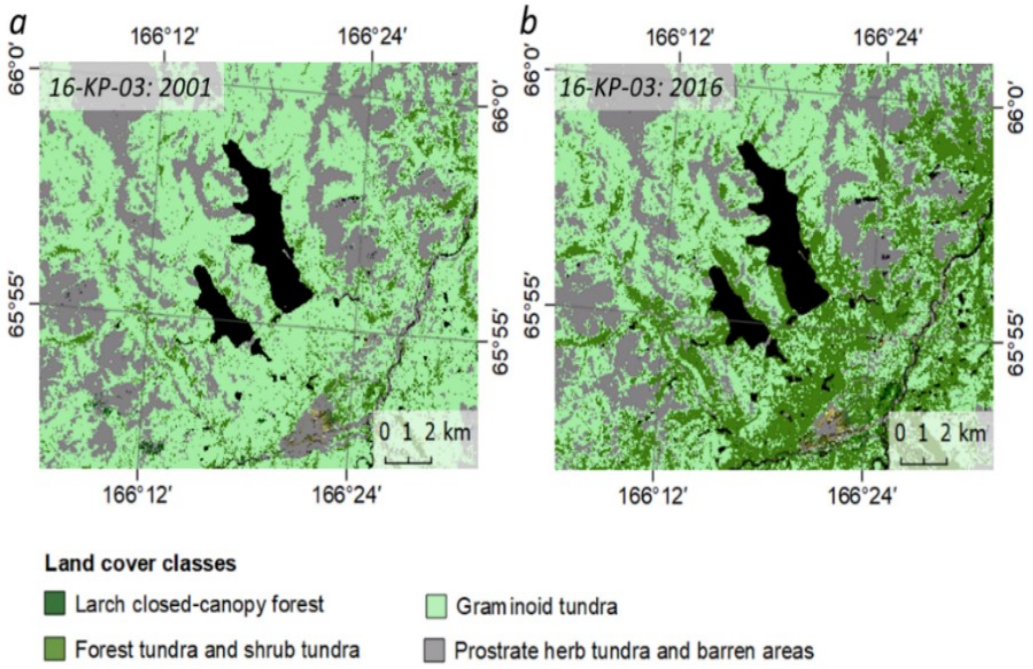

Figure F3. Colour-coded land-cover classes of 16-KP-03 (southern border of tundra–taiga ecotone): a) for 2001, where dominant classes are graminoid tundra (57%) and prostrate herb tundra and barren areas (34%). Forest tundra and shrub tundra occurs along the waterways and on the gentle slopes of the lakes (8%); b) for 2016, where the dominant classes are graminoid tundra (42%), forest tundra and shrub tundra (28%) and prostrate herb tundra and barren areas (29%). Larch closed-canopy forest (<1%) can barely be seen as patches along the river.

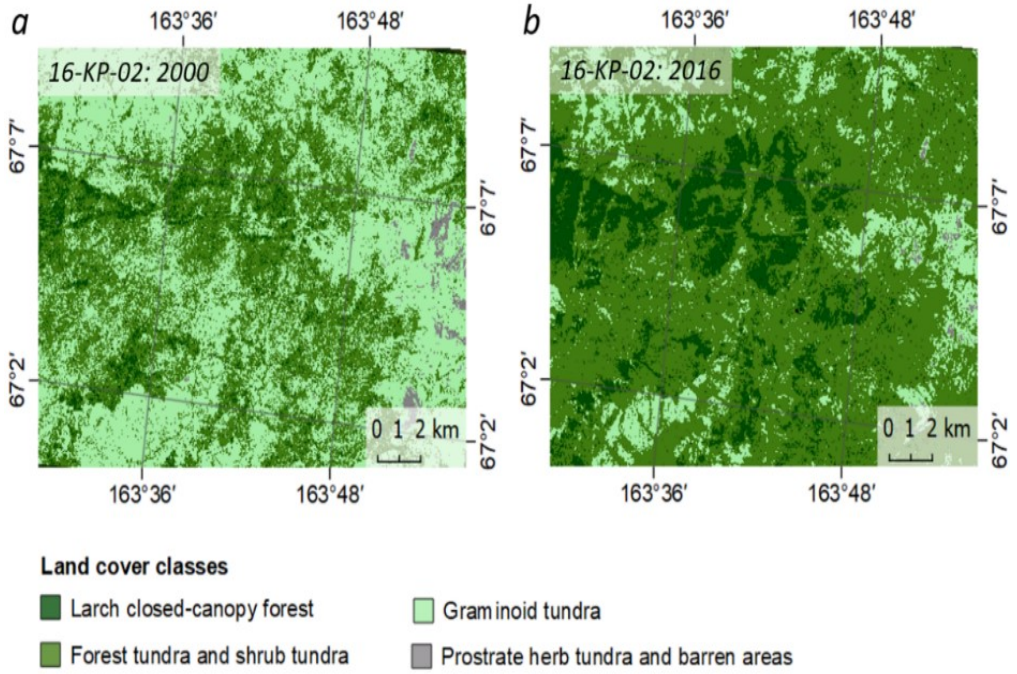

Figure F4. Colour-coded land-cover classes of 16-KP-02 (northern taiga): a) for 2000, where the dominant classes are graminoid tundra (55%) and forest tundra and shrub tundra (39%). To the east one can see a mountain complex where graminoid tundra turns into prostrate herb tundra and barren areas (1%). Larch closed-canopy forest (5%) is better represented in this area than in the other explored areas; b) for 2016, where the dominant classes are forest tundra and shrub tundra (69%), graminoid tundra (17%) and larch closed-canopy forest (13%). The prostrate herb tundra and barren areas class is poorly represented (<1%).

Appendix G. Heterogeneity of natural landscapes and mixed pixels of satellite data

Figure G1. At site V26 (16-KP-03) the lichen understorey significantly lowers the most important vegetation index (NDVI) compared with other tree-covered areas with grass or shrub understorey. While having high percentages of green healthy tree cover, the understorey is mostly covered with highly red-reflecting lichens (and green-reflecting *Larix cajanderi* needles) (360x180 degree panoramic image, Stefan Kruse).

Figure G2. Despite the dense healthy-green *Pinus pumila* patches at site V23 (16-KP-03), a great proportion of the area around is covered by far less green lichen communities. These cause a significant increase in red reflectance which results in lower NDVI values for the 30x30m pixel size (360x180 degree panoramic image, Stefan Kruse).

Appendix H. Distribution of land-cover classes and their changes by study area

Table H1. Distribution of land-cover classes and their changes by study area given in %.

Area	Year	Proportion of land-cover class [%]			
		Larch closed-canopy forest	Forest tundra and shrub tundra	Graminoid tundra	Prostrate herb tundra and barren areas
16-KP-04	2002	0.10	0.24	32.49	67.17
	2017	0.08	1.12	35.70	63.10
	change 2017-2002	-0.02	0.88	3.21	-4.07
16-KP-01	2001	0.04	2.76	93.23	3.96
	2016	0.20	27.49	69.08	3.23
	change 2016-2001	0.16	24.72	-24.15	-0.74
16-KP-03	2001	0.63	7.87	58.70	32.80
	2016	0.39	28.73	42.31	28.57
	change 2016-2001	-0.23	20.86	-16.39	-4.24
16-KP-02	2000	4.02	39.63	54.74	1.60
	2016	12.35	70.99	16.15	0.51
	change 2016-2000	8.32	31.36	-38.59	-1.09

Table H2. Distribution of land-cover classes and their changes by study area given in km^2.

Area	year	Portion of land-cover class [km^2]			
		Larch closed-canopy forest	Forest tundra and shrub tundra	Graminoid tundra	Prostrate herb tundra and barren areas
	2002	0.17	12.08	17.33	407.5
16-KP-04	2017	0.89	120.14	14.1	301.94
	change 2017-2002	0.72	108.05	-3.22	-105.55
	2001	4.51	56.71	236.43	423.06
16-KP-01	2016	2.82	207.04	205.89	304.97
	change 2016-2001	-1.69	150.33	-30.54	-118.1
	2001	0.12	0.29	81.13	39.24
16-KP-03	2016	0.09	1.35	76.21	43.12
	change 2016-2001	-0.03	1.07	-4.92	3.88
	2000	12.63	124.45	5.03	171.87
16-KP-02	2016	38.76	222.9	1.61	50.71
	change 2016-2000	26.13	98.46	-3.42	-121.17

5 Recent above-ground biomass changes in central Chukotka (NE Siberia) combining field-sampling and remote sensing

Iuliia Shevtsova[1,2], Ulrike Herzschuh[1,2,3], Birgit Heim[1], Luise Schulte[1,2], Simone Stünzi[1,6], Luidmila A. Pestryakova[4], Evgeniy S. Zakharov[4,5], and Stefan Kruse[1]

[1]Polar Terrestrial Environmental Systems, Alfred Wegener Institute (AWI), Helmholtz Centre for Polar and Marine Research, Potsdam, 14473, Germany
[2]Institute of Biochemistry and Biology, University of Potsdam, Potsdam, 14476, Germany
[3]Institute of Environmental Sciences and Geography, University of Potsdam, Potsdam, 14476, Germany
[4]Institute of Natural Sciences, North-Eastern Federal University of Yakutsk, Yakutsk, 677000, Russia
[5]Institute for Biological Problems of the Cryolithozone, Russian Academy of Sciences, Siberian branch, Yakutsk, 677000, Russia
[6]Geography Department, Humboldt-Universität zu Berlin, Unter den Linden 6, 10099, Berlin, Germany

Correspondence to: Iuliia Shevtsova (iuliia.shevtsova@awi.de), Stefan Kruse (stefan.kruse@awi.de)

Abstract

Upscaling plant biomass distribution and dynamics is essential for estimating carbon stocks and carbon balance. In this respect, the Russian Far East is among the least investigated sub-Arctic regions despite its known vegetation sensitivity to ongoing warming. We representatively harvested above-ground biomass (AGB; separated by dominant taxa) at 40 sampling plots in central Chukotka. We used ordination to relate field-based taxa projective cover and Landsat-derived vegetation indices. A general additive model was used to link the ordination scores to AGB. We then mapped AGB for paired Landsat-derived time slices (i.e., 2000/2001/2002 and 2016/2017), in four study regions covering a wide vegetation gradient from closed-canopy larch forests to barren alpine tundra. We provide AGB estimates and changes in AGB that were previously lacking for central Chukotka at a high spatial resolution and a detailed description of taxonomical contributions. Generally, AGB in the study region ranges from 0 to 16 kg m−2, with Cajander larch providing the highest contribution. Comparison of changes in AGB within the investigated period shows that the greatest changes (up to 1.25 kg m−2 yr−1) occurred in the northern taiga and in areas where land cover changed to larch closed-canopy forest. As well as the notable changes, increases in AGB also occur within the land-cover classes. Our estimations indicate a general increase in total AGB throughout the investigated tundra–taiga and northern taiga, whereas the tundra showed no evidence of change in AGB.

1 Introduction

Estimated global mean surface temperature has increased by 0.87 °C since pre-industrial times and continues to rise (IPCC, 2018). The Arctic is warming 2 to 3 times faster than the global annual average. Here, vast amounts of terrestrial carbon are stored in the soil organic matter and living plant biomass (McGuier et al., 2009; ACIA, 2005), and, therefore, changes in the carbon cycle potentially affected by climate change are a central issue. In the course of global warming, positive feedbacks can be observed: for example, encroachment of deep-rooted vegetation due to shrubification can lead to deeper carbon deposition and act as a potential carbon sink (Jobbágy and Jackson, 2000). Therefore, estimation of above-ground biomass (AGB) stocks and detailed knowledge about the individual taxa contributing to it is of prime interest in understanding whether the northernmost forests and tundra also change in biomass in analogy to the widespread observed shrubification. This information is essential for modelling terrestrial carbon cycling in vulnerable high-latitude ecosystems and will help predict future carbon dynamics that may accelerate or slow down future warming.

Detailed (species/taxa level) estimation of AGB can provide more valuable information on an ecosystem's functioning and its development than AGB estimates at a plant functional type (PFT) level. For example, a loss of specific species from one PFT can be replaced by taxa from another PFT in response to climate change even though total AGB production remains similar (Bret-Harte et al., 2008). Thus, the change in AGB between PFTs can be caused by changing species contributions within PFTs. However, many studies of Arctic and sub-Arctic regions present AGB state or change at a PFT level (Räsänen et al., 2018; Berner et al., 2018; Webb et al., 2017; Walker et al., 2005). Some focus only on shrub biomass of one or more species (Vankoughnett and Grogan, 2015; Berner et al., 2018), while others focus on tree biomass (Berner et al., 2012) or on species and PFT AGB of one specific community (e.g., Hudson and Henry, 2009). Occasionally, a study presents results of AGB on a PFT level despite sampling methods that suggest a division by species in the field (Maslov et al., 2016; Chen et al., 2009). Very seldom is AGB presented at a species/taxa level (e.g., Shaver and Chapin, 1991). In consequence, only a few estimations of species or taxon-specific AGB are available to assess species/taxa contributions.

Whereas for some Arctic regions in North America, AGB state and change have been well studied (e.g. Canada in Hudson, 2009), the Russian Far East has received less attention and AGB has never been investigated in the vast areas of central Chukotka, which is our study region. The very few existing circumpolar AGB estimations that also cover these areas (Raynolds et al., 2011; Santoro and Cartus, 2019) have a coarse spatial resolution (1 km and 100 m, respectively) and, therefore, show only the general AGB gradient of the lowest in tundra to the highest in taiga. Similarly, the circumpolar

estimation of Epstein et al. (2012) covers AGB change until 2010 and shows only a general zonal pattern of change. In consequence, it remains unknown how the landscape of central Chukotka, with its characteristic treeline formed by needle-leaf deciduous trees, mountainous terrain, and high diversity of vegetation communities, responds to climate warming in terms of terrestrial carbon stocks.

For vegetation and AGB investigations the remote-sensing index – the normalised difference vegetation index (NDVI) – is often used. It incorporates information from red and near-infra-red regions of the light spectrum that reflect plant biomass of various ecological systems (Pettorelli, 2005). In the Arctic and sub-Arctic regions remote-sensing algorithms based on satellite-derived NDVI and field measurements have been used to predict the total and exclusively shrub AGB in Alaska (Epstein et al., 2008; Berner et al., 2018) and for Cajander larch in north-eastern Siberia (Berner et al., 2012). Some studies have used very high spatial resolution imagery (Räsanen et al., 2018) and hyperspectral field spectrometry for AGB investigations in north-western and northern Siberia and Alaska (Bratsch, 2017) that enable spatially restricted studies on estimations of local AGB. However, the NDVI can be affected by water content and tall vegetation shadows, which can influence the spectral signal of vegetated land (Pattison et al., 2015) and decouple it from the biomass relationship. Such decoupling or similar biomass ranges make distinguishing between different plant functional types (PFT) or communities difficult. Furthermore, the NDVI may not capture differences in the understorey of moderately closed forests (Loranty et al., 2018) because the remote-sensing signal comes from the top of the canopy.

To capture land cover and land-cover change in central Chukotka related to taxa, Shevtsova et al. (2020a) established a redundancy analysis (RDA) model that incorporates the Landsat NDVI, normalised difference water index (NDWI), and normalised difference snow index (NDSI). This model, together with the extensive Landsat satellite data archive, also made it possible to assess the strength and direction of AGB changes in central Chukotka over the last few decades. We used Landsat satellite data and field data from a 2018 expedition in a statistical model for AGB mapping. The aim was to provide an estimation of AGB stocks and their change between paired time points (2000/2001/2002 to 2016/2017) at four focus areas along a tundra–taiga gradient, in central Chukotka. Our first objective was to reconstruct the AGB of each sampling plot using individual plant biomass samples and their corresponding distribution within these plots. The second objective was to upscale AGB in the focus areas for the most recent time covered by Landsat 8 satellite data via statistical modelling. Finally, the third objective was to apply the developed upscaling approach to the oldest available good-quality Landsat 7 acquisitions to investigate AGB changes in the focus areas.

2 Materials and methods

2.1 Study region and field surveys

Our study covers six areas of central Chukotka, Russian Far East (Fig. 1). Four of them (16-KP-01, 16-KP-02, 16-KP-03, 16-KP-04) are our focus areas for biomass mapping and previous vegetation investigations (Shevtsova et al., 2020a); two further areas (18-BIL-01, 18-BIL-02) are supplementary and were investigated for representative AGB sampling. All investigated areas are underlain by continuous permafrost, and all four focus areas are mountainous.

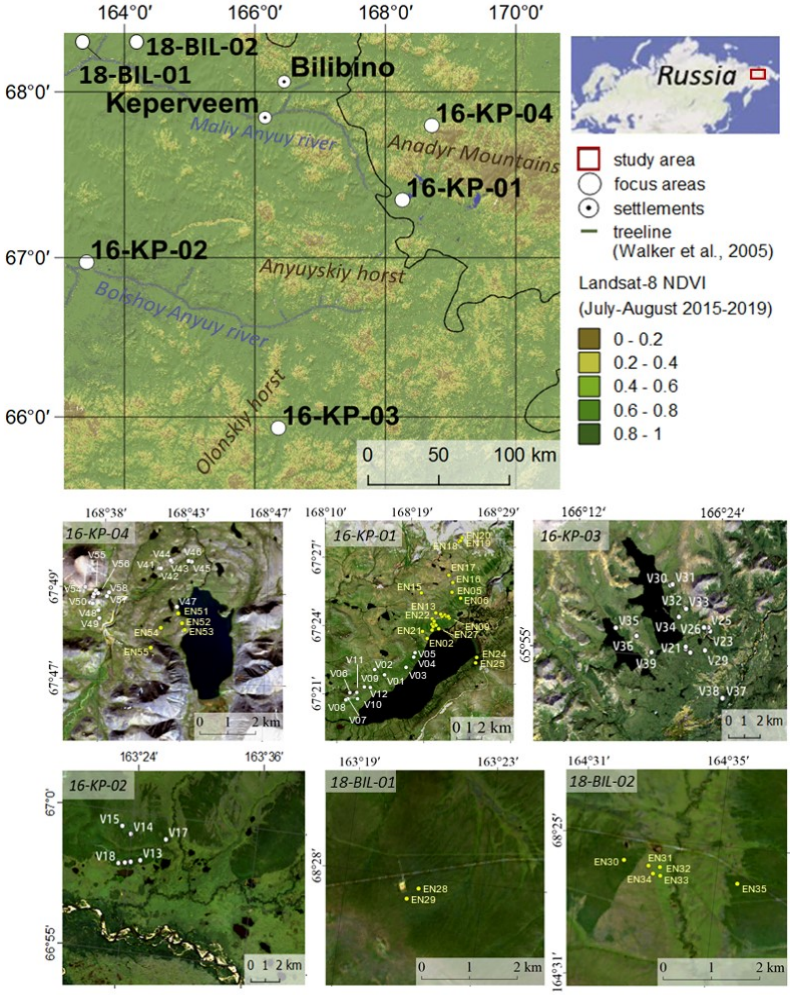

Figure 1: Overview of the study region and four focus areas: tundra (16-KP-04), northern tundra–taiga (16-KP-01), southern tundra–taiga (16-KP-03), and northern taiga (16-KP-02), and two areas with supplementary ABG sampling: 18-BIL-01 and 18-BIL-02 (tundra–taiga to northern taiga). Sample plot names of the 2016 expedition are V01-V58, sample plot names of the 2018 expedition are EN01-EN55 (abbreviated here to EN# rather than EN18#). Overview map modified from Shevtsova et al., 2020a. Base maps of study areas are Landsat-8 RGB composites. Black colour represents no data or water.

During the expedition “Chukotka 2018” in July 2018, we inventoried 40 sample plots (Fig. 1; Biskaborn et al., 2019): 5 sample plots in treeless tundra (16-KP-04), 27 sample plots in the tundra-taiga ecotone (16-KP-01), and 8 sample plots in northern taiga (18-BIL-01, 18-BIL-02). Numbers of plots per habitat are different but align with the concept of stratified random sampling by placing a higher number of plots in the well-represented typical habitats and fewer in the atypical habitats. In the most homogeneous locations, 15 m radius sampling plots were demarcated. Heterogeneity was accommodated by roughly assorting vegetation into two to three vegetation types per sampling plot. Within each area of roughly estimated vegetation types we selected three representative 2 × 2 m subplots for ground-layer foliage projective cover assessment. In these subplots, a 50 × 50 cm area was selected for ground-layer AGB harvesting (major taxa and others), as well as a 10 × 10 cm area for moss and lichen biomass harvesting (Fig. 2). Trees and tall shrubs were sampled directly from the 15 m radius plots. AGB was sampled in 38 sample plots of the 40 inventoried.

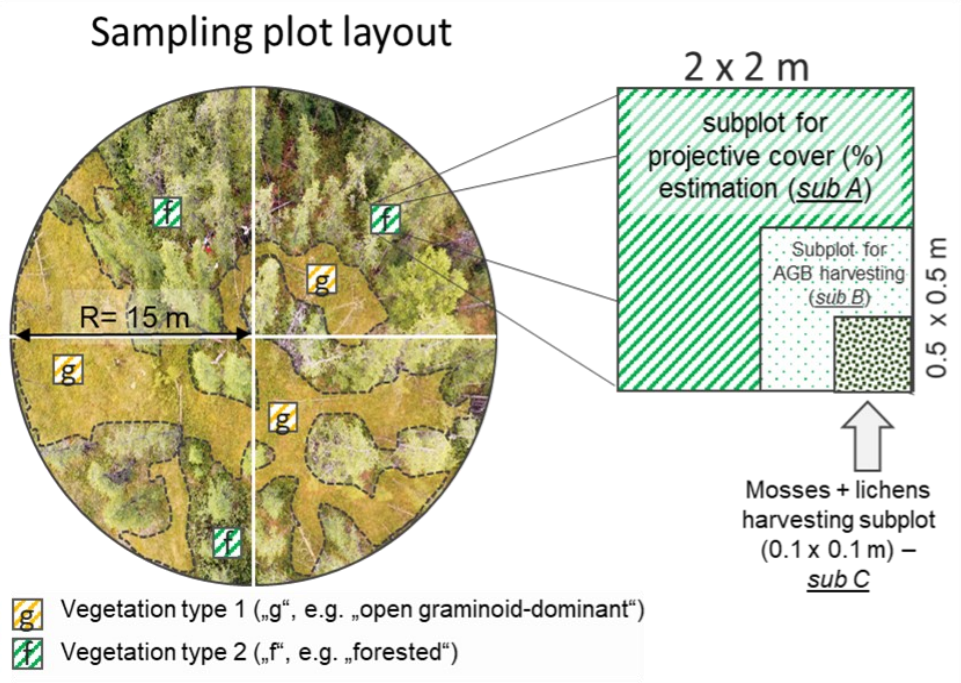

Figure 2: Sampling scheme of the 2018 expedition vegetation survey. To accommodate heterogeneity in the main sample plot with a radius of 15 m, two to three dominant vegetation types were roughly estimated, e.g., in the example we identified two types (‘g’ and ‘f’). Within every vegetation type, three sampling subplots (sub A, 2 x 2 m) were placed for projective cover assessment. Inside one of these, the most representative subplot per vegetation type, we placed a subplot (sub B, 0.5 x 0.5 m) for harvesting above-ground biomass (AGB) from the ground-layer plants, excluding mosses and lichens, which were instead sampled from a representative smaller subplot (sub C, 0.1 x 0.1 m).

All biomass samples were weighed fresh in the field. In general, biomass samples with a weight of more than 15 g were subsampled to reduce the volume of biomass as there were limits to what was logistically possible to transport to the laboratory for drying. All samples were oven dried (60 °C, 24 h for ground-layer and moss and lichen samples, 48 h for shrub and tree branch samples, up to 1 week for tree stem discs) and weighed again.

Our 2018 vegetation and biomass sampling plots were consistently placed in similar vegetation communities to those investigated in 2016. In 2016, we investigated only projective cover, whereas in 2018 both projective cover and AGB were estimated. Only tall dense *Alnus viridis* ssp. *fruticosa* (Rupr.) Nyman (hereafter *Alnus fruticosa*) shrub associations were not sampled during the expedition in 2018; this association is a rare type of vegetation community that only occurs in a few places in the area of interest. Additionally, we sampled the vegetation at an old fire scar, mostly consisting of patches of tall non-creeping *Salix* spp. shrubs with graminoids and dead, upright tree stems of *Larix cajanderi Mayr.*

The sampling protocols for projective cover and AGB sampling are different for (1) trees (*Larix cajanderi*), (2) non-creeping shrubs (*Salix* spp., *Alnus fruticosa*, *Pinus pumila* (Pall.) Regel), and (3) ground-layer plants (including creeping shrubs, herbs, mosses, and lichens).

Tree cover and heights of all trees were visually estimated in the 15 m radius plot after training with a clinometer (Suunto, Finland). Detailed parameters of 10 trees per 15 m radius plot were recorded: height, crown diameter, crown start, stem perimeter at basal and at 1.3 m height, and vitality. We aimed to representatively sample at least three (tall, medium, low) of these trees for AGB. Samples included, if available, needle biomass, one small living branch, one medium-sized living branch, one big living branch, one dead branch, and ideally three stem discs (basal height at 0 cm, breast height at 130 and 260 cm). We estimated the number of branches on each felled tree before felling by eye as follows: (1) number of big branches, (2) number of medium branches on a representative big branch, and (3) number of small branches on a representative medium branch. From the 107 trees sampled, 53 trees were fully sampled, 41 trees were sampled only from the tree trunk, and 13 trees were sampled only from branches and needles. Stem biomass was reconstructed using allometric equations (Appendix A) based on the assumption of a cone-shaped tree form. Using exponential models (Appendix A), we were able to reconstruct total and partial (wood, needle) AGB of all trees (separately for dead and living trees) in each 15 m radius plot. We converted our AGB estimates into averages of kg m^{-2} for each 15 m radius plot.

Non-creeping shrub cover was estimated in the 15 m radius plot. If present, three representative shrub individuals from each species were sampled for AGB: leaf/needle and branch. The average total and partial AGB from representative shrubs was then converted to kg m^{-2} for each sample plot (Appendix A).

Ground-layer vegetation cover was estimated in 2×2 m representative subplots. AGB of ground-layer plants was estimated by harvesting 50×50 cm subplots; AGB of mosses and lichens was estimated by harvesting 10×10 cm subplots. By accounting for the vegetation types within each 15 m radius plot, the total average AGB of each sampled taxon was estimated in kg m^{-2} per sample plot (details in Appendix A).

All AGB estimations (total and per taxon) were analysed in four land-cover classes (1, larch closed-canopy forest; 2, forest tundra and shrub tundra; 3, graminoid tundra; 4, prostrate herb tundra and barren areas; Shevtsova et al., 2020a) and are reported by their median with their interquartile range (IQR) as a measurement of statistical dispersion.

2.2 Above-ground biomass upscaling and change derivation

A redundancy analysis (RDA) model was built with foliage projective cover of 36 taxa from the 2016 expedition sample plots as dependent variables and Landsat spectral indices (normalised difference vegetation index (NDVI), normalised difference water index (NDWI), normalised difference snow index (NDSI)) as predictors (Shevtsova et al., 2020a; Appendix B). We used the RDA model to predict RDA scores for the 40 new sample plots of the 2018 expedition. Foliage projective cover of the new sample plots covered the same taxonomical resolution and was standardised by applying a Hellinger transformation (Legendre and Legendre, 2012). Every position in the ordination space describes a specific vegetation composition with specific coverage, as well as a combination of Landsat spectral indices associated with it. Using the RDA scores, we assigned sample plots from the 2018 expedition to the four established land-cover classes using *k*-means classification: (1) larch closed-canopy forest, (2) forest tundra and shrub tundra, (3) graminoid tundra, and (4) prostrate herb tundra and barren areas (Shevtsova et al., 2020a).

For predicting the total AGB for the 2018 sample plots, the RDA scores of the two first axes were used to build a generalised additive model (GAM; R package "mgcv") using Eq. (1).

$$Total\ AGB = RDA1 + s(RDA1, RDA2)\ , \quad (1)$$

where RDA1 and RDA2 are the ordination scores of the first and second axes, respectively, of the 2018 expedition data from sample plots where AGB was sampled and *s* is a smooth monotonic function. The parameterised GAM was subsequently used to estimate the total AGB for the four focus areas based on the RDA scores of Landsat spectral indices (Table 1). Specifically, for each focus area the AGB was mapped for each of two time points: recent (2016 or 2017) and historical (2000, 2001, or 2002). From AGB maps with a 15–16 years difference covering the same focus area, AGB change maps were produced. The state of and any change in AGB were estimated within and between

land-cover classes for land-cover state and change maps (Shevtsova et al., 2020a). All final estimations of AGB state are presented in kg m^{-2} as the median with the IQR.

Table 1: The four focus areas with corner coordinates (decimal degrees (DD), WGS 84) and acquisition times of the historical and recent Landsat spectral indices (NDVI and NDWI for peak summer, NDSI for snow-covered conditions) used for the redundancy analysis (RDA).

focus area	ecological zone/ ecotone	upper left coordinates (DD)	lower right coordinates (DD)	(historical image product) Landsat 7 ETM+ spectral indices	(recent image product) Landsat 8 OLI spectral indices
16-KP-01	northern tundra-taiga	67.226 N, 168.096 E	67.401 N, 168.621 E	NDVI, NDWI 30 July 2001 NDSI 24 March 2001	NDVI, NDWI 31 July 2016 NDSI 16 March 2016
16-KP-02	northern taiga	67.020 N, 163.432 E	67.173 N, 163.938 E	NDVI, NDWI 8 August 2000 NDSI 22 March 2001	NDVI, NDWI 12 August 2016 NDSI 5 March 2016
16-KP-03	southern tundra-taiga	65.876 N, 166.103 E	65.998 N, 166.509 E	NDVI, NDWI 30 July 2001 NDSI 24 March 2001	NDVI, NDWI 31 July 2016 NDSI 16 March 2016
16-KP-04	tundra	67.735 N, 168.587 E	67.831 N, 168.862 E	NDVI, NDWI 9 August 2002 NDSI 24 March 2001	NDVI, NDWI 10 August 2017 NDSI 16 March 2016

All analyses were performed in R (R Core Team, 2017) using the packages “vegan” version 2.5–4 (Oksanen et al., 2019), “raster” version 2.6–7 (Hijmans, 2017), mgcv (Wood, 2011), “sp” (Pebesma and Bivand, 2005), “factoextra” version 1.0.5.999 (Kassambra and Mundt, 2017), and “ggplot2” (Wickham, 2016).

3 Results

3.1 Vegetation composition and above-ground biomass

In situ projective cover data of all 2018 expedition vegetation sample plots are described in Shevtsova et al. (2021). The main vegetation communities of the study region assessed were (1) barren areas, covered only by rock lichens; different vegetation associations of the open tundra such as (2) non-hummock poorly vegetated areas with *Dryas octopetala* L. and various herbs dominant

or (3) hummock tundra with graminoid dominance (*Eriophorum vaginatum*) and creeping shrubs (*Salix* spp., *Betula nana*); (4) high dense *Pinus pumila* shrub associations; and (5) *Larix cajanderi* tree stands with different degrees of openness and different understorey compositions.

The predictions of the 40 new sample plots categorised into RDA space assigned 2 sample plots to the class "larch closed-canopy forest", 17 sample plots to "forest tundra and shrub tundra", 13 sample plots to "graminoid tundra", and 7 sample plots to "prostrate herb tundra and barren" (Fig. 3). In situ AGB values for each investigated 2018 expedition vegetation sample plot (Fig. 4) are published in Shevtsova et al. (2020c).

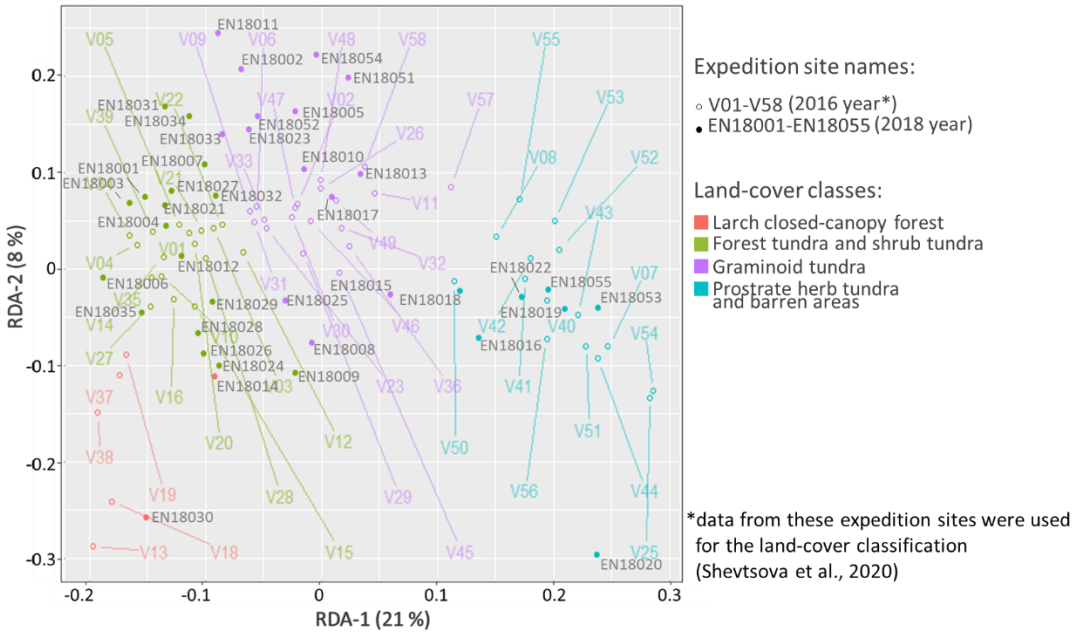

Figure 3: 2018 expedition vegetation data predicted into RDA-space built using the 2016 expedition vegetation data and assigned to four land-cover classes: (1) larch closed-canopy forest, (2) forest tundra and shrub tundra, (3) graminoid tundra, and (4) prostrate herb tundra and barren areas.

In the larch closed-canopy forest *L. cajanderi* makes the highest contribution to AGB (92% or 10.20 kg m^{-2} (IQR=5.09 kg m^{-2}) on average of the total of 11.04 kg m^{-2} (IQR=4.98 kg m^{-2})). Other major vegetation groups are mosses and lichens (4%; 0.43 kg m^{-2} (IQR=0.004 kg m^{-2}))
and low and dwarf shrubs (4%; 0.41 kg m^{-2} (IQR=0.10 kg m^{-2})), among them *Betula exilis* (0.21 kg m^{-2} (IQR=0.017 kg m^{-2})), *Ledum palustre* L. (0.10 kg m^{-2} (IQR=0.019 kg m^{-2})), *Vaccinium vitis-idaea* L.(0.08 kg m^{-2} (IQR=0.061 kg m^{-2})),
Salix spp. (0.006 kg m^{-2} (IQR=0.004 kg m^{-2})),

Empetrum nigrum L. (0.006 kg m^{-2} (IQR=0.006 kg m^{-2})),
and *V. uliginosum* L. (0.003 kg m^{-2} (IQR=0.003 kg m^{-2})).

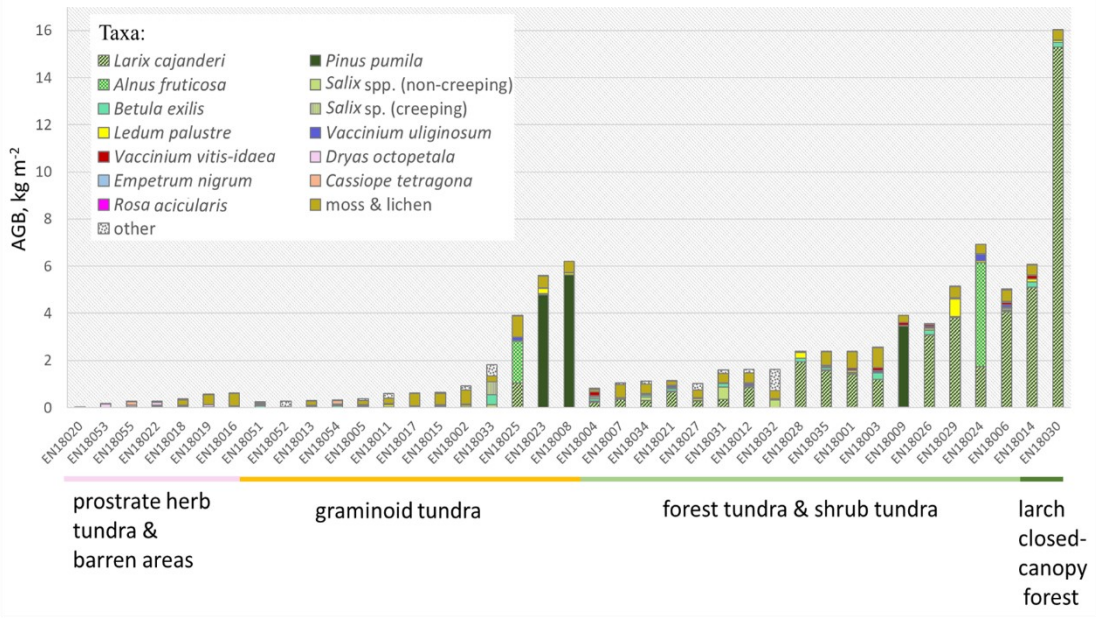

Figure 4: In situ above-ground biomass (AGB) in kg m^{-2} in each investigated sample plot according to the taxa present, ordered by the predicted land-cover class (below names of the sample plots).

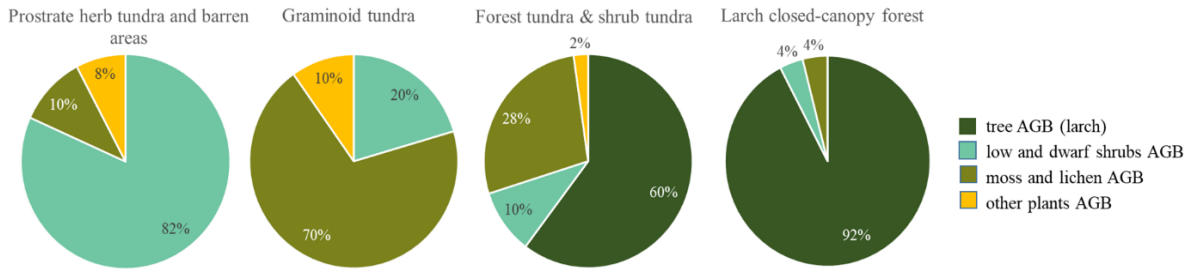

Figure 5: Plot-scale average (median) partial AGB in the four vegetation classes. Tall shrubs (*Alnus fruticosa, Pinus pumila*) were rare and made up less than 1% of the average plot AGB and are not included here.

In the forest tundra and shrub tundra, 60% of the average sample plot AGB (1.44 kg m^{-2} (IQR=2.40 kg m^{-2})) is *Larix cajanderi* which accounts for 0.86 kg m^{-2} (IQR=1.45 kg m^{-2}), followed by mosses and lichens (28%; 0.40 kg m^{-2} (IQR=0.19 kg m^{-2})). Low and dwarf shrubs are 10% (0.14 kg m^{-2} (IQR=0.27 kg m^{-2}) of total sample plot AGB, among them *Betula nana* (0.05 kg m^{-2} (IQR=0.09 kg/m^2)), *V. vitis-idaea* (0.04 kg m^{-2} (IQR=0.06 kg m^{-2})), *Ledum palustre* (0.03 kg m^{-2} (IQR=0.05 kg m^{-2})), *V. uliginosum* (0.02 kg m^{-2} (IQR=0.06 kg m^{-2})), *Salix* spp. (0.003 kg m^{-2} (IQR=0.118 kg m^{-2}))

and *E. nigrum* (0.001 kg m^{-2} (IQR=0.010 kg m^{-2})). The remaining 2% (0.03 kg m^{-2} (IQR=0.01 kg m^{-2})) are mostly graminoids or other herbs.

In the graminoid tundra, 56% (0.25 kg m^{-2} (IQR=0.32 kg m^{-2})) of the average sample plot AGB (0.36 kg m^{-2} (IQR=1.49 kg m^{-2})) are mosses and lichens, 20% (0.07 kg m^{-2} (IQR=0.98 kg m^{-2})) are low and dwarf shrubs, and the remaining 10% (0.04 kg m^{-2} (IQR=0.17 kg m^{-2})) are other plants (grasses and forbs). Low and dwarf-shrub contributors are *B. nana* (0.02 kg m^{-2} (IQR=0.04 kg m^{-2})), *L. palustre* (0.018 kg m^{-2} (IQR=0.067 kg m^{-2})), *Salix* spp. (0.019 kg m^{-2} (IQR=0.03 kg m^{-2})), *V. vitis-idaea* (0.013 kg m^{-2} (IQR=0.019 kg m^{-2})), and *V. uliginosum* (0.008 kg m^{-2} (IQR=0.024 kg m^{-2})).

The average (median) sample plot AGB of the prostrate herb tundra and barren areas is 0.11 kg m^{-2} (IQR=0.25 kg m^{-2}) of which 82% is dwarf-shrub biomass with a dominance of *Dryas octopetala* (0.07 kg m^{-2} (IQR=0.08 kg m^{-2})) and minor contributions of *V. uliginosum* (0.006 kg m^{-2} (IQR=0.014 kg m^{-2})), *V. vitis-idaea* (0.005 kg m^{-2} (IQR=0.005 kg m^{-2})), *L. palustre* (0.002 kg m^{-2} (IQR=0.008 kg m^{-2})), and *Salix* spp. (0.001 kg m^{-2} (IQR=0.002 kg m^{-2})). Moss and lichens account for 10% or 0.11 kg m^{-2} (IQR=0.32 kg m^{-2}) of the average sample plot AGB. The other 8% (0.08 kg m^{-2} (IQR=0.08 kg m^{-2})) of AGB is biomass of different herbs.

Additionally, we analysed the individual partial AGB of four taxa: *Larix cajanderi*, *Alnus fruticosa*, *Pinus pumila*, and non-creeping *Salix* spp. (Fig. 6). *Pinus pumila* had a very wide range of needle-to-wood mass ratios, including a ratio indicating a higher weight of needle biomass compared to wood biomass from an individual shrub. For all other investigated species this is not the case. In contrast, deciduous needled larch has the lowest weight ratio of needles to wood when compared to *P. pumila*, *Salix* spp., and *A. fruticosa.* In the different areas of investigation, we observe generally higher leaf (needle)-to-wood mass ratios in the tundra–taiga area (16-KP-01) thanin the northern taiga (18-BIL-01, 18-BIL-02).

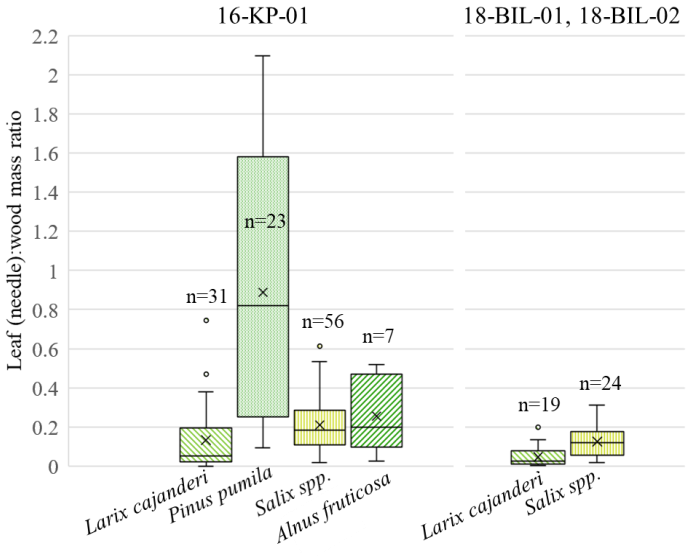

Figure 6: Distribution of leaf (needle) to wood dry mass ratio among studied species: *Larix cajanderi*, *Pinus pumila*, *Salix* spp. (non-creeping), and *Alnus fruticosa* in two ecological regions: tundra–taiga ecotone (16-KP-01) and northern taiga (18-BIL-01, 18-BIL-02); "n" is number of individuals sampled.

3.2 Upscaling above-ground biomass using GAM

In the GAM, the RDA scores are explanatory variables and total AGB is the dependent variable. The first two RDA axes explain 87 % of the variance in the AGB data (Table 2). Both variables (parametric coefficient RDA1 and the smooth term *s*(RDA1, RDA2)) are highly significant in the model.

Table 2: Estimates and significance values of generalised additive model (GAM) parameters.

Formula: total AGB ~ RDA1 + s(RDA1, RDA2)

Parametric coefficients:

	Estimate	Standard error	t value	p
Intercept	2.30	0.20	11.32	<0.005
RDA1	-0.42	0.06	-6.84	<0.005

Approximate significance of smooth terms:

	estimated degrees of freedom	F-value	p
s(RDA1, RDA2)	10.53	12.04	<0.005

We plotted fitted values against residuals for the GAM to visualise residual standard deviations (SDs) for every sample plot used in the modelling (Fig. 7). There is some slight heteroscedasticity, and the SD increases with an increase in absolute AGB values. The RMSE of the model is 1.08 kg.

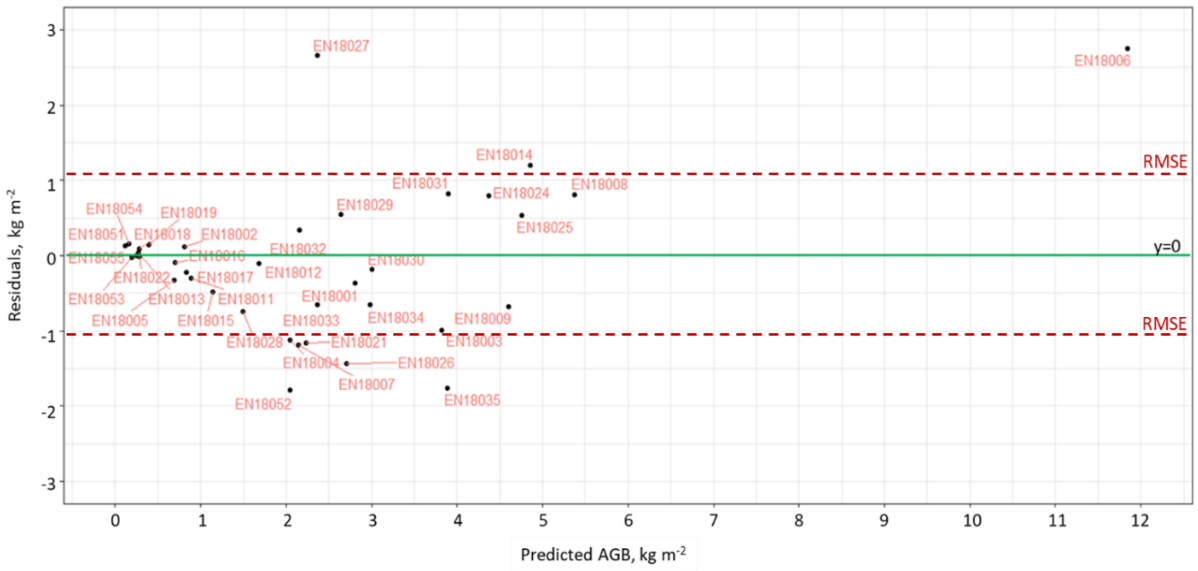

Figure 7: The distribution of residuals of the generalised additive model (GAM) trained for AGB biomass prediction.

Based on the most recent Landsat data acquisitions, the maximum total AGB estimated within our study area is found in the northern taiga in the larch closed-canopy forests (20–24 kg m^{-2}, 16-KP-02, Fig. 8). In the southern tundra–taiga transition (16-KP-03) the maximum AGB reached 12 kg m^{-2} at places in a river valley that are covered by azonal dense forests. In the northern tundra-taiga (16-KP-01) the maximum AGB is 4–6 kg m^{-2} in the forest tundra and shrub tundra. In the tundra (16-KP-04) it is 3–4 kg m^{-2} on the slopes of rivers' valleys.

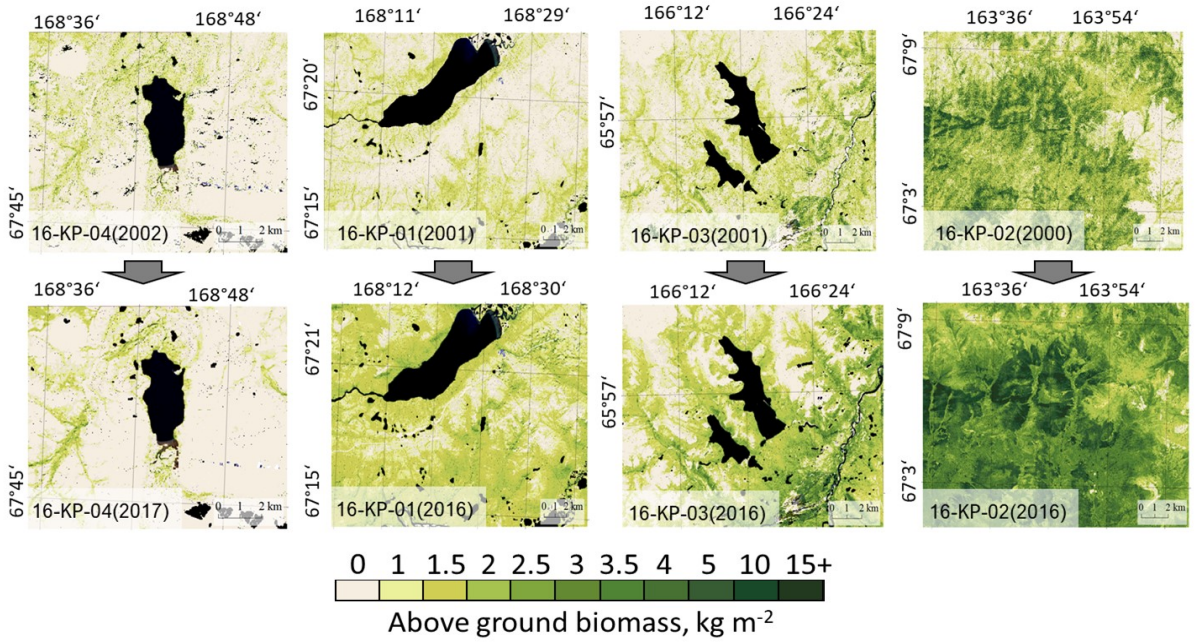

Figure 8: Landsat-derived maps of total above-ground biomass (AGB) in historical years (2000, 2001 or 2002) and recent years (2016 or 2017) in four focus areas: treeless tundra (16-KP-04), northern tundra–taiga (16-KP-01), southern tundra–taiga (16-KP-03) and northern taiga (16-KP-02).

3.3 Change of above-ground biomass between 2000 and 2017 in the four focus areas

The compiled change maps of recent years (20016/2017) versus 15–16 years earlier (2000/2001/2002) show the rates and spatial patterns of AGB change in the four focus areas (Fig. 9).

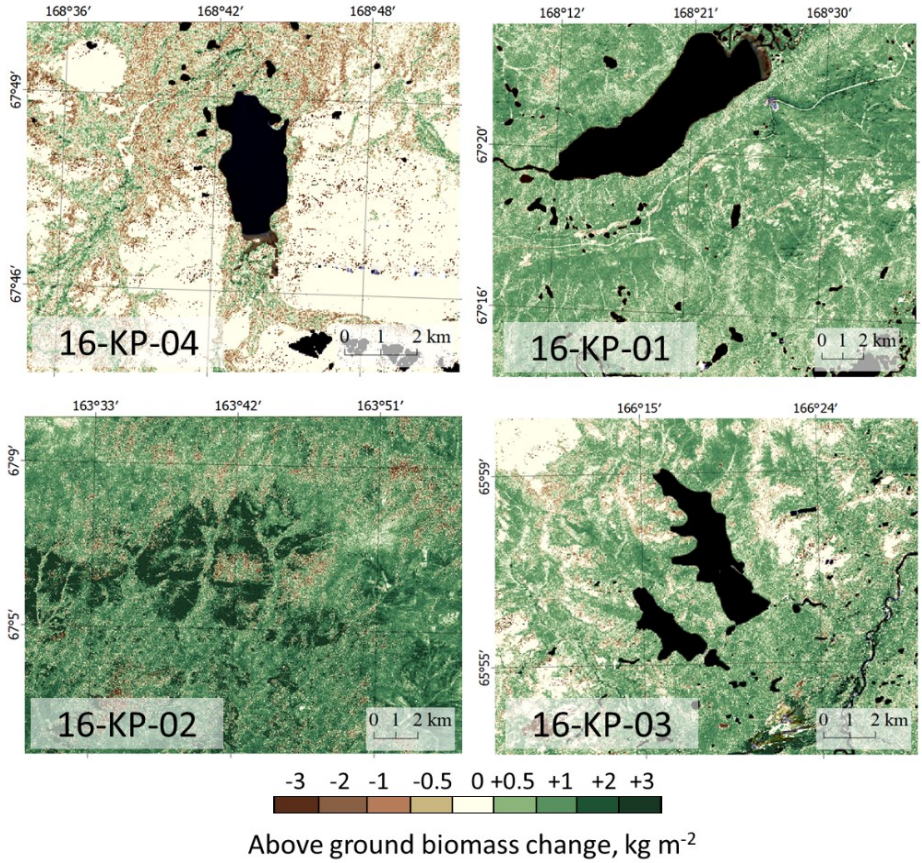

Figure 9: Maps of change in Landsat-derived total above ground biomass (AGB) from historical years (2000/2001/2002) to recent years (20016/2017) in the four focus areas: treeless tundra (16-KP-04), northern tundra–taiga (16-KP-01), southern tundra–taiga (16-KP-03), and northern taiga (16-KP-02). A generally positive trend in AGB change is detected in the tundra–taiga and northern taiga, whereas AGB in the tundra largely remains stable or is decreasing.

Tundra area 16-KP-04, 2002–2017. AGB of prostrate herb tundra vegetation has not changed within the investigated period (0 kg m^{-2}, IQR = 0.12 kg m^{-2} in 2002 and IQR = 0 kg m^{-2} in 2017); AGB of graminoid tundra vegetation has slightly decreased (0.69 kg m^{-2}, IQR = 0.83 kg m^{-2} in 2002; 0.58 kg m^{-2}, IQR = 0.99 kg m^{-2} in 2017). A change in land-cover class from graminoid tundra to forest tundra and shrub tundra between 2002 and 2017 resulted in AGB increase from 1.42 kg m^{-2} (IQR = 0.49 kg m^{-2}) to 1.71 kg m^{-2} (IQR = 0.44 kg m^{-2}), whereas a change

from prostrate herb tundra to graminoid tundra resulted in AGB decrease from 0.48 kg m^{-2} (IQR = 0.87 kg m^{-2}) to 0 kg m^{-2} (IQR = 0.23 kg m^{-2}).

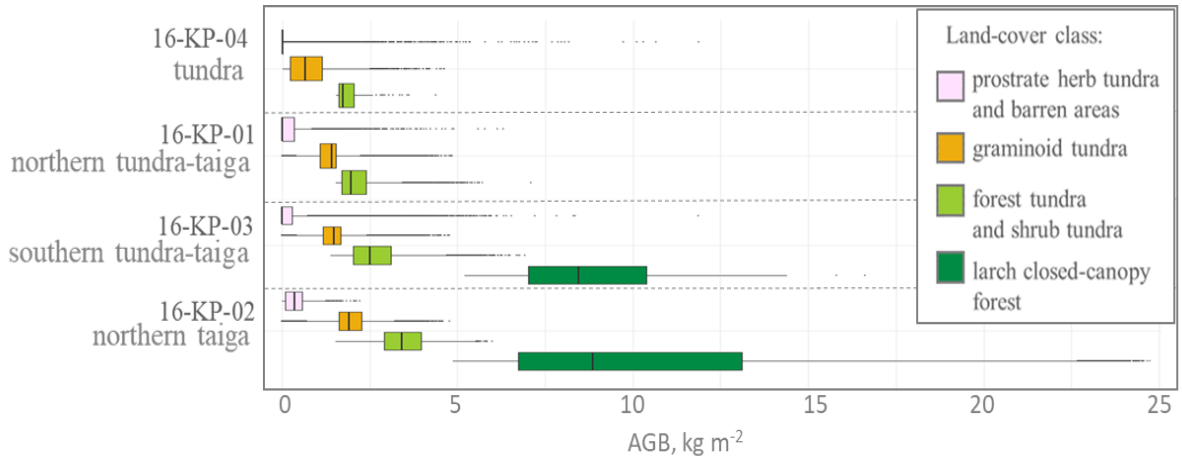

Figure 10: Average above ground biomass (AGB) in recent years (2016/2017) within land-cover classes that have not changed between 2000 and 2017 for four investigated locations, covering a vegetation gradient from tundra (16-KP-04) via tundra–taiga (16-KP-01, 16-KP-03) to northern taiga (16-KP-02).

Northern tundra–taiga area 16-KP-01, 2001–2016. AGB of prostrate herb tundra vegetation stayed stable at 0 kg m^{-2} (IQR = 0.29 kg m^{-2} in 2001; IQR = 0.34 kg m^{-2} in 2016) on average, while the graminoid tundra AGB increased from 0.65 kg m^{-2} (IQR = 1.04 kg m^{-2}) to 1.40 kg m^{-2} (IQR = 0.48 kg m^{-2}) and the forest tundra and shrub tundra AGB did not change (1.73 kg m^{-2}, IQR = 0.50 kg m^{-2} in 2001; 1.70 kg m^{-2}, IQR = 0.32 kg m^{-2} in 2016). A change in land-cover class from prostrate herb tundra into graminoid tundra resulted in AGB increase from 0 kg m^{-2} (IQR = 0.24 kg m^{-2}) in 2001 to 0.34 kg m^{-2} (IQR = 0.67 kg m^{-2}) in 2016, as did a change from graminoid tundra to forest tundra and shrub tundra from 1.27 kg m^{-2} (IQR = 0.53 kg m^{-2}) in 2001 to 1.69 kg m^{-2} (IQR = 0.29 kg m^{2}) in 2016.

Southern tundra–taiga area 16-KP-03, 2001–2016. AGB of prostrate herb tundra vegetation did not change and stayed at 0 kg m^{-2} (IQR = 0.50 kg m^{-2} in 2001; IQR = 0.31 kg m^{-2} in 2016) on average, while graminoid tundra AGB increased from 1.00 kg m^{-2} (IQR = 0.91 kg m^{-2}) in 2001 to 1.50 kg m^{-2} (IQR = 0.57 kg m^{-2}) in 2016. The forest tundra and shrub tundra AGB only slightly changed (2.00 kg m^{-2}, IQR = 0.99 kg m^{-2} in 2001; 2.10 kg m^{-2}, IQR = 0.79 kg m^{-2} in 2016). A change in land-cover class from prostrate herb tundra to graminoid tundra resulted in AGB increase from 0.46 kg m^{-2} (IQR = 0.82 kg m^{-2}) in 2001 to 0.88 kg m^{-2} (IQR = 1.03 kg m^{-2}) in 2016, and a change from graminoid tundra to forest tundra and shrub tundra resulted in AGB increase from 1.43 kg m^{-2} (IQR = 0.48 kg m^{-2}) in 2001 to 2.02 kg m^{-2} (IQR = 0.66 kg m^{-2}) in 2016. A major AGB change is associated with forest tundra and shrub tundra becoming larch closed-canopy

forest resulting in AGB increase from 3.02 kg m^{-2} (IQR = 1.29 kg m^{-2}) in 2001 to 7.29 kg m^{-2} (IQR = 2.53 kg m^{-2}) in 2016.

Northern taiga area 16-KP-02, 2000–2016. AGB of prostrate herb tundra vegetation increased from 0 kg m^{-2} (IQR = 0.09 kg m^{-2}) to 0.60 kg m^{-2} (IQR = 2.60 kg m^{-2}); graminoid tundra AGB increased from 1.30 kg m^{-2} (IQR = 0.82 kg m^{-2}) to 1.90 kg m^{-2} (IQR = 0.69 kg m^{-2}); forest tundra and shrub tundra AGB slightly increased from 2.70 kg m^{-2} (IQR = 1.33 kg m^{-2}) to 3.10 kg m^{-2} (IQR = 1.09 kg m^{-2}); and larch closed-canopy forest AGB increased from 7.00 kg m^{-2} (IQR = 2.49 kg m^{-2}) to 7.50 kg m^{-2} (IQR = 4.65 kg m^{-2}) within the time studied. A change in land-cover class from prostrate herb tundra into largely graminoid tundra resulted in AGB increase from 0 kg m^{-2} (IQR = 0.08 kg m^{-2}) in 2000 to 1.45 kg m^{-2} (IQR = 0.93 kg m^{-2}) in 2016, and a change from graminoid tundra to forest tundra and shrub tundra resulted in AGB increase from 1.44 kg m^{-2} (IQR = 0.61 kg m^{-2}) in 2000 to 2.78 kg m^{-2} (IQR = 0.96 kg m^{-2}) in 2016. Some areas classed as forest tundra and shrub tundra became larch closed-canopy forest, which resulted in AGB increase from 3.25 kg m^{-2} (IQR = 1.49 kg m^{-2}) in 2000 to 7.20 kg m^{-2} (IQR = 4.12 kg m^{-2}) in 2016.

AGB of land-cover classes that did not change within the investigated period tends to have higher values moving from the tundra to northern taiga (Fig. 10).

We find an increase in AGB for those areas where land-cover class has changed (Table 3). The highest changes in the paired years occurred in the southern tundra-taiga (16-KP-03; +4.30 kg m^{-2}) and the northern taiga (16-KP-02: +4.09 kg m^{-2}) associated with a change in land-cover class from forest tundra and shrub tundra to larch closed-canopy forest. The lowest AGB change rates are associated with a change in land-cover class from graminoid tundra to forest tundra and shrub tundra in the northern taiga (16-KP-02) and southern tundra–taiga (16-KP-03). In general, total AGB in the tundra focus area has not changed over the time studied (0 kg m^{-2}, IQR = 0.2 kg m^{-2}), while in the northern tundra–taiga it has increased by 0.69 kg m^{-2} (IQR = 0.69 kg m^{-2}) and in the southern tundra–taiga by 0.44 kg m^{-2} (IQR = 0.91 kg m^{-2}). In the northern taiga total AGB has increased by 1.3 kg m^{-2} (IQR = 1.4 kg m^{-2}), which is much more than in the other focus areas.

Table 3: Above-ground biomass (AGB) change associated with land-cover class change in four focus areas from 2000/2001/2002 to 2016/2017.

Land-cover class change	Tundra 16-KP-04, (kg m^{-2})	Northern tundra–taiga 16-KP-01, (kg m^{-2})	Southern tundra–taiga 16-KP-03, (kg m^{-2})	Northern taiga 16-KP-02, (kg m^{-2})
Prostrate herb tundra and barren areas -> graminoid tundra	-0.30 (IQR=0.80)	+0.20 (IQR=0.54)	+0.35 (IQR=0.95)	+1.31 (IQR=0.98)
Graminoid tundra -> forest tundra and shrub tundra	+0.34 (IQR=0.67)	+0.51 (IQR=0.60)	+0.65 (IQR=0.76)	+1.46 (IQR=1.04)
Forest tundra and shrub tundra -> larch closed-canopy forest	-	-	+4.30 (IQR=2.55)	+4.09 (IQR=3.99)

4 Discussion

4.1 Recent state of above-ground biomass at the field sites

We estimated total and partial dry AGB for the 2018 expedition sample plots, which cover a wide range of vegetation associations (Shevtsova et al., 2020c, d). From these field biomass samples, AGB estimates range from 0 to 15 kg m^{-2} and as expected, reflect a gradient of land-cover classes from the least vegetated prostrate herb tundra and barren areas to the larch closed-canopy forests.

As in other subarctic and arctic vegetation studies the taxa found in our study region can be grouped into similar PFTs for a convenient comparison. Thus, deciduous shrubs are largely represented by *Betula nana*, *Vaccinium uliginosum*, and *Salix* sp., which are typical circumpolar subarctic species (Grigoryev, 1946) and are widely found, for example in the tundra in Alaska near Toolik Lake (Shaver and Chapin, 1991). In graminoid tundra, which, by its characteristics, is comparable to tussock tundra in Alaska, deciduous shrubs contribute 33 % to the total AGB (tundra, median = 0.09 kg m^{-2} and IQR = 0.05 kg m^{-2}) or 9 % (tundra–taiga, median = 0.07 kg m^{-2} and IQR = 0.05 kg m^{-2}), which is similar to deciduous shrub AGB of Alaskan tussock tundra (0.09 ± 0.02 kg m^{-2}). However, in Alaska, deciduous shrub contribution to the total AGB is 16 %, which is lower than for the central Chukotka graminoid tundra but higher than for the graminoid tundra in the central Chukotkan tundra–taiga. Evergreen shrub taxa are also similar in our study region to those near Toolik Lake, Alaska, being mainly represented by *Ledum palustre*, *Vaccinium vitis-idaea*, *Dryas octopetala*, and *Empetrum nigrum*, with *Pinus pumila* in our study region in contrast to Alaska. Evergreen shrubs generally have a lower AGB in the graminoid tundra of our study region (tundra, median = 0.08 and IQR = 0.11; tundra–taiga, median = 0.03 and IQR = 0.10) than in the tussock tundra of Alaska (0.17 ± 0.02 kg m^{-2}), but the percentage of this PFT is slightly higher (31 %) in central Chukotka than in Alaska (24 %). In the graminoid tundra of the central Chukotka tundra–taiga, AGB of evergreen shrubs is poorly represented (4 %). Graminoids in our region were not separately sampled but are included as "other". However, especially in graminoid tundra, the other class

mostly consists of graminoids and other taxa inclusions are rare, so it can be a good approximation of graminoid AGB. The main taxa here, as in Alaska, are *Carex* sp. and *Eriophorum vaginatum*. Compared to the tussock tundra in the Toolik Lake vicinity in Alaska, graminoid tundra of both tundra and tundra–taiga areas in central Chukotka has much less graminoid AGB. For the tundra area it is 9 % of total AGB (median = 0.02 kg m^{-2}; IQR = 0.11 kg m^{-2}) and in the tundra–taiga it is 5 % (median = 0.04 kg m^{-2}; IQR = 0.14 kg m^{-2}), whereas in Alaskan tussocks it is 16 % of the total AGB (0.11 ± 0.02 kg m^{-2}). All vascular plant AGB is similar for all compared areas of graminoid/tussock tundra. Graminoid tundra AGB contribution in the tundra area in central Chukotka is 0.25 kg m^{-2} (median, IQR = 0.04 kg m^{-2}), and in the tundra–taiga area it is 0.34 kg m^{-2} (median, IQR = 2.46 kg m^{-2}; the high IQR is caused by *P. pumila* contributions at two sites). This compares to AGB of 0.37 ± 0.03 kg m^{-2} in the tussock tundra of Alaska. The contribution of vascular plants versus non-vascular plants is much higher in the graminoid tundra of the Chukotka tundra area (96 %) than in Alaska (53 %), whereas for the graminoid tundra of the Chukotka tundra–taiga ecotone their contribution is similar to that in Alaska (42 %). Total AGB of graminoid tundra in central Chukotka is strongly different between tundra (median = 0.26 kg m^{-2}) and tundra–taiga (median = 0.81 kg m^{-2}), with the latter being similar to total AGB of the Alaskan tussock tundra (0.71 kg m^{-2}), while the former is similar to total AGB of open areas and open north-boreal fen in northern Finland (0.30 kg m^{-2}; Räsanen et al., 2018). However, major taxa such as *Betula nana*, *Salix* sp., and graminoids have different contributions in these investigated areas. The tundra area in central Chukotka (only graminoid tundra class) has higher AGB from *B. nana* (median = 0.07 kg m^{-2}; IQR = 0.03 kg m^{-2}) and *Salix* sp. (median = 0.01 kg m^{-2}; IQR = 0.009 kg m^{-2}) than these taxa in northern Finland (0.02 ± 0.05 and 0.0005 ± 0.008 kg m^{-2}, respectively) but similar AGB of graminoids (0.02 kg m^{-2}, IQR = 0.11 kg m^{-2} versus 0.03 ± 0.011 kg m^{-2}).

The highest contribution to partial AGB in central Chukotka is from Cajander larch (*Larix cajanderi*), the only tree species present in the study region. Despite many studies using complex allometric equations, mostly including tree height and stem diameter (e.g., Dong et al., 2020; Heather et al., 2012; Bjarnadottir et al., 2007) to estimate AGB of an individual tree, we used only tree height because stem diameter measurements (stem perimeter) were not available for all trees. However, where measurements of tree stem diameters were available, these are shown to be highly correlated with height (Appendix A, Fig. A3), which makes it rational to use only height to estimate tree AGB to avoid multicollinearity in the model. Other parameters (crown height, crown width) were also measured on a subset of trees and proved to be insignificant predictors. Thus, using estimated tree height we provide coherent AGB estimation models by accounting for living state (live or dead) and ecological zone (tundra–taiga, northern taiga). We also estimated leaf and wood biomass separately and summed them in the data processing procedure (Appendix A). These established

allometric equations can be applied at a broad scale in central Chukotka to a range of tree heights (up to 20 m), as covered by our study.

4.2 Recent state of above-ground biomass upscaled for central Chukotka

The AGB of the studied focus areas of central Chukotka varies along a gradient from <0.5 kg m^{-2} in the sparsely vegetated areas of the tundra to 25 kg m^{-2} in the dense larch forests of the northern taiga. When comparing areas in the circumpolar region with a similar vegetation to that of our study region it can be seen that graminoid tundra in central Chukotka generally has less AGB than tussock tundra in Alaska (Toolik research station; Shaver and Chapin, 1991), whereas forest tundra in central Chukotka has more larch AGB than in the Kolyma region (Berner et al., 2018).

Circumpolar remote-sensing-based estimations such as in Santoro and Cartus (2019) and Raynolds et al. (2011) have lower spatial resolution and less precise AGB estimates for central Chukotka than our mapped AGB estimates. The most recent (2017) European Space Agency (ESA) global AGB map (Santoro and Cartus, 2019) shows generally lower AGB estimates for non-mountainous regions of central Chukotka than our AGB estimates: shrublands in tundra with AGB of 1.5–4 kg m^{-2} (our estimations) only range from 0.3 to 0.6 kg m^{-2} in the ESA AGB product; our AGB estimates for forest tundra in the tundra–taiga ecotone range from 2.5 to 3 kg m^{-2} but are 0.07–0.16 kg m^{-2} in the ESA AGB product; for graminoid tundra in the tundra–taiga ecotone our AGB estimates are 0.7–3 kg m^{-2}, while ESA AGB is 0.1–0.8 kg m^{-2}; and our larch closed-canopy forests AGB estimates are 22–24 kg m^{-2} versus 2.8–4 kg m^{-2} in the ESA product. In contrast, mountainous regions show unrealistically high AGB values in the ESA AGB product that are most likely due to topographical artefacts in the synthetic aperture radar (SAR) processing of the ESA AGB product (see also Santoro and Cartus, 2019). However, other spatial distribution patterns of AGB, especially in the tundra–taiga areas (16-KP-01, 16-KP-03) are very similar to our AGB results. The dissimilarities in the AGB magnitudes can be explained by the different remote-sensing methods: the ESA AGB product was derived from SAR remote sensing while our AGB estimates are based on optical Landsat data. SAR-based biomass estimation is sensitive to vegetation structure and can only derive higher vegetation layers. Therefore, ESA AGB can only represent a "living-tree AGB", while our AGB estimates include other plant groups (lower shrubs, ground vegetation, mosses and lichens) of central Chukotka and are thus more suitable for the investigated area.

Two of our focus areas overlap with the circumpolar above-ground phytomass map of peak-summer season (Raynolds et al., 2011), and a comparison reveals that AGB estimates for the tundra-taiga area (16-KP-01) are similar to each other: 0.65 kg m^{-2} (IQR = 1.1 kg m^{-2}) in 2001 and 1.5 kg m^{-2} (IQR = 0.46 kg m^{-2}) in 2016 (our estimates) versus 0.61–0.97 kg m^{-2} in 2010. However, for the second area, 16-KP-04, our average AGB estimate is lower during the whole investigation period

at 0 kg m^{-2} (IQR = 0.7 kg m^{-2}) in 2002 and 0 kg m^{-2} (IQR = 0.37 kg m^{-2}) in 2017 versus 0.61–0.97 kg m^{-2} in 2010 as estimated by Raynolds et al. (2011).

Further comparison with AGB of similar vegetation types in Alaska (Toolik research station; Shaver and Chapin, 1991) shows that tussock tundra has higher AGB in Alaska (0.71 kg m^{-2}) than graminoid tundra in central Chukotka (0.36 kg m^{-2}), despite having a similar composition that includes tussocks and also being dominated by *Eriophorum vaginatum*. This may be because the AGB of graminoids and forbs in Alaska (0.12 kg m^{-2}) is higher than in central Chukotka (0.04 kg m^{-2}) as is the AGB of dwarf shrubs (0.26 kg m^2 versus 0.07 kg m^{-2}). The prostrate herb tundra and barren areas land-cover class in central Chukotka has a similar composition to heath communities in Alaska with evergreen dwarf shrubs and extensive exposed ground. Prostrate herb tundra AGB of central Chukotka is lower (0.11 kg m^{-2}) compared to that of Alaska (0.32 kg m^{-2}), having more lichen and dwarf-shrub biomass. Forest tundra and shrub tundra in central Chukotka is challenging to compare to Alaskan communities, but generally, average AGB in this land-cover class is slightly lower (1.33 kg m^{-2}) than AGB of even shrub-only communities in Alaska (1.39 kg m^{-2}), which are formed of tall deciduous shrubs such as *Salix* spp. growing on river bars and well-drained floodplains. In contrast to Alaska, forest tundra and shrub tundra in central Chukotka includes mostly dwarf or sparse low shrubs, as well as some tall shrubs and open larch tree stands, and is found on more diverse landscape features than river bars. In addition, the AGB of the central Chukotka tundra and also, partly, the northern tundra–taiga is generally comparable to the AGB of the North Slope of Alaska, which ranges from 0 to 4 kg m^{-2} (Berner et al., 2018).

Comparing our AGB estimates of *Larix cajanderi* to those in the area around the river Kolyma (western Chukotka; Berner et al., 2012) – a close match to our study region by vegetation composition and partly by environmental settings – reveals similarities in the spatial patterns of AGB distribution. The highest AGB tends to occur on protected mountain valley slopes in both investigated regions. AGB of *Larix cajanderi* open forests in the river Kolyma area ranges, on average, from 0.5 to 5 kg m^{-2}, reaching the maximum of 6.7 kg m^{-2}, which is comparable with our forest tundra and shrub tundra AGB assuming a 57 % representation of *Larix cajanderi* in this land-cover class.

Many factors can influence the AGB estimates such as the number of reference samples, prediction method, and remote-sensing sensor type (optical, radar), as well as spatial and temporal resolution of the satellite imagery and products (Fassnacht et al., 2014). Overall, a comparison with global and circumpolar AGB estimates highlights great improvements in the accuracy of the estimates and a better way to resolve a more landscape related spatial pattern of our AGB estimates for the study region.

4.3 Change in above-ground biomass within the investigated 15–16 years in central Chukotka

We derived total AGB changes in the central Chukotka from Landsat satellite data spanning 15–16 years and found the greatest change in the dense forests of the northern taiga (16-KP-02). In the northern tundra–taiga area (16-KP-01), AGB increased from 2001 to 2016 by 0.046 kg m^{-2} yr^{-1} (IQR = 0.046 kg m^{-2} yr^{-1}), which is much faster than the rate estimated by Epstein et al. (2012) for 1982 to 2010 (0.004–0.015 kg m^{-2} yr^{-1}). Further, we estimated AGB change from 2002 to 2017 in the tundra focus area (16-KP-04) as being close to 0 kg m^{-2} yr^{-1} (IQR = 0.013 kg m^{-2} yr^{-1}) on average, which is lower than estimations from 1982 to 2010 given in the circumpolar above-ground phytomass map for the Russian Far East (Walker and Raynolds, 2018). Our results of tundra AGB change being close to zero are similar to experiments with modelling extreme temperature increases in Alaskan tundra (Hobbie and Chapin, 1998). In their study, Hobbie and Chapin (1998) conclude that, in tundra, plant biomass accumulation depends on nutrient availability and AGB will only increase if mineralisation of soil organic nutrients is stimulated together with climate warming. Given differences in soil development between the focus areas of tundra, tundra–taiga, and northern taiga, their conclusion may also apply to our results. In general, the comparison with circumpolar estimated AGB changes from 1982 to 2010 (Walker and Raynolds, 2018) shows that changes in AGB in our focus areas of central Chukotka between 2000 and 2017 were much faster, probably because of the stronger warming in the first decades of the 21st century in these regions.

Our estimates of AGB change within our land-cover classes show that AGB change does not necessarily lead to a change in land-cover class. We assume that changes for different regions within the same stable land-cover classes could be associated with population size change but also likely with changes in the plant's parameters (height, crown density, etc.). This could explain why the change in AGB estimated for the graminoid tundra in the northern taiga (16-KP-02) is greater than for the tundra (16-KP-04, Fig. 10).

5 Conclusions

We successfully used field-based AGB data and Landsat satellite data in statistical modelling to map recent (2016/2017) and historical (2000/2001/2002) states of AGB in four focus areas along a tundra–taiga gradient in central Chukotka. The total AGB values consist of major taxon-specific (and other) estimates that allow us together with the taxon-related land cover to achieve a more detailed picture of AGB change and to reveal changes in major species contributions from areas with diverse ecology. In addition, we were able to analyse changes in AGB together with changes in land-cover classes.

AGB of the investigated areas in the field ranged from 0 to 16 kg m^{-2}. Taxa making the most contribution to AGB in our study region include Cajander larch (*Larix cajanderi*) in forest stands and dwarf birch, dwarf willows, heathers, *Dryas octopetala* (only in prostrate herb tundra and barren areas), mosses, and lichens in tundra areas. Forested sites generally had higher AGB (2.38 kg m^{-2}, IQR = 3.06 kg m^{-2}) than open tundra (hummocks with dwarf or low shrubs 0.65 kg m^{-2}, IQR = 0.76 kg m^{-2}; prostrate tundra 0.32 kg m^{-2}, IQR = 0.22 kg m^{-2}). Tall *Pinus pumila* shrub communities have the highest total AGB (5.57 kg m^{-2}, IQR = 1.14 kg m^{-2}) but are rare at the landscape level and are azonal. Thus, an expansion of forest would make the strongest change to total AGB, but it is still unclear how fast taiga could colonise tundra areas in the upcoming decades. Nevertheless, taxon-specific estimations allow us to separate tree biomass from other vegetation forms, expanding the usefulness of our study to treeline migration assessment and forest management in the study region.

Estimation of recent AGB (2016/2017) in our four focus areas found the highest AGB (24 kg m^{-2}) in the larch closed-canopy forests of the southern tundra–taiga and northern taiga. The lowest AGB occurred in the prostrate herb tundra and barren land-cover class and largely in the tundra on a landscape scale. On average, above-ground vegetation of the closed-canopy forest class has AGB of 8.9 kg m^{-2} (IQR = 6.4 kg m^{-2}), the forest tundra and shrub tundra class has AGB of 3.3 kg m^{-2} (IQR = 1.2 kg m^{-2}), the graminoid tundra class has AGB of 1.4 kg m^{-2} (IQR = 0.53 kg m^{-2}), and the prostrate herb tundra and barren areas class has AGB close to 0 kg m^{-2} (IQR = 0 kg m^{-2}; for non-barren areas 0.4 kg m^{-2}, IQR = 0.52 kg m^{-2}). A comparison with other available estimations of AGB for central Chukotka revealed that other studies considerably overestimate mountainous prostrate herb tundra and barren areas and underestimate tundra–taiga and northern taiga areas. Our satellite-derived estimations match the magnitude of the ground data and show greater detail in the spatial phytomass distribution for the study region.

We found that the greatest AGB changes occurred in the northern taiga, particularly in the larch closed-canopy forest class (+4.09 kg m^{-2}), which also has the highest AGB and most favourable

environment for the expansion of *Larix cajanderi* which contributes highly (92 % on average) to AGB. The less favourable environments in the tundra–taiga and tundra would need more time to adapt to recent climate changes. We found changes in AGB not only that are associated with changes in land-cover classes but also within areas with no changes in land-cover class. This could indicate either that vegetation composition changes are not yet prominent enough to trigger a change in land-cover class or that there has been a change in plant properties (height, crown diameter, leaf size, etc.) within the investigated period.

Overall, our mapped AGB of recent and historical times in central Chukotka is of value in helping to understand regional ecosystem dynamics as well as circumpolar processes, especially in the light of recent climate changes. The specific parameterisation of plant biomass from central Chukotka makes our AGB maps the most suitable for the region and more precise in terms of spatial resolution than global and circumpolar estimations of AGB. Future uses of our AGB state and change maps could include modelling of carbon stocks and investigating habitat changes in the area. Knowing the recent and historical AGB distribution and the contributing taxa is useful for modelling studies that aim to project future AGB changes, as well as for policymaking, particularly in relation to mitigation of climate-change impacts and conservation.

Data availability statement

The data that support the findings of this study are published in the PANGAEA® Data Repository for Earth and Environmental Science. The following data sets are accessible via the stated links:

1. Kruse, S., Herzschuh, U., Schulte, L., Stuenzi, S. M., Brieger, F., Zakharov, E. S., Pestryakova, L. A.: Forest inventories on circular plots on the expedition Chukotka 2018, NE Russia, PANGAEA, doi.pangaea.de/10.1594/PANGAEA.923638, 2020.
2. Shevtsova, I., Kruse, S., Herzschuh, U., Schulte, L., Brieger, F., Stuenzi, S. M., Heim, B., Troeva, E. I., Pestryakova, L. A., Zakharov, E. S.: Foliage projective cover of 40 vegetation sites of central Chukotka from 2018, PANGAEA, https://doi.pangaea.de/10.1594/PANGAEA.923664, 2020.
3. Shevtsova, I., Kruse, S., Herzschuh, U., Schulte, L., Brieger, F., Stuenzi, S. M., Heim, B., Troeva, E. I., Pestryakova, L. A., Zakharov, E. S.: Total above-ground biomass of 39 vegetation sites of central Chukotka from 2018, PANGAEA, https://doi.pangaea.de/10.1594/PANGAEA.923719, 2020.
4. Shevtsova, I., Kruse, S., Herzschuh, U., Schulte, L., Brieger, F., Stuenzi, S. M., Heim, B., Troeva, E. I., Pestryakova, L. A., Zakharov, E. S.: Individual tree and tall shrub partial above-ground biomass of central Chukotka in 2018, PANGAEA, https://doi.pangaea.de/10.1594/PANGAEA.923784, 2020.

Author contributions

IS, UH and SK designed the study. SK, IS, UH, LS, SS, LP, EZ collected the field data. SK and IS processed the field samples. BH advised the processing of remote sensing data. IS developed R code for processing all data used in the study, performed the formal analyses and visualisation, and prepared and edited the original manuscript. SK, UH and BH supervised the research activity and provided critical review during manuscript preparation. UH, LP and SK were responsible for the management and coordination of the planning and execution of the expedition project.

Competing interests

The authors declare that they have no conflict of interest.

Acknowledgements

This study has been supported by the German Federal Ministry of Education and Research (BMBF), which enabled the Russian-German research programme "Kohlenstoff im Permafrost KoPf" (grant no. 03F0764A), by the Initiative and Networking Fund of the Helmholtz Association and by the ERC consolidator grant Glacial Legacy of Ulrike Herzschuh (grant no. 772852), by Russian Foundation for Basic Research (grant no. 18-45-140053 r_a), Ministry of Science and Higher Education of the Russian Federation (grant no. FSRG-2020-0019). Birgit Heim acknowledges funding by the Helmholtz Association Climate Initiative REKLIM. We thank our Russian and German colleagues from the joint German-Russian expedition "Chukotka 2018" for support in the field.

References

Alexander, H., Mack, M., Goetz, S., Loranty, M., Beck, P., Earl, K., Zimov, S., Davydov, S. and Thompson, C.: Carbon Accumulation Patterns During Post-Fire Succession in Cajander Larch (*Larix cajanderi*) Forests of Siberia, Ecosystems, 15(7), 1065-1082, doi:10.1007/s10021-012-9567-6, 2012.

Berner, L., Beck, P., Loranty, M., Alexander, H., Mack, M. and Goetz, S.: Cajander larch (*Larix cajanderi*) biomass distribution, fire regime and post-fire recovery in northeastern Siberia, Biogeosciences, 9(6), 7555-7600, doi:10.5194/bgd-9-7555-2012, 2012.

Berner, L., Jantz, P., Tape, K. and Goetz, S.: Tundra plant above-ground biomass and shrub dominance mapped across the North Slope of Alaska, Environmental Research Letters, 13(3), 035002, doi:10.1088/1748-9326/aaaa9a, 2018.

Bratsch, S., Epstein, H., Buchhorn, M., Walker, D. and Landes, H.: Relationships between hyperspectral data and components of vegetation biomass in Low Arctic tundra communities at Ivotuk, Alaska, Environmental Research Letters, 12(2), 025003, doi:10.1088/1748-9326/aa572e, 2017.

Biskaborn, B. K., Brieger, F., Herzschuh, U., Kruse, S., Prestakova, L., Shevtsova, I. and Zakharov, E.: Glacial lake coring and treeline forest analyses at the northeastern treeline extension in Chukotka, in: Kruse S., Bolshiyanov D., Grigoriev M. N., Morgenstern A., Pestryakova L., Tsibizov L. and Udke A., Russian-German Cooperation: Expeditions to Siberia in 2018, Berichte zur Polar-und Meeresforschung [Reports on polar and marine research], 734, 139–147, Bremerhaven, Alfred Wegener Institute for Polar and Marine Research, doi:10.2312/BzPM_0734_2019, 2019.

Bjarnadottir, B., Inghammar, A., Brinker, M.-M. and Sigurdsson, B.: Single tree biomass and volume functions for young Siberian larch trees (*Larix sibirica*) in eastern Iceland, Icelandic Agricultural Sciences, 20, 125-135, 2007

Dong, L., Zhang, Y., Zhang, Z., Xie, L. and Li, F.: Comparison of Tree Biomass Modeling Approaches for Larch (*Larix olgensis* Henry) Trees in Northeast China, Forests, 11(2), 202, doi:10.3390/f11020202, 2020.

Epstein, H., Raynolds, M., Walker, D., Bhatt, U., Tucker, C. and Pinzon, J.: Dynamics of aboveground phytomass of the circumpolar Arctic tundra during the past three decades, Environmental Research Letters, 7(1), 015506, doi:10.1088/1748-9326/7/1/015506, 2012.

Epstein, H., Walker, D., Raynolds, M., Jia, G. and Kelley, A.: Phytomass patterns across a temperature gradient of the North American arctic tundra, Journal of Geophysical Research, 113(G3), doi:10.1029/2007jg000555, 2008.

Grigoryev, A. A.: Subarktyka [Subarctic], Publ. Acad. Sci. SSSR., Moscow-Leningrad, 1946 (in Russian).

Hijmans R J.: Raster: Geographic Data Analysis and Modeling, R package version 2.6-7, https://CRAN.R-project.org/package=raster, 2017.

Hobbie, S. and Chapin, F.: The Response of Tundra Plant Biomass, Aboveground Production, Nitrogen, and CO_2 Flux to Experimental Warming, Ecology, 79(5), 1526, doi:10.2307/176774, 1998.

IPCC: Global Warming of 1.5°C. An IPCC Special Report on the impacts of global warming of 1.5°C above pre-industrial levels and related global greenhouse gas emission pathways, in the context of strengthening the global response to the threat of climate change, sustainable development, and efforts to eradicate poverty, V. Masson-Delmotte, P. Zhai, H. O. Pörtner, D. Roberts, J. Skea, P.R.Shukla,A. Pirani, W. Moufouma-Okia, C.Péan, R. Pidcock, S. Connors, J. B. R. Matthews, Y. Chen, X. Zhou, M. I. Gomis, E. Lonnoy, T. Maycock, M. Tignor, T. Waterfield (eds.), 2018.

Jobbágy, E. and Jackson, R.: The vertical distribution of soil organic carbon and its relation to climate and vegetation, Ecological Applications, 10(2), 423-436, doi:10.1890/1051-0761(2000)010[0423:tvdoso]2.0.co;2, 2000.

Kassambara A. and Mundt F.: factoextra: Extract and Visualize the Results of Multivariate Data Analyses, R package version 1.0.5.999, http://www.sthda.com/english/rpkgs/factoextra, 2017.

Kruse, S., Herzschuh, U., Schulte, L., Stuenzi, S. M., Brieger, F., Zakharov, E. S. and Pestryakova, L. A.: Forest inventories on circular plots on the expedition Chukotka 2018, NE Russia, PANGAEA, doi.pangaea.de/10.1594/PANGAEA.923638, 2020.

Legendre, P. and Legendre, L.: Numerical Ecology, 3rd ed., Elsevier, Amsterdam, 2012.

Loranty, M.M.; Davydov, S.P.; Kropp, H.; Alexander, H.D.; Mack, M.C.; Natali, S.M.; Zimov, N.S.. Vegetation Indices Do Not Capture Forest Cover Variation in Upland Siberian Larch Forests, *Remote Sens.*, *10*, 1686. https://doi.org/10.3390/rs10111686, 2018.

Pettorelli, N.: Erratum: Using the satellite-derived NDVI to assess ecological responses to environmental change, Trends in Ecology and Evolution, 21(1), 11, doi:10.1016/j.tree.2005.11.006, 2006.

Räsänen, A., Juutinen, S., Aurela, M. and Virtanen, T.: Predicting aboveground biomass in Arctic landscapes using very high spatial resolution satellite imagery and field sampling, International Journal of Remote Sensing, 40(3), 1175-1199, doi:10.1080/01431161.2018.1524176, 2018.

McGuire A. D., Anderson L. G., Christensen T. R., Dallimore S., Guo L., Hayes D. J., Heimann M., Lorenson T. D., Macdonald R. W. and Roulet N.: Sensitivity of the carbon cycle in the Arctic to climate change, Ecological Monographs 79 523–55, doi: 10.1890/08-2025.1, 2009.

Oksanen, J., Blanchet, F. G., Friendly, M., Kindt, R., Legendre, P., McGlinn, D., Minchin, P.R., O'Hara, R.B., Simpson, G.L,Solymos, P., Stevens, M.H.H., Szoecs, E. and Wagner H.: vegan: Community Ecology Package, R package version 2.5-4, https://CRAN.R-project.org/package=vegan, 2019.

Pattison, R.R., Jorgenson, J.C., Raynolds, M.K. and Welker J. M.: Trends in NDVI and Tundra Community Composition in the Arctic of NE Alaska between 1984 and 2009, *Ecosystems* **18,** 707–719, doi.org/10.1007/s10021-015-9858-9, 2015.

Pebesma, E.J. and Bivand, R.S.: Classes and methods for spatial data in R, R News 5 (2), https://cran.r-project.org/doc/Rnews/, 2005.

R Core Team: R: A language and environment for statistical computing, R Foundation for Statistical Computing, Vienna, Austria, https://www.R-project.org/, 2017.

Raynolds, M., Walker, D., Epstein, H., Pinzon, J. and Tucker, C.: A new estimate of tundra-biome phytomass from trans-Arctic field data and AVHRR NDVI, Remote Sensing Letters, 3(5), 403-411, doi:10.1080/01431161.2011.609188, 2011.

Santoro, M. and Cartus, O.: ESA Biomass Climate Change Initiative (Biomass_cci): Global datasets of forest above-ground biomass for the year 2017, v1, Centre for Environmental Data Analysis, doi: 10.5285/bedc59f37c9545c981a839eb552e4084, 2019.

Shaver, G. and Chapin, F.: Production: Biomass Relationships and Element Cycling in Contrasting Arctic Vegetation Types, Ecological Monographs, 61(1), 1-31, doi:10.2307/1942997, 1991.

Shevtsova, I., Heim, B., Kruse, S., Schröder, J., Troeva, E., Pestryakova, L., Zakharov, E. and Herzschuh, U.: Strong shrub expansion in tundra-taiga, tree infilling in taiga and stable tundra in central Chukotka (north-eastern Siberia) between 2000 and 2017, Environmental Research Letters, 15(8), 085006, doi:10.1088/1748-9326/ab9059, 2020a.

Shevtsova, I., Kruse, S., Herzschuh, U., Schulte, L., Brieger, F., Stuenzi, S. M., Heim, B., Troeva, E. I., Pestryakova, L. A., and Zakharov, E. S.: Foliage projective cover of 40 vegetation sites of central Chukotka from 2018, PANGAEA, https://doi.pangaea.de/10.1594/PANGAEA.923664, 2020b.

Shevtsova, I., Kruse, S., Herzschuh, U., Schulte, L., Brieger, F., Stuenzi, S. M., Heim, B., Troeva, E. I., Pestryakova, L. A., and Zakharov, E. S.: Total above-ground biomass of 39 vegetation sites of central Chukotka from 2018, PANGAEA, https://doi.pangaea.de/10.1594/PANGAEA.923719, 2020c.

Shevtsova, I., Kruse, S., Herzschuh, U., Schulte, L., Brieger, F., Stuenzi, S. M., Heim, B., Troeva, E. I., Pestryakova, L. A., and Zakharov, E. S.: Individual tree and tall shrub partial above-ground biomass of central Chukotka in 2018, PANGAEA, https://doi.pangaea.de/10.1594/PANGAEA.923784, 2020d.

Walker, D.A. and M.K. Raynolds: Circumpolar Arctic Vegetation, Geobotanical, Physiographic Maps, 1982-2003, ORNL DAAC, Oak Ridge, Tennessee, USA, doi: 10.3334/ORNLDAAC/1323, 2018.

Wickham, H.: ggplot2: Elegant Graphics for Data Analysis, Springer-Verlag, New York, 2016.

Wood, S.N.: Fast stable restricted maximum likelihood and marginal likelihood estimation of semiparametric generalized linear models, Journal of the Royal Statistical Society (B) 73(1):3-36, 2011.

Appendix A. Sampling and above-ground biomass (AGB) calculation protocol for field data

Here we present the step-by-step protocol for harvesting and calculating ground-layer AGB for a 30 x 30 m sample plot in kg m^{-2}:

1) Fresh biomass harvested and weighed (sample of a particular taxon from a 0.25 m^2 plot): GFW

2) Fresh biomass subsample from the GFW sample: $subFW$ (g/0.25 m^2)

3) Dry biomass from the subsample: $subGDW$ (g/0.25 m^2)

4) Dry weight from the sample (g/0.25 m^2):

$$GDW = \frac{GFW * subGDW}{subGFW}, \quad \text{(A1)}$$

for moss samples

$$GDW = \frac{GFW * subGDW}{0.04 subGFW} \quad \text{(A2)}$$

5) Dry weight of all samples per subplot *sub B* (as in Fig. 2, kg m^{-2})

$$GDWsubplotb = 0.004 \sum_1^k GDW \quad \text{(A3)}$$

k is number of taxa sampled on the subplot B

6) Total dry weight for the whole 30 x 30 m plot (kg 30 m^2):

$$GDWplot = 9a * GDWsubplotb1 + 9b * GDWsubplotb2, \quad \text{(A4)}$$

a and b are proportions of vegetation represented by subplot B1 and B2 (estimated subjectively during field data inventory) on the 30 x 30 m plot, respectively.

7) Average total dry weight (kg m^{-2}):

$$GDWavg = \frac{GDWplotplot}{900}, \quad \text{(A5)}$$

Calculation for *Pinus pumila* shrub AGB. We sampled three (small, medium, big) individual pine plants on each 30 x 30 m sample plot that contained the species. With the following steps we calculated the AGB for each individual plant:

1) Woody AGB of all small living branches (g):

$$DWSmBrsB\ (S, M\ or\ B) = \frac{nSBr(FWSmBrB * subFWSmBrB)}{subDWSmBrB}, \quad \text{(A6)}$$

where $subDWSmBrB$ is dry weight of subsample of a small branch wood; S, M or B are size of an individual plant; $nSBr$ is the number of small branches, $FWSmBrB$ or $subFWSmBrB$ is the fresh weight of a whole sample or subsample of a small branch wood, respectively.

2) Needle AGB of all small living branches (g):

$$DWSmLsB\ (S, M\ or\ B) = \frac{nSBr(FWSmLB * subFWSmLB)}{subDWSmLB}, \quad \text{(A7)}$$

where $subDWSmLB$ *is* dry weight of subsample of a small branch needles, $FWSmLB$ or $subFWSmLB$ is the fresh weight of a whole sample or subsample of a small branch needles, respectively.

3) Woody AGB of all big living branches (g):

$$DWBiBrsB\ (S, M\ or\ B) = \frac{nBiBr(FWBiBrB * subFWBiBrB)}{subDWBiBrB}, \quad \text{(A8)}$$

where $subDWBiBrB$ is dry weight of subsample of a big branch wood, $nBiBr$ is the number of big branches, $FWBiBrB$ or $subFWBiBrB$ is the fresh weight of a whole sample or subsample of a big branch wood, respectively.

4) Woody AGB of all dead branches (g):

$$DWdBrsB\ (S, M\ or\ B) = \frac{ndBr(FWdBrB * subFWdBrB)}{subDWdBrB}, \quad \text{(A9)}$$

where $subDWdBrB$ is dry weight of subsample of a big branch wood, $ndBr$ is the number of dead branches, $FWdBrB$ or $subFWdBrB$ is the fresh weight of a whole sample or subsample of a dead branch wood, respectively.

5) Average AGB of small living branch wood (across the three different-sized samples, g):

$$DWSmBrsBAv = \frac{DWSmBrsB\ (S) + DWSmBrsB\ (M) + DWSmBrsB\ (B)}{3}. \quad \text{(A10)}$$

6) Average AGB of small living branch needles (g):

$$DWSmLsBAv = \frac{DWSmLsB\ (S) + DWSmLsB\ (M) + DWSmLsB\ (B)}{3}. \quad \text{(A11)}$$

7) Average AGB of big living branch wood (g):

$$DWBiBrsBAv = \frac{DWBiBrsB\ (S) + DWBiBrsB\ (M) + DWBiBrsB\ (B)}{3}. \quad \text{(A12)}$$

8) Average AGB of dead branch wood (g):

$$DWdBrsBAv = \frac{DWdBrsB\ (S) + DWdBrsB\ (M) + DWdBrsB\ (B)}{3}. \quad \text{(A13)}$$

9) Average individual plant wood total AGB (including cones biomass, g):

$$AvWoodDW = DWSmBrsBAv + DWBiBrsBAv + DWdBrsBAv + nc * cB, \quad \text{(A14)}$$

where $AvWoodDW$ is the average dry weight for only the woody part of a plant, nc is number of cones, and cB is cones biomass.

10) Average volume of a shrub crown (cm^3):

$$CrV = \frac{SH*SCr1*SCr2 + MH*MCr1*MCr2 + BH*BCr1*BCr2}{3}, \quad \text{(A15)}$$

where SH, MH and BH is height of a small, medium and big plant respectively; $Cr1$ and $Cr2$ are two measurements of a diameter of a crown perpendicular directions.

11) Average wood AGB of *Pinus pumila* (g m^{-2}):

$$DWAvWood = AvWoodDW * \frac{10000}{CrV}, \quad \text{(A16)}$$

where $DWAvWood$ is the average woody mass of a plant per m^2.

12) Average needle AGB of *Pinus pumila* (g m^{-2}):

$$DWAvLs = DWSmLsB * \frac{10000}{CrV}, \quad \text{(A17)}$$

where $DWAvLs$ is the average needles' mass of a plant per m^2.

13) Total average AGB of *Pinus pumila* shrub on a 30 x 30 m sample plot (kg m^{-2}):

$$TDAGBPp = 0.1\ e(DWAvWood + DWAvLs), \quad \text{(A18)}$$

$TDAGBPp$ is the total average AGB of a plant on the 30 x 30 m sample plot, e is cover of *Pinus pumila* shrubs on the 30 x 30 m sample plot (%).

Calculation for *Alnus fruticosa* and *Salix* sp. shrubs AGB. We sampled three (small, medium, big) individuals as for *Pinus pumila* at each plot if present. Calculations are similar as for pine, but include not only big and small branches, but also medium branches.

Calculation for *Larix cajanderi* AGB. *Larix cajanderi* trees were representatively subsampled at the following parts: living branches (small, medium, big), dead branches, needles from small branches, stem (ideally three tree discs at 0, 1.3, and 2.6 m heights), and cones. Total AGB of an individual tree (g) from the field survey of 2018 expedition was calculated as following:

1) $$TDAGB = DBrLB + DTrB, \quad \text{(A19)}$$

where $TDAGB$ is total dry AGB of a tree, $DBrLB$ is dry weight of biomass of branches and leaves, $DTrB$ is dry weight of stem biomass.

2) $$DBrLB = nSBr * SmBrB + nSBr * SmLB + nMBr * MBrB + \\ + nBiBr * BiBrB + ndBR * dBrB + nc * cB, \quad \text{(A20)}$$

where $nSBr$ is the number of small branches, $SmBrB$ is the small branch dry biomass, $SmLB$ is the small branch needles dry biomass, $nMBr$ is the number of medium branches, $MBrB$ is medium branch dry biomass, $nBiBr$ is number of big branches, $BiBrB$ is dry biomass of big branches, $ndBR$ is number of dead branches, $dBrB$ is dead branch biomass, nc is number of cones, and cB is cones biomass.

3) $$DTrB = V_{A-B} * TrDens_{A-B} + V_{B-C} * TrDens_{B-C} + V_C * TrDens_C, \quad \text{(A21)}$$

where V is volume ($_{A-B}$ is a base of a tree stem from 0 to 130 cm, $_{B-C}$ is a middle part of a tree stem from 130 to 260 cm, $_C$ is a top part of a tree stem from 260 to the top), $TrDens$ is the wood density of a tree part (base, middle or top).

4) $$TrDens_{A-B} = \frac{TrDens_A + TrDens_B}{2}, \quad \text{(A22)}$$

where $TrDens_A$ is the wood density of tree disc A and $TrDens_B$ is the wood density of tree disc B.

5) $$TrDens_{B-C} = \frac{TrDens_B + TrDens_C}{2}, \quad \text{(A23)}$$

where $TrDens_C$ is the wood density of a tree disc C.

6) $$TrDens_A = \frac{V_{Adisc}}{B_{Adisc}} = \pi\ h_{Adisc}(\frac{DAdisc}{2})^2 - \pi\ h_{Adisc}(\frac{Dz}{2})^2 - Crl * Crw * h_{Adisc}, \quad \text{(A24)}$$

where V_{Adisc} is the volume of a tree disc sampled at 0 cm tree stem height, B_{Adisc} is dry weight of a tree disc sampled at 0 cm tree stem height, h_{Adisc} is height of a tree disc sampled at 0 cm tree stem height, D_{Adisc} is diameter of a tree disc sampled at 0 cm tree stem height, D_z is diameter of a circular

hole in the central part of a disc (if present), and Crl and Crw are length and average width of a crack in the tree disc, respectively (if present). $TrDens_B$ and $TrDens_C$ are calculated by analogy with $TrDens_A$.

7) Calculation of volume of a tree part (base, middle or top) varies depending on presence or absence of a central hole in the tree stem.

Scenario 1: A hole in the tree disc is absent $Dz = 0$:

$$V_{A-B} = \frac{130\pi}{3}\left(\left(\frac{D_A}{2}\right)^2 + \left(\frac{D_B}{2}\right)^2 + \left(\frac{D_A * D_B}{4}\right)\right), \quad \text{(A25)}$$

where V_{A-B} is the volume of a tree stem part from 0 (A) to 130 cm (B), D_A is diameter of disc A, and D_B is diameter of disc B.

$$V_C = \frac{\pi(H-260)}{3} * \left(\frac{DC}{2}\right)^2, \quad \text{(A26)}$$

where V_c is the volume of a top part of a tree stem from 260 cm to the full height of a tree (H) and D_C is the diameter of disc C.

Scenario 2: A hole in the tree disc is present only in disc A $Dz \neq 0$ (only A):

$$V_{A-B} = \frac{130\pi}{3}\left(\left(\frac{D_A}{2}\right)^2 + \left(\frac{D_B}{2}\right)^2 + \left(\frac{D_A * D_B}{4}\right)\right) - \frac{130\pi}{3}\left(\frac{Dz_A}{2}\right)^2, \quad \text{(A27)}$$

where Dz_A is the diameter of a central circular hole in disc A.

V_c – by analogy with Scenario 1.

Scenario 3: A hole in the tree disc is present in discs A and B $Dz \neq 0$ (A and B):

$$V_{A-B} = \frac{130\pi}{3}\left(\left(\frac{D_A}{2}\right)^2 + \left(\frac{D_B}{2}\right)^2 + \left(\frac{D_A * D_B}{4}\right)\right) - \frac{130\pi}{3}\left(\left(\frac{Dz_A}{2}\right)^2 + \left(\frac{Dz_B}{2}\right)^2 + \left(\frac{Dz_A * Dz_B}{4}\right)\right), \quad \text{(A28)}$$

where Dz_B is the diameter of a central circular hole in disc B.

V_c – by analogy with Scenario 1.

The next step in estimation of Larix cajanderi AGB was to estimate partial individual tree AGB for the 15 m radius sample plot, limited to tree height as a predictor (Eqs. A29–A34, Fig. A2). We did not use the tree stem diameter or perimeter for this purpose, because AGB is highly correlated with tree height (Fig. A3). We differentiated between allometric equations to estimate partial individual larch AGB from trees from two ecological regions (tundra–taiga and northern taiga).

To assess the different models for different regions we used a Wilcoxon rank sum test on measurements of tree stem perimeters. It showed significant differences between the basal perimeter and perimeter at a 1.3 m height of trees from 16-KP-01 (tundra–taiga, 178 samples) and BIL-18 (northern taiga, 74 samples) (Fig. A1). In both cases, the tree basal perimeter (p=0.007453) and tree perimeter at 1.3 m (p=0.03014) in the tundra–taiga is statistically greater than in northern taiga. Since individual trees are significantly different in the two regions, different AGB-prediction models are required for the tundra–taiga and northern taiga focus areas.

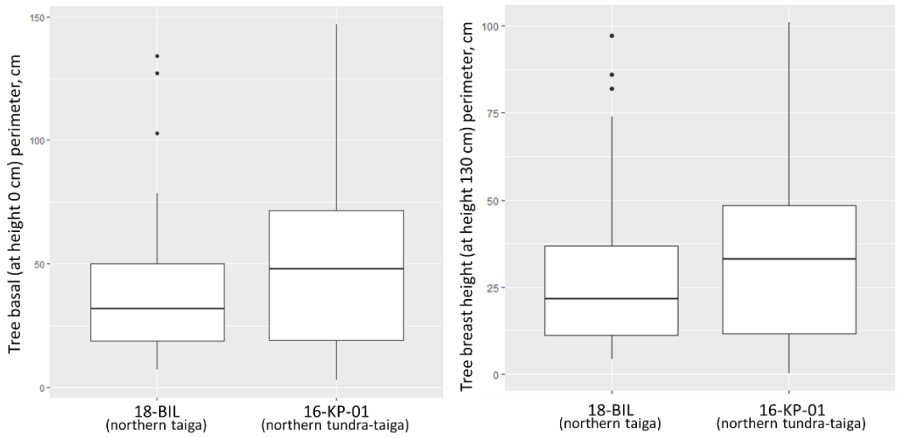

a b

Figure B1. Distribution of basal (a) and breast height (b) diameters values of trees from two focus areas: northern taiga (18-BIL) and northern tundra–taiga (16-KP-01). We also made separate models for living and dead trees as there are obvious differences in the wood densities and no needle material for dead trees. Total AGB of a tree was calculated from partial needle and wood biomass estimations.

Below are the allometric equations that we established:

1) Needle biomass of a living tree (area 16-KP-01, g):

$$AGBn\ (16-KP-01)\ =\ \frac{703.62}{1+e^{-\frac{H-579.5}{208.69}}},\qquad (A29)$$

where AGB is above ground biomass and H is tree height in cm (Kruse et al., 2020).

2) Needle biomass of a living tree (areas 18-BIL-01/18-BIL-02, g):

$$AGBn\ (18-BIL)\ =\ 12.176e^{0.0029H}\qquad (A30)$$

3) Needle biomass of a dead tree (both regions, g):

$$AGBnd\ =\ 0\qquad (A31)$$

4) Wood biomass of a living tree (area 16-KP-01, g):

$$AGBwl\ (16-KP-01)\ ==\ \frac{78713.63}{1+e^{-\frac{H-793.64}{73.91}}}\qquad (A32)$$

5) Wood biomass of a living tree (area 18-BIL, g):

$$AGBwl\ (18-BIL)\ =\ 170.69e^{0.0046H}\qquad (A33)$$

6) Wood biomass of a dead tree (both areas, g):

$$AGBwd\ =\ 203.3e^{0.0057H}\qquad (A34)$$

Larix cajanderi AGB for a 30 x 30 m sample plot was calculated as following:

$$LCAGB = \sum_1^k\ \ AGBn + \sum_1^k\ \ AGBw,$$

where k is number of trees on the 15 m radius sample plot, $AGBn$ is the needle biomass of a tree, and $AGBw$ is the woody biomass of a tree.

Appendix B: Landsat satellite data and statistical analysis as preparation for the AGB upscaling

For each time stamp (2000/2001/2002 and 2016/2017) we used available Landsat acquisitions: peak-summer and snow-covered (table B1, Shevtsova et al., 2020a). We used peak-summer acquisitions to derive two Landsat spectral Indices (Normalised Difference Vegetation Index (NDVI), Normalised Difference Water Index (NDWI)) and snow-covered acquisition for derivation of Normalised Difference Snow Index (NDSI). Before calculating the indices the Landsat data were topographically corrected. The subsets that we used for land-cover classification were cloud free and cloud-shadow free. Additionally, we masked all water bodies. Latdsat-8 data were transformed to Landsat-7-like.

Table B1. Dates and short description of Landsat data used for retrieving spectral indices and further land-cover classification. (in Shevtsova et al. 2020a)

Focus area	Landsat acquisition			Short description(season/ Landsat mission/ spatial resolution)
	year	Month	day	
16-KP-01	2001	7	30	peak-summer, Landsat-7, 30 m
	2001	3	24	snow-covered, Landsat-7, 30 m
	2016	7	31	peak-summer, Landsat-8, 30 m
	2016	3	16	snow-covered, Landsat-8, 30 m
16-KP-02	2000	8	8	peak-summer, Landsat-7, 30 m
	2001	3	22	snow-covered, Landsat-7, 30 m
	2016	8	12	peak-summer, Landsat-8, 30 m
	2016	3	5	snow-covered, Landsat-8, 30 m
16-KP-03	2001	7	30	peak-summer, Landsat-7, 30 m
	2001	3	24	snow-covered, Landsat-7, 30 m
	2016	7	31	peak-summer, Landsat-8, 30 m
	2016	3	16	snow-covered, Landsat-8, 30 m
16-KP-04	2002	8	9	peak-summer, Landsat-7, 30 m
	2001	3	24	snow-covered, Landsat-7, 30 m
	2017	8	10	peak-summer, Landsat-8, 30 m
	2016	3	16	snow-covered, Landsat-8, 30 m

Landsat spectral indices NDVI, NDWI and NDSI and projective cover of different taxa were used in the RDA analysis, which made it possible to distinguish two RDA axes, which in total described 29% of the variance in the projective cover through the Landsat spectral indices (Fig. B1).

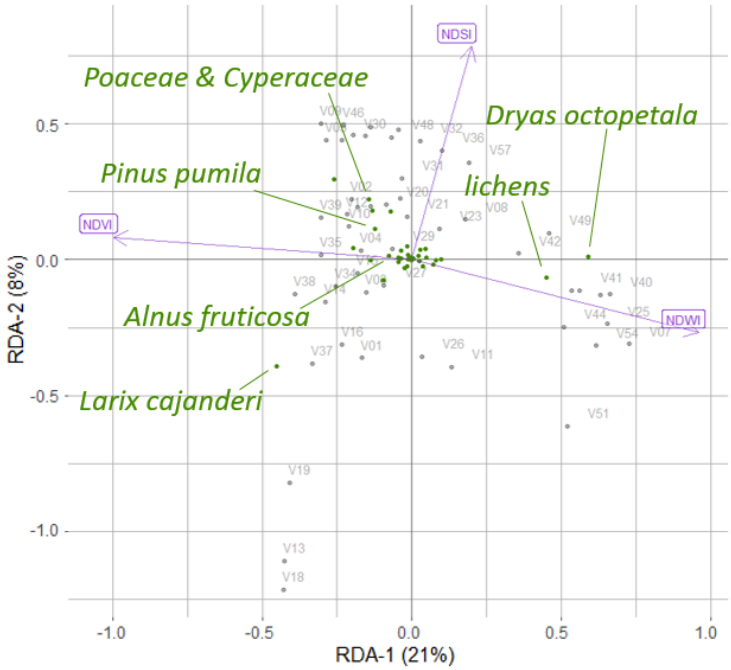

Figure B1: The positions of the major taxa in the RDA space, based on foliage projective cover data of the plot taxa and Landsat spectral indices (Normalised Difference Vegetation Index (NDVI), Normalised Difference Water Index (NDWI) and Normalised Difference Snow Index (NDSI)), where V01-V58 are the 52 vegetation field sites (Shevtsova et al., 2020a).

Based on RDA scores we build a classification using the *k*-means method. We were able to derive four stabe land-cover classes: 1) larch closed-canopy forest, 2) forest tundra and shrub tundra, 3) graminoid tundra, 4) prostrate herb tundra and barren areas (Fig. B2).

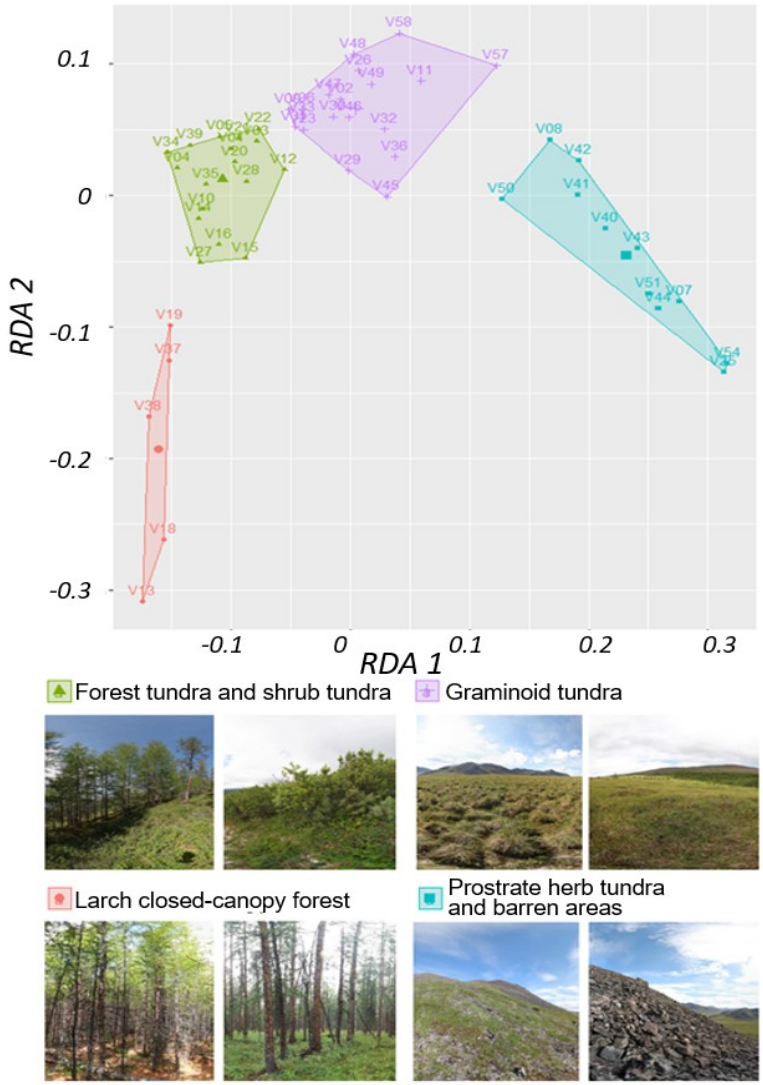

Figure B2: *K*-means classes based on two redundancy analysis (RDA) axes using Normalised Difference Vegetation Index (NDVI), Normalised Difference Water Index (NDWI) and Normalised Difference Snow Index (NDSI) as predictors. Images: extracts from 360x180 degree panoramic images, Stefan Kruse (Figure in Shevtsova et al., 2020a).

Future spatially explicit tree above-ground biomass trajectories revealed for a mountainous treeline ecotone using the individual-based model LAVESI

Submitted to Arctic, Antarctic, and Alpine Research.

Iuliia Shevtsova[1,2], Ulrike Herzschuh[1,2,3], Birgit Heim[1], Luidmila A. Pestryakova[4], Evgeniy S. Zakharov[5] and Stefan Kruse[1]

[1]Alfred Wegener Institute (AWI), Helmholtz Centre for Polar and Marine Research, Research Unit Potsdam, Germany
[2]Institute of Biochemistry and Biology, University of Potsdam, Karl-Liebknecht-Straße 24–25, 14476 Potsdam, Germany
[3]Institute of Environmental Sciences and Geography, University of Potsdam, Karl-Liebknecht-Straße 24–25, 14476 Potsdam, Germany
[4]Institute for Biological problems of the Cryolithozone, Russian Academy of Sciences, Siberian branch, Yakutsk, Russia
[5] Institute of Natural Sciences, North-Eastern Federal University of Yakutsk, 677000 Yakutsk, Russia

Abstract

Future above-ground biomass (AGB) changes will heavily depend on climate changes under global warming. In the subarctic region, the tundra-taiga ecotone is one of the most vulnerable ecological regions worldwide. Forest changes could substantially influence carbon balance and general ecosystem functioning but are understudied especially in complex landscapes such as the mountainous regions of Chukotka, Far East Russia. We investigated potential tree AGB change in central Chukotka by applying the individual-based spatially explicit vegetation model LAVESI to simulate forest dynamics until 3000 CE under different climate scenarios, depending on representative concentration pathways (RCPs) RCP 2.6, RCP 4.5, and RCP 8.5 with and without hypothetical cooling after 2300 CE to 20th century levels. The spatial distribution and the current state of tree AGB were validated against data obtained from direct field investigations and extracted from Landsat satellite imagery, and additionally compared to a high spatial resolution (~0.5 m) satellite image with distinctive trees visible. Our results suggest mostly densification of existing tree stands within the current century in the study region and a lagged forest expansion (up to 39% of total area in the RCP 8.5) under all considered climate scenarios without cooling in different local areas depending on the closeness to the current treeline. In scenarios with cooling air temperature after 2300 CE, forests stopped expanding at 2300 CE (up to 10%, RCP 8.5) and then gradually retreated to their pre-21st century position. The average tree AGB rates of increase are the strongest in the first 300 years of the 21st century. The rates depend on the RCP scenario, where the highest are as expected are under RCP 8.5. Knowing the rates of tree AGB change and the future distribution of trees for this long period in the landscape can be particularly useful for conservation strategies and modelling of future above-ground carbon-stock dynamics.

1 Introduction

Under most scenarios of future climate change, such as the well-known representative concentration pathways (RCPs), global surface temperature will exceed 1.5 °C (RCP 4.5) or 2 °C (RCP 8.5) warming with high confidence by the end of 2100 (IPCC, 2014). However, due to the phenomenon of Arctic amplification, the high latitudes are warming faster than the rest of the world (IPCC, 2014; Miller et al., 2010; Holland & Blitz, 2003) and the warming rates are even predicted to increase (IPCC, 2014). Mean annual precipitation is also predicted to rise at high latitudes under RCP 8.5, whereas spring snow cover is likely to decrease (by 7% in RCP 2.6 and 25% in RCP 8.5). As a consequence of the thermal regime shift, the permafrost extent is expected to shrink by 37% in RCP 2.6 and 81% in RCP 8.5. These and other environmental changes are expected to play a major role in vegetational changes, especially in the Arctic and Subarctic (Zhang et al., 2018; Rupp et al., 2000; Bonan et al., 1995). Above-ground biomass (AGB) is one of the most important parameters of vegetation, which is directly connected to above-ground carbon stocks and ecosystem primary production. Estimation of its future dynamics in the high latitudes is crucial to predict and timely manage mitigation measures and define adaptation strategies in respond to future ecosystem changes (biodiversity, wildlife, natural habitat loss etc) and climate feedbacks.

There are not many studies on future subarctic vegetation dynamics and even fewer on future AGB dynamics. Currently, vegetation or parameters associated with vegetation change are mostly simulated by global models (e.g., Druel et al., 2019; Sitch et al., 2008; Bergengren et al., 2001; Bonan et al., 2003) with a lack of local accuracy in complex environments (Epstein et al., 2007). Therefore, for more accurate results, landscape-scale future estimations of vegetation changes are necessary and expected when applying an individual-based and spatially explicit model (Kruse et al., 2019).

The Individual tree-based gap model University of Virginia Forest Model Enhanced (UVAFME) was used to simulate forest carbon biomass in response to climate change for boreal Russia (Shuhman et al. 2014) and interior Alaska (Foster et al., 2019). The simulations were successful in the different regions mostly highlighting that climate change resulted in species composition. However, North-eastern Russian subarctic at landscape level stays unexplored by individual-based models.

In the subarctic region, the expected major outcome of vegetation change is a northern boreal treeline extension that is associated with tundra loss (Foley et al., 1998). This treeline is represented by the tundra-taiga ecotone region, and its size and geographical borders vary in different parts of the subarctic region. Here, tree growth is controlled by soil moisture (Liang et al., 2014; Kagawa et al., 2003), air and soil temperature, length of the growing season, frost events, wind, permafrost, and nutrient deficiency (Holtmeier & Broll, 2009). These factors are in turn influenced

topography (Holtmeier & Broll, 2009). In mountainous regions, the treeline area tends to be narrower than on the flatlands and is thus more sensible to climate changes. This is the case for the easternmost treeline ecotone in central Chukotka, Far East Russia, which covers a complete vegetation gradient from prostrate mountainous tundra to open forest tundra on complex topography (Shevtsova et al., 2020a), but despite its valuable character as a study region it is understudied.

There are several tree species across the subarctic region of Eurasia, each covering millions of square kilometres and forming the northern treeline (Abaimov, 2010). The approximate 5000 km long treeline in Siberia is formed by four deciduous conifer species of the genus *Larix* Mill. (larch) (Abaimov, 2010). In our central Chukotka study region, the northern treeline is comprised of *Larix cajanderi* Mayr, which covers 2.6 million km^2 of Siberia in total (Abaimov, 2010; Abaimov et al., 1980). *Larix cajanderi* grows on a wide variety of soils: dry, waterlogged, permafrost, peaty, stony, and on soils poor in nutrients (Osipov & Burundukova, 2015).

Recently, extensive investigations of vegetation cover and AGB were made in central Chukotka (Shevtsova et al., 2020a; Shevtsova et al., 2021), namely the area around Lower and Upper Lake Ilirney, including field inventories in 2016 and 2018 (Shevtsova et al., 2020c, Shevtsova et al., 2020d, Kruse et al., 2020). We therefore selected this study area to predict changes in forest distribution and AGB in the complex landscape.

Due to successional and immigrational processes such as seed dispersal, establishment of seedlings, seedlings growth to reproductive maturity, even the rapid warming occupation of open tundra by forest occurs with time lags (Kirilenko & Solomon, 1998). Furthermore, in subarctic forest tundra even under increasing air temperatures due to the warming, establishment of tree stands in the open tundra could be delayed because of wind-exposed conditions, which decrease tree growth (Gamache & Payette, 2004). To disentangle the spatial dynamics of tree AGB for future climate-change scenarios, the use of the individual-based and spatially explicit model LAVESI, which is able to reveal complex migrational behaviour that has a non-linear response to climate change (e.g., Kruse et al., 2016), is the key.

The aim of this study is to assess future change of tree AGB in the treeline ecotone of central Chukotka for climate changes between 2000 and 3000 BC. We focus on spatial dynamics of tree AGB in the upcoming centuries in the mountainous focus area. With this, we also focus on the rates of tree AGB change in the region of Lower and Upper Lake Ilirney and estimate how AGB will potentially be distributed within the investigated period. We formulated two research questions to guide this study: (1) What are the future dynamics of tree AGB at a plot level (2) What are the future dynamics of tree AGB at the landscape level?

2 Materials and methods

2.1 Study region

Our study region in central Chukotka (north-eastern Siberia, Russia) is set up in the Lower Lake Ilirney area, at the north-eastern margin of the northern treeline ecotone (Fig. 1). It supports a wide range of vegetation types from relatively dense tree stands at lower elevations to tree-free prostrate lichen-dominated tundra generally at higher elevations (Shevtsova et al., 2020a). According to field data collected in 2018 (Shevtsova et al., 2020c), total above-ground biomass (AGB) ranges from a minimum close to 0 kg m^{-2} in the mountains (800–1600 m a.s.l.), to intermediate around 0.56 kg m^{-2} in the graminoid tundra (600–700 m a.s.l. or in some places at lower elevations) to around 2.48 kg m^{-2} in the forest tundra (430–600 m a.s.l.). The tree stands are represented by only one tree species *Larix cajanderi* Mayr, which has the highest proportion of up to 60% of the total vegetation AGB on the forest tundra sites (Shevtsova et al., 2021). The typical climate for the area can be characterised as continental with average January temperatures of -30 °C, an average July temperature of +13 °C, and annual precipitation of 200 mm yr^{-1} (Menne et al., 2012). Growing season is short (100 days yr^{-1}).

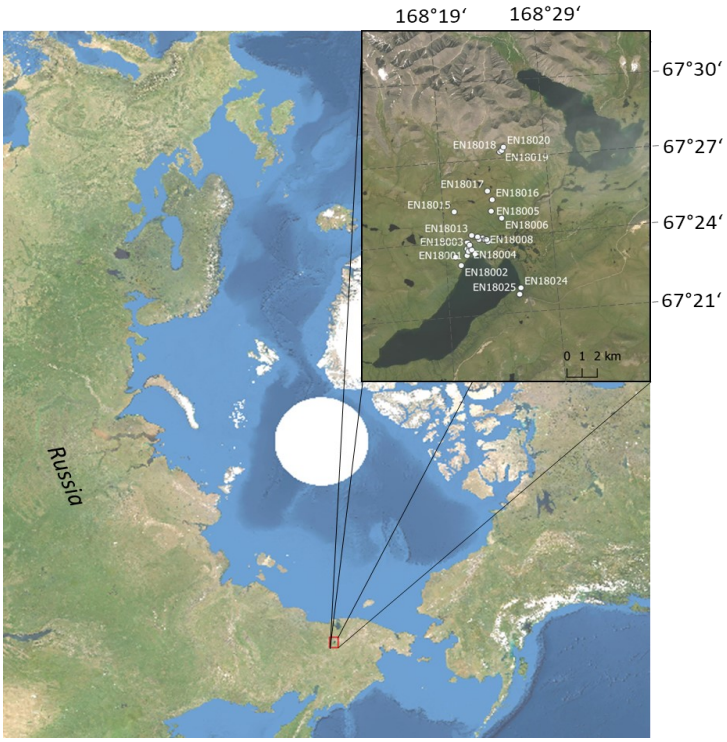

Figure 1. View on the circum-Arctic and location and close-up of the study region with the Lake Ilirney area lake system in the northern tundra-taiga. On the inset, points mark the 26 sites, where above-ground biomass (AGB) was sampled in 2018. Source of background maps: ESRI World Imagery.

2.2 LAVESI model setup, parameterisation, and validation

The *Larix* vegetation simulator (LAVESI) is an individual-based spatially explicit model that simulates larch stand dynamics (Kruse et al., 2016; Kruse et al., 2018). The current model version of LAVESI uses temperatures of the coldest and warmest months (January, July) and monthly precipitation series as climate forcing, as well as data on wind speed and direction and biological specifics of larch to simulate seed distribution and tree reproduction, growth, and death (Kruse et al., 2019; Kruse et al., 2018; Kruse et al., 2016).

To make LAVESI simulate AGB dynamics at landscape scales representing a complex environment including mountainous topography we improved LAVESI by the following. We added elevation and auxiliary and environmental factors as new boundary conditions by using the slope angle and the topographical wetness index (TWI). To convert from tree stand structure based on tree diameter growth to AGB we implemented AGB equations and applied them on the simulated tree heights in LAVESI.

2.2.1 Implementing topographical parameters: elevation, aspect, slope angle, and topographical wetness index

Topography modulates regional climate and controls the spatial patterns of the treeline limits (Holtmeier & Broll, 2009). We used the TanDEM-X 90 m digital elevation model (DEM) product (Krieger et al., 2013) for extracting the relevant spatial topographical parameters, namely: elevation, slope angle, and topographical wetness index (TWI). Prior to spatial topographical parameters extraction, the DEM was resampled from the 90-m cell spacing to a 30-m resolution. We also investigated aspect, but when evaluating the topographical parameters for implementation, it did not have a strong effect. Slope angle and aspect were calculated in SAGA 2.3.2 (as QGIS 3.16.0 plugin) using Zevenberger & Thorne's second-order polynomial adjustment algorithm (1987). The TWI represents the moisture content, spatially distributed on the landscape. The TWI was calculated using the basic terrain analysis tool (SAGA GIS plugin) with the default setting of "the channel density" set to five. The final topography layers – elevation, slope angle, and TWI – were masked for areas of present surface water, such as Lower and Upper Lake Ilirney, small ponds, and rivers. We created the water mask by applying the land-water threshold technique to the Landsat-8 short-wave infrared (SWIR) 1 band on a summer acquisition on 07.12.2018 with the Landsat spatial resolution of 30 m.

The topographical data (elevation, slope angle, TWI) were introduced in the source code of LAVESI as 30 x 30 m gridded input data, featuring a user-defined area. Based on this, the values are linearly interpolated to the internally used environmental grid of 20 x 20 cm tiles.

The seed dispersal that already depended on wind direction and speed, release height, and species-specific fall rates (Kruse et al., 2018, 2019), was further improved for this study by shortening the upslope dispersal distance and restricting it to locations below release height.

2.2.2 Calculation of above-ground biomass (AGB)

To predict the above-ground biomass (AGB) of each of the simulated larch trees, we used two separate models for needle and woody biomass established previously for the field sites in the study region (Shevtsova et al., 2021) based on a set of sampled trees (Shevtsova et al., 2020c) and simplified to estimate the biomass of all trees on the sites based on the recorded height of the present trees (Kruse et al., 2020). Needle biomass of a living tree was calculated from the LAVESI-simulated tree height as followed:

$$AGBn = \frac{703.62}{1 + e^{-\frac{H - 579.5}{208.69}}} \text{ (g)}, \quad (1)$$

where AGB is above-ground biomass and H is tree height in cm. Wood biomass from a LAVESI-simulated living tree was calculated as followed:

$$AGBwl = \frac{78713.63}{1 + e^{-\frac{H - 793.64}{73.91}}} \text{ (g)}. \quad (2)$$

2.2.3 Parameterisation of influence of the topography and wetness on tree presence and growth

To extract the dependence of tree presence from the topographic parameters – aspect, slope angle, and TWI – we used a high-resolution satellite acquisition from early summer in 2010 (ESRI World Imagery), which allows identification of single trees and covering a representative part of the study region. In the first step, 6488 sampling points for evaluation of the presence of trees (were selected by stratified random sampling from 589 different possible combinations of elevation, slope angle, aspect, and TWI (Fig. 2; Appendix A). The samples cover 2% of the area shown in Figure 2, from southern forested areas via hummock tundra to the non-vegetated northern mountainous areas.

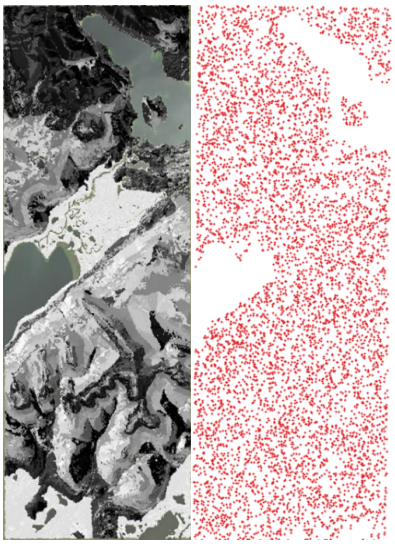

a b

Figure 2. a) Visualisation of the combinations of elevation, slope angle, and topographic wetness index (TWI) in the area for parameterisation of the new topographic components in LAVESI with 589 categories distinguished, shown in grey shades, and (b) 6488 samples, marked as red dots.

The visual assessment of the established relationship showed that aspect did not play an important role in the presence of trees in the study region (Fig. 3). Areas both with and without trees show the same pattern of sample distributions in relation to the aspect data. In contrast, one can clearly observe that trees prefer higher slope angles, rather than lower.

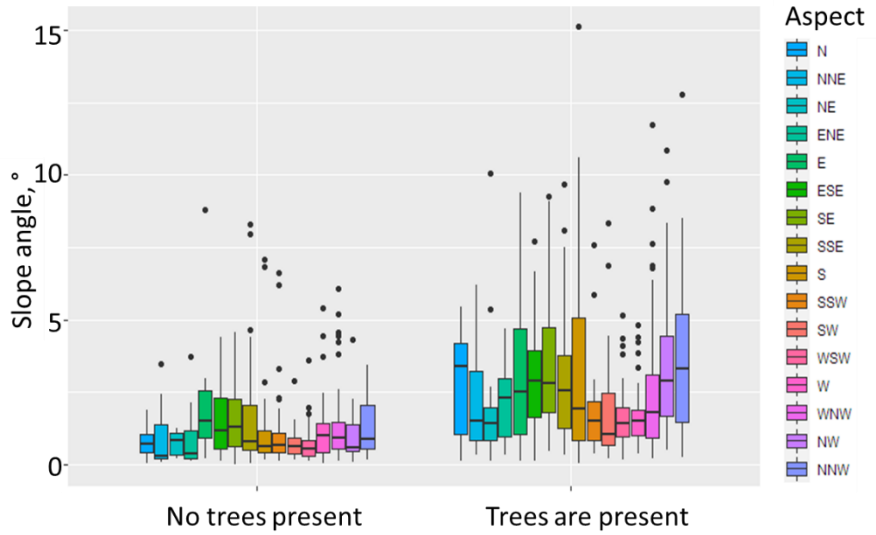

Figure 3. Tree presence depends strongly on slope angle and very slightly on aspect in the study region (based on 6488 stratified random samples). The patterns of aspect and slope angle combinations are generally similar for each direction of the treeless and tree areas, whereas areas with trees are found on slopes with higher angles in comparison to treeless areas for most of the aspect directions.

In consequence, we could separately establish two statistically significant linear models predicting tree presence (in percent of observations) depending on slope angle and TWI:

$$TrPrSA = e^{-0.5\frac{(slope\ angle - a)^2}{b^2}} = e^{-0.5\frac{(slope\ angle - 12.58)^2}{12.78^2}}, \quad (3)$$

where TrPrSA is tree presence depending on slope angle, and a and b are coefficients (Table 1).

$$TrPrT = -c * TWI + 0.98 = -0.05 * TWI + 0.98, \quad (4)$$

where TrPrT is tree presence depending on TWI, and c is a coefficient (Table 2).

The models have good accuracy with residual standard errors of 0.013 (model under formula 3) and 0.011 (model under formula 4) and all significant coefficients (Appendix B, tables B1 and B2).

The coefficients of these models were introduced into the model LAVESI to control environmental impact on individual growth simply by using the predicted forest presence at a certain location as a factor for the actual individual tree growth:

$$Envirgrowth = 0.5\,TrPrT + 0.5e^{2TrPrSA} \quad (5)$$

2.2.4 LAVESI simulation setup for this study

We ran LAVESI simulations for three different RCP climate scenarios (RCP 2.6, RCP 4.5, RCP 8.5 with and without cooling after 2300 CE) to see potential future paths of larch AGB change in the study region. Simulation runs were started with the updated LAVESI version with an empty landscape with true topography starting at 500 CE to allow for spin up and ending in 2018 CE. Into this, seeds (N=100000) for initiating the population establishment were introduced across a subset of 12 x 15 km in the southwestern corner of the simulation area (18 x 25 km) for the first 50 years. Only 1000 seeds were introduced yearly after 550 CE allowing for re-establishment after a complete die-out of trees on the whole simulated area.

As historical climate data for the forcing, we used the 0.5° x 0.5° Climate Research Unit gridded Time Series (CRU TS) monthly data (1901–2019) (Harris et al., 2020; Fig. 4). This data was used to prepare a processed towards proceeding monthly series by linking air temperature to $\delta^{18}O$ and precipitation to ice layer thickness series from for 501 to 1900 CE from the Severnaya Zemlya/AN ice core data (Opel et al. 2013, Arkhipov et al. 2008). Six hourly wind data was extracted for the study region from the ECMWF Re-Analysis ERA-Interim 0.75° x 0.75° (Dee et al., 2011). For future predictions, we used a coupled climate model run output from MPI-ESM driven by three available RCP scenarios (Giorgetta et al., 2012a; Giorgetta et al., 2012b; Giorgetta et al., 2012c) from 2019 to 2300 CE and prolonged it until 3000 CE. Therefore, we added climate data following the trend until 2500, subsequently keeping the reached temperature level at 2400-2500 until 3000 CE, or in the case of the cooling scenarios, we brought temperatures back to the years 1901-1987 CE of the series in a loop (Fig. 4).

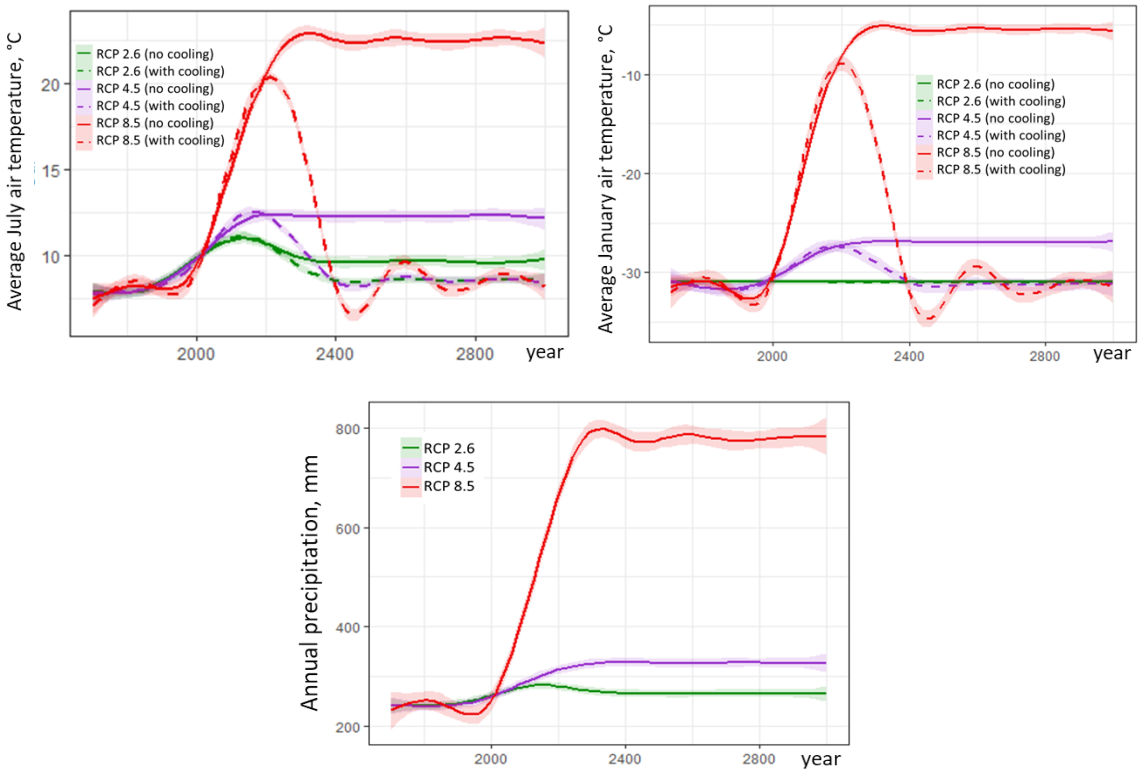

Figure 4. Air temperature and precipitation changes for the Lakes Ilirney area, central Chukotka. Historical CRU TS data are shown from 1700 until 2019 CE and ECMWF Re-Analysis ERA-Interim data are shown from 2019 until 3000 CE according to different representative concentration pathways (RCP) scenarios. To visualise the data generalised additive model (GAM) was used.

According to the 2018 field inventories (Shevtsova et al., 2021), forest tundra as opposed to open tundra in this region has at minimum tree AGB of 0.68 kg m^{-2}. Using this threshold, we calculated the percent of areas with tree stands reaching this AGB threshold for the simulated data from 2000 to 3000 CE to derive dynamics of forest and/or forest tundra in the study area under different climate scenarios. We visualised results as the overall dynamics throughout the investigated period, as well as its spatial representation for selected years.

All statistical analyses in this study were performed in R 3.4.2 (R Core Team, 2017), mostly using included standard functions, with the addition of functions from the package "raster" version 2.6-7 (Hijmans, 2017) for treating and exporting raster AGB data and functions from the package "ggplot2" (Wickham, 2016) for visualisation of the results. Maps were visualised with R 3.4.2.

2.2.5 Validation of the model's performance

For a spatial validation of data simulated with LAVESI, we compared the simulated larch distribution at local scales in 2018 CE with field larch AGB estimations from the 2018 expedition (Shevtsova et al., 2020c). In addition, for ensuring temporal validation, we compared LAVESI-based larch AGB values in 2001 and 2016 CE with AGB estimations from field and Landsat data from 2001 and 2016 (Appendix C, table C1). For this purpose, we calculated the percent of the total AGB using the 2018 larch AGB of the samples and took the same percent of the total AGB in 2001 and 2016 derived from Landsat-based estimations (Shevtsova et al., 2021). Thus, we got estimates of larch AGB for 2001 and 2016 based on field and Landsat data, which we compared to our simulated estimations for 2001 and 2016 CE.

3 Results

3.1 Dynamics and spatial distribution changes of tree above-ground-biomass

3.1.1 Predicted rates of tree above-ground biomass changes at the plot level

We selected representative focus sites along the vegetation gradient and tracked how larch AGB changes yearly from the present (2020 CE) to 3000 CE under scenarios of RCP 2.6, 4.5, 8.5 with and without cooling. Temporal tree AGB changes of currently forested areas were investigated at two sites: EN18001 and EN18024, which are west and east of the Lower Lake Ilirney, respectively (Fig. 5). Changes in tree AGB have a similar character at both sites, tending generally to fluctuate around a certain value.

In detail, under RCP 2.6 without cooling tree AGB generally increases (with big fluctuations) in the beginning of the 21st century (until around 2050 CE) reaching its highest values of 1.5-1.6 kg m^{-2} (Fig. 7), followed by a decrease until 2300 CE with its lowest AGB of around 1 kg m^{-2} From 2300 CE to 2700 CE the tree AGB fluctuates differently on the two inspected sites, showing increase until 1.5 kg m^{-2} in around 2650 CE and gradual decrease afterwards (EN18001) or faster increase until 1.3 kg m^{-2} in around 2500 CE, fast decrease until 0.9 kg m^{-2} in around 2650 CE and fast increase again (EN18024). Under RCP 4.5 without cooling the highest tree AGB is reached in around 2500 CE (EN18001) or around 2250 CE (EN024), which is 1.6 kg m^{-2}. In this scenario tree AGB follows generally the same fluctuation pattern as under RCP 2.6. Under RCP 8.5 it takes more time for larch AGB to reach the highest value, but the values themselves fluctuate less and on the site EN18024 it is even clearly an increasing trend to observe. In scenarios without cooling tree AGB firstly increases until 2300 CE, reaching 1.5-1.6 kg m^{-2} and then decreases gradually with less fluctuations, reaching around 0.75 kg m^{-2}, which is even less than in 2000 CE (beginning of investigated period).

However closer to 3000 CE under the warmest scenario RCP 8.5 second tree AGB increase is predicted, which is not the case under RCP 2.6 and 4.5.

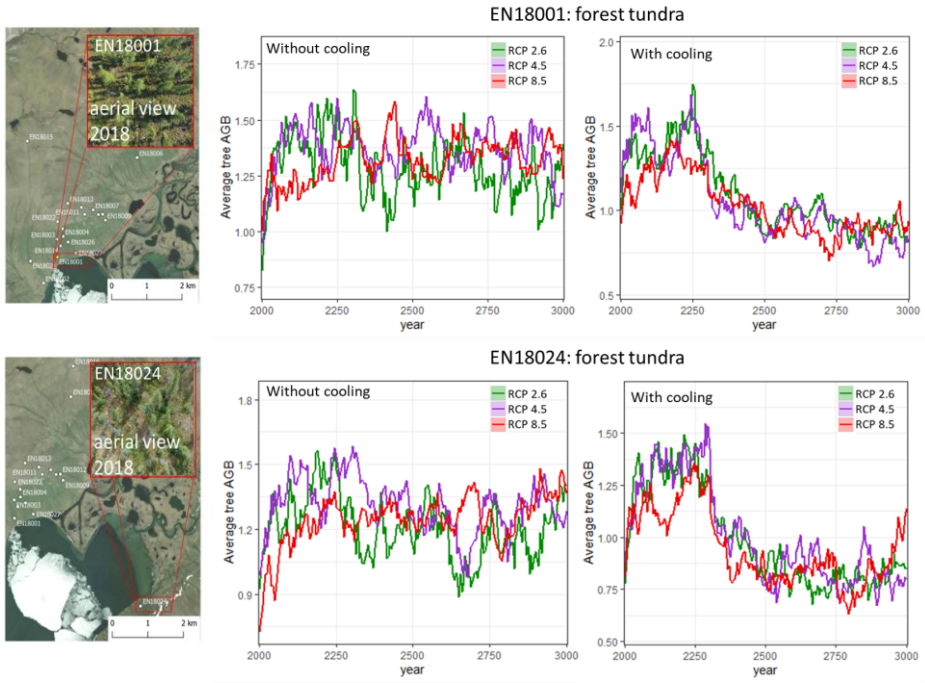

Figure 5. Temporal changes in LAVESI-based larch above-ground biomass (AGB) of the forest tundra sites from 2000 to 3000 CE. Source of background maps: ESRI World Imagery.

We have chosen several representative sites of open graminoid (hummock) tundra close to and far from the current treeline (Fig. 6). The trend in tree AGB change for the sites close to the current treeline is similar to the trend on the forested sites with the difference that it takes longer for tree AGB to increase, because of the tree establishment phase. On the closest to the current treeline site (EN18011) the increase in tree AGB starting from the 2000s, whereas on the site a little bit further away from the current treeline (EN18013) strong increase in tree AGB is predicted to start later after around 2100 CE. Until stabilisation, larch tree AGB steadily increases until 2250 CE for EN18011 and until 2500 CE for EN18013. After that in both cases tree AGB fluctuate about a certain value, depending on the RCP scenario. Here the highest values are reached under RCP 8.5 (1.1-1.3 kg m^{-2}), moderate under 4.5 (0.9-1.2 kg m^{-2}) and the lowest under RCP 2.6 (0.6-1 kg m^{-2}). Under scenarios with cooling after 2300 CE tree AGB as on the currently forested sites increases before cooling starts and decreases afterwards, but in contrast, staying at higher values, then in the beginning of the 21st century. On the sites, far from the treeline tree AGB is reaching generally lover values and it takes even longer for tree AGB to stabilise after increase. Under cooling scenarios tree AGB generally stays close to 0 kg m^{-2}, rising before the cooling and drop back to very little values after cooling.

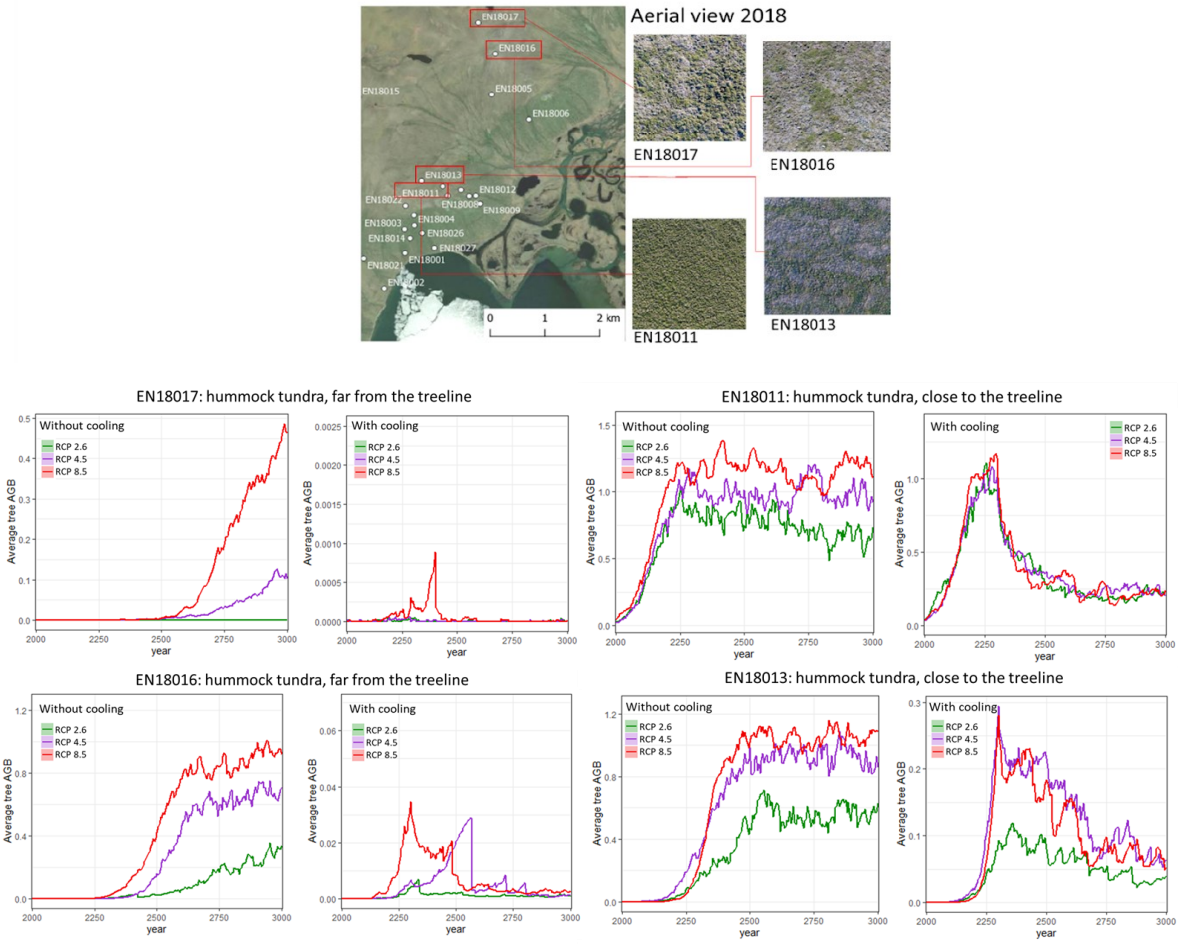

Figure 6. Temporal changes in LAVESI-based larch above-ground biomass (AGB) of the hummock tundra sites from 2000 to 3000 CE. Source of the background map: ESRI World Imagery.

The last group of sites used to investigate tree AGB changes include poorly vegetated open tundra with lichen communities, herbs, and *Dryas* sp. dominance (Fig. 7). On all three sites the highest value of tree AGB is predicted to be around 1 kg m^{-2} under RCP 8.5 (with no cooling). For the site EN18022, which is very close to the current treeline the trend in tree AGB changes is similar to the described before fast increase and then stabilisation (like on the tundra sites with hummock vegetation, close to the treeline), whereas for the sites with very poor current vegetation up in the hills increase in tree AGB is predicted only in the second half of millennia and only under RCP scenarios 4.5 and 8.5 without cooling. If the cooling event occurs, on both sites tree establishment is disabled. On the site, close to the treeline, tree AGB increases to 0.4 kg m^{-2} until 2300 CE in the cooling scenarios with a following decrease. This trend is also similar to that on the graminoid tundra sites, closer to the treeline.

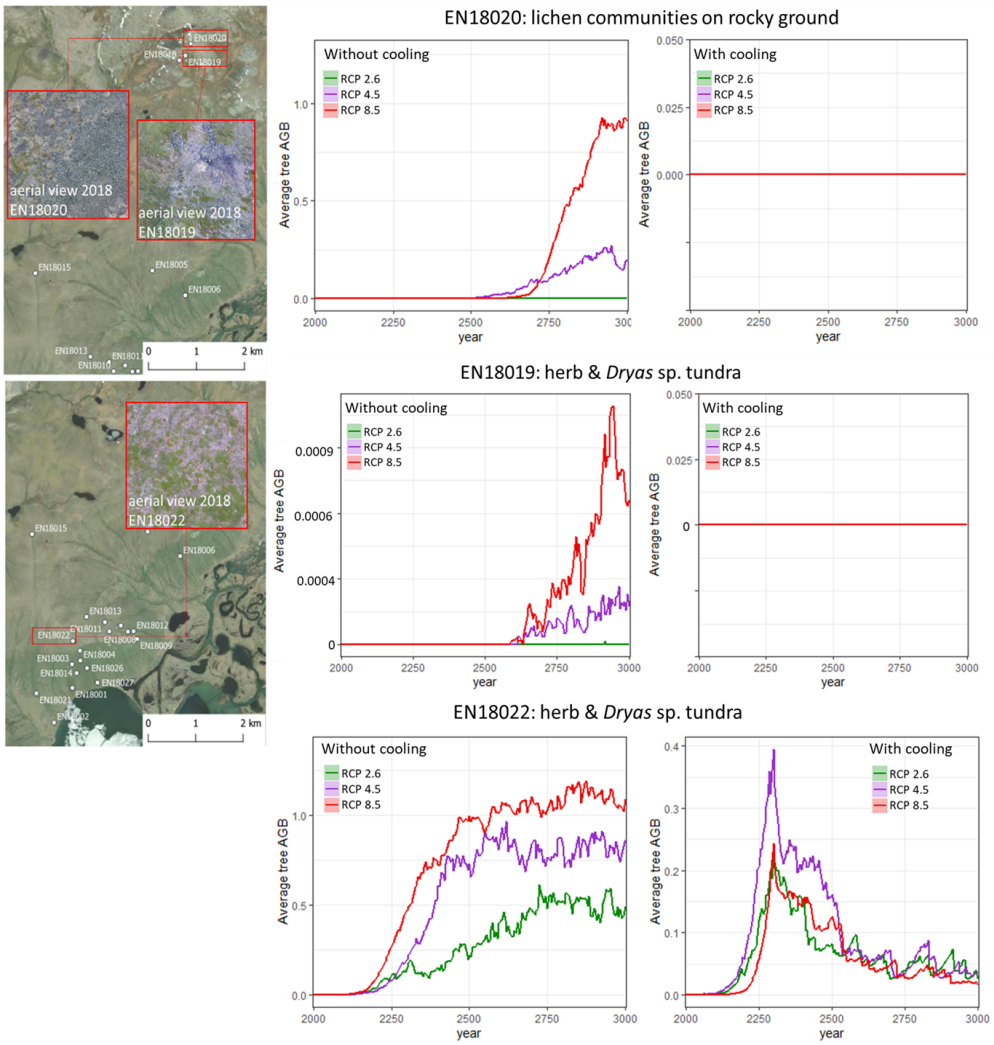

Figure 7. Temporal changes in LAVESI-based larch above-ground biomass (AGB) of the poorly vegetated tundra sites from 2000 to 3000 CE. Source of background maps: ESRI World Imagery.

3.1.2 Temporal and spatial changes of tree above-ground biomass at the landscape level

The average (median) larch AGB across the whole study region for all scenarios is predicted to stay close to 0 kg m^{-2} until around the year 2550 CE (Fig. 8). From 2550 CE, it increases exponentially in the warm RCP 8.5 scenario reaching 0.009 kg m^{-2} by the year 3000 CE. The increase in larch AGB is delayed under the RCP 4.5 scenario reaching 0.008 to 0.009 kg m^{-2} by the year 3000 CE. Under RCP 2.6, larch AGB is predicted to stay around 0 kg m^{-2} in its median during the investigated period. In the cooling scenarios warming occurs only until 2300 CE, until which average (median) tree AGB in the region stays close to 0 kg m^{-2} in every case. The average tree AGB rates of increase are the strongest in the first 300 years of the 21st century: for 2020-2100 CE they are 48.79±0.32 (RCP 2.6), or 62.43±0.21 (RCP 4.5), or 33.06±0.07 (RCP 8.5) t yr^{-1}; for 2100-2200 CE they are 60.68±0.41 (RCP 2.6), or 47.73±0.11 (RCP 4.5), or 100.06±0.01 (RCP 8.5) t yr^{-1}; for 2200-2300 CE

they are 47.68±0.44 (RCP 2.6), or 84.86±0.16 (RCP 4.5), or 80.39±0.81 (RCP 8.5) kg yr^{-1}; for 2300-3000 CE they are 15.56±0.02 (RCP 2.6), or 39.31±0.13 (RCP 4.5), or 63.52±0.09 (RCP 8.5) t yr^{-1}; for the whole study region. In case of cooling after 2300 CE tree AGB decrease from 2300 to 3000 CE with the rates of -18.13±0.19 (RCP 2.6), or -23.46±0.14 (RCP 4.5), -25.25±0.004 (RCP 8.5) t yr^{-1}.

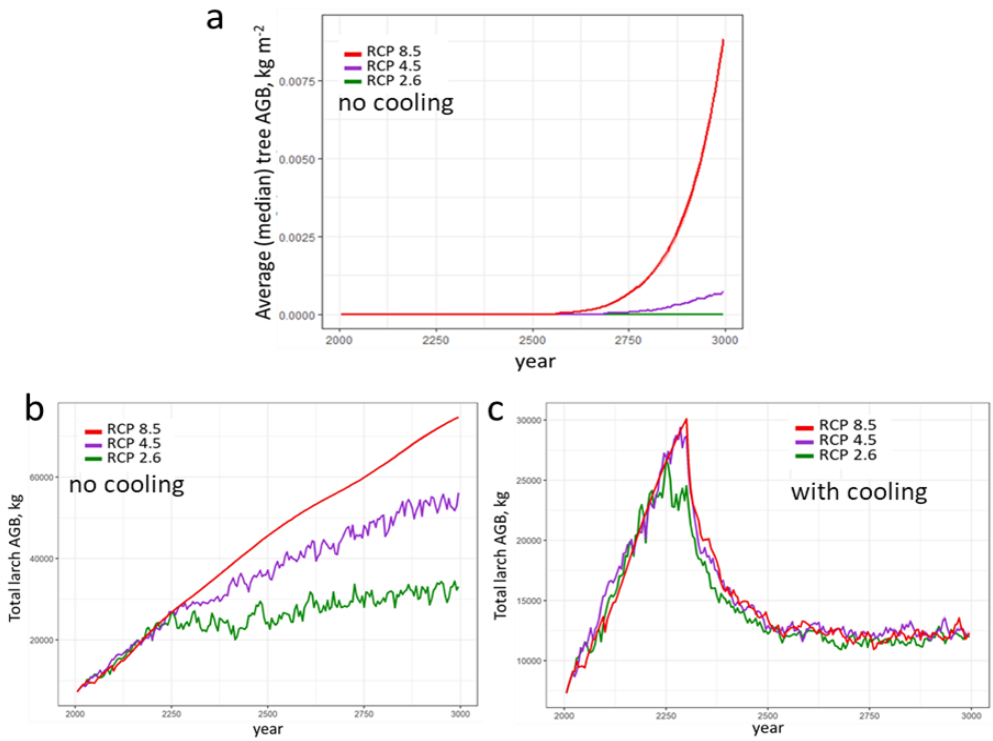

Figure 8. Predictions of temporal change of overall: a – average (median) larch above-ground biomass (AGB) in the study region under different climate scenarios until 3000 CE, b – total larch AGB under scenarios without cooling in the study region under different climate scenarios until 3000 CE, b – total larch AGB under scenarios with cooling after 2300 CE in the study region under different climate scenarios until 3000 CE.

The detailed observations at the plot level (Fig. 9) depict population dynamics that cause the spatial distribution and spreading of larch AGB (Fig. 11 and Fig. 12). Following the simulations, increase in larch AGB gradually occurs from 2020 to 3000 CE independent of the RCP scenario. Until 2200 CE it is mostly associated with densification of existing tree stands. Starting from the year 2200 CE larch is predicted to spread more across the landscape, colonizing upslope areas. After 2400 CE in case of RCP 2.6 larch tree stands are predicted to become sparser, while establishment of larch tree stands is continuing in the newly colonised areas. By the end of the investigated period differences between the RCP scenarios are in the scales of tree AGB in the same areas on the landscape, as well as,

in speed of spreading northwards: the highest values tree AGB and the most northward spread are observed in the scenario RCP 8.5.

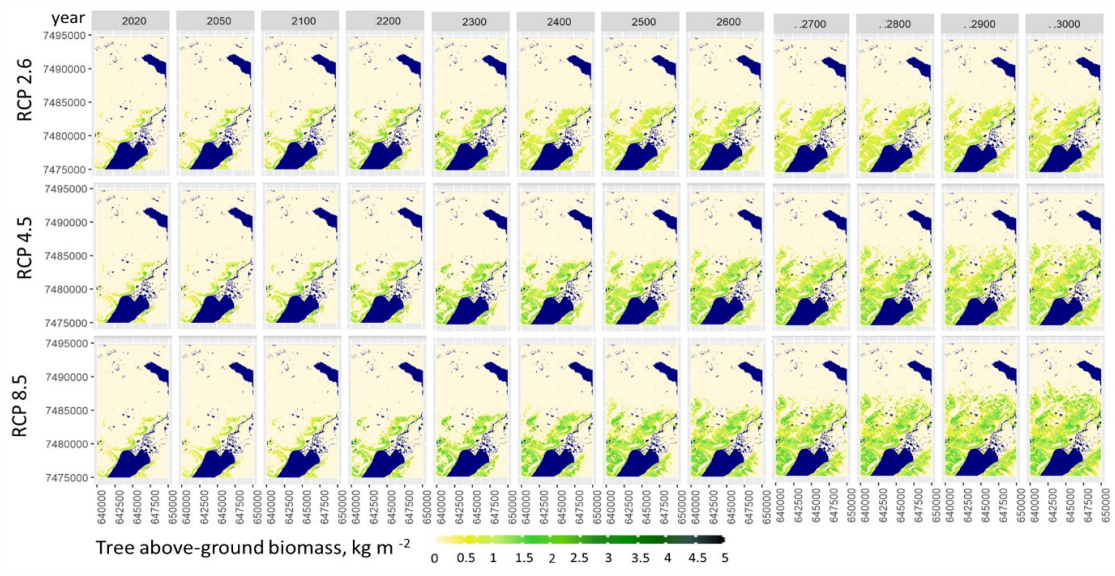

Figure 9. Larch above-ground biomass (AGB) predicted for years 2020-3000 CE under three representative concentration pathway (RCP) scenarios.

In the cooling scenarios before 2300 CE tree AGB increase is similar to that in the scenarios without cooling (Fig. 10). After 2300 CE there is a vast decrease in the larch tree AGB, finally reaching lowest values in the whole area in every cooling scenario.

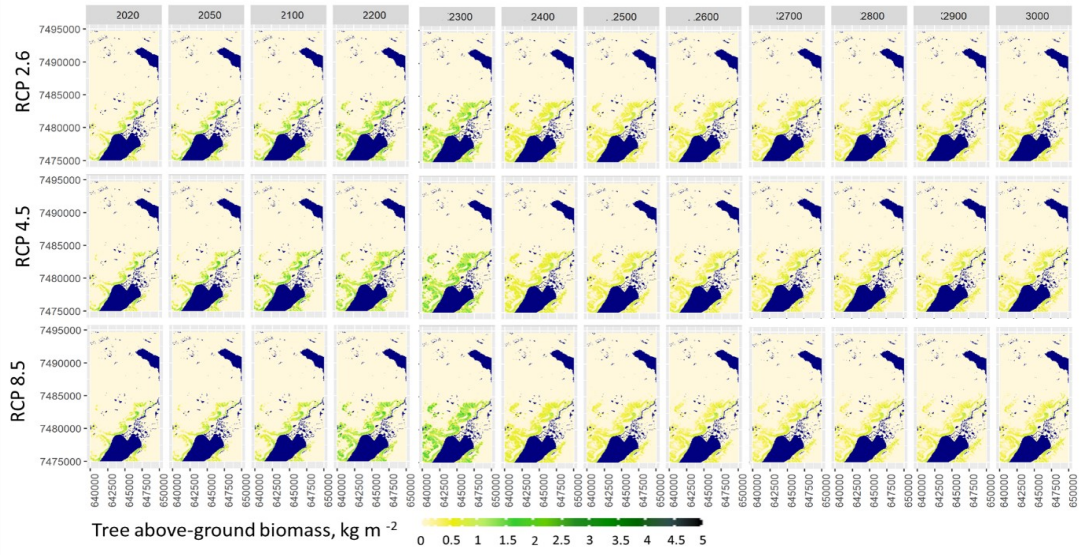

Figure 10. Larch above-ground biomass (AGB) predicted for years 2020-3000 CE under three representative concentration pathway (RCP) scenarios with cooling after 2300 CE.

Changes in larch AGB predicted between 3000 and 2020 for most currently forested areas are predicted to reach the rates of 0.0005-0.002 kg m^{-2} yr^{-1} (0.5-2 kg m^{-2} per 980 years, Fig. 11) depending on the RCP scenario with the lowest under RCP 2.6 and the highest under RCP 8.5. Under scenarios with cooling, the rates of increase are not exceeding 0.0005 kg m^{-2} yr^{-1} and decrease -0.0005 kg m^{-2} yr^{-1}. An increase is predicted for mostly newly colonised areas, and a decrease for the currently existing tree stands. In the period until 2300 CE, all scenarios with or without cooling similar increase in the tree AGB up to 0.002 kg m^{-2} yr^{-1} is predicted (Fig. 12).

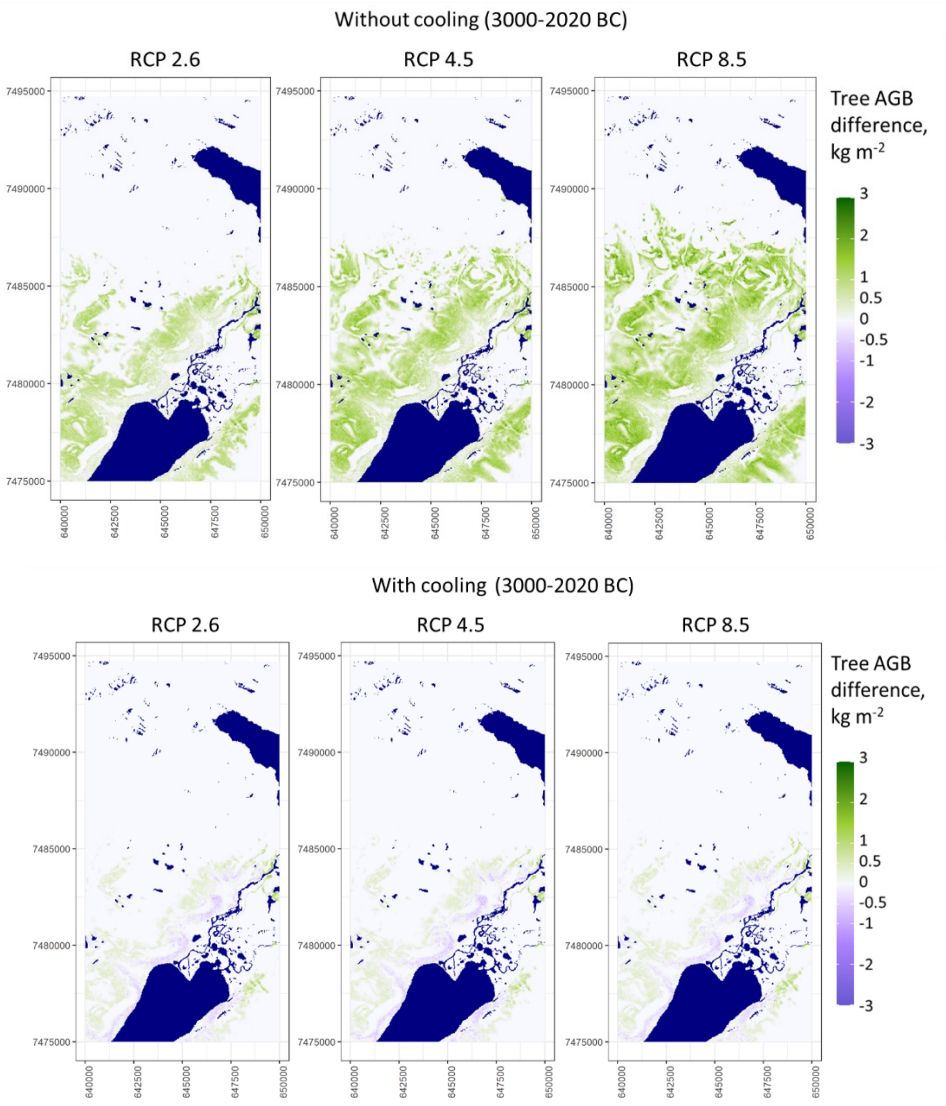

Figure 11. Predicted larch above-ground biomass (AGB) change between 2020 and 3000 CE in the vicinity of the Ilirney lake system under three representative concentration pathway (RCP) scenarios with cooling and without cooling after 2300 CE.

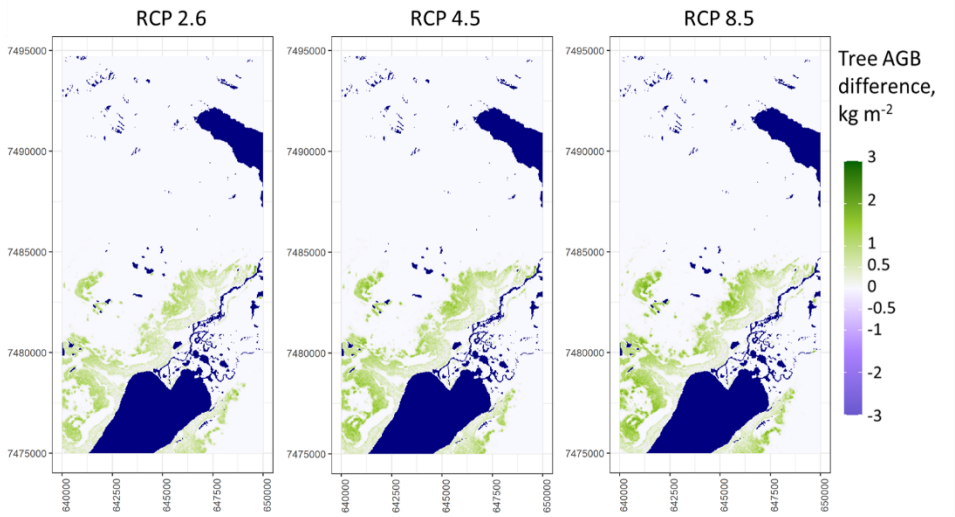

Figure 12. Predicted larch above-ground biomass (AGB) change between 2020 and 2300 CE in the vicinity of the Ilirney lake system under three representative concentration pathway (RCP) scenarios with cooling or without cooling after 2300 CE.

With respect to temporal and spatial dynamics of forest tundra in comparison to open tundra, our results are showing that the higher the temperatures (e.g., RCP 8.5 in comparison to RCP 2.6), the higher percent of forested areas and lesser fluctuations of this percent during the investigating period (Fig. 13). Under RCP 8.5 forest tundra is predicted to occupy up to 39% of the investigated region by the end of the investigated period (3000 CE), whereas under RCP 4.5 it is predicted to occupy around 33% of the whole investigated region, under RCP 2.6 forest tundra is predicted only to occupy up to around 25% (Fig. 14). In case of cooling scenarios, the highest percent of forest tundra is reached in 2300 CE, which depending on the RCP scenario would be 22% (RCP 2.6), 23% (RCP 4.5) or 24% (RCP 8.5). After the cooling started, forested areas are predicted to decrease to the level of 2-3% of the investigated region.

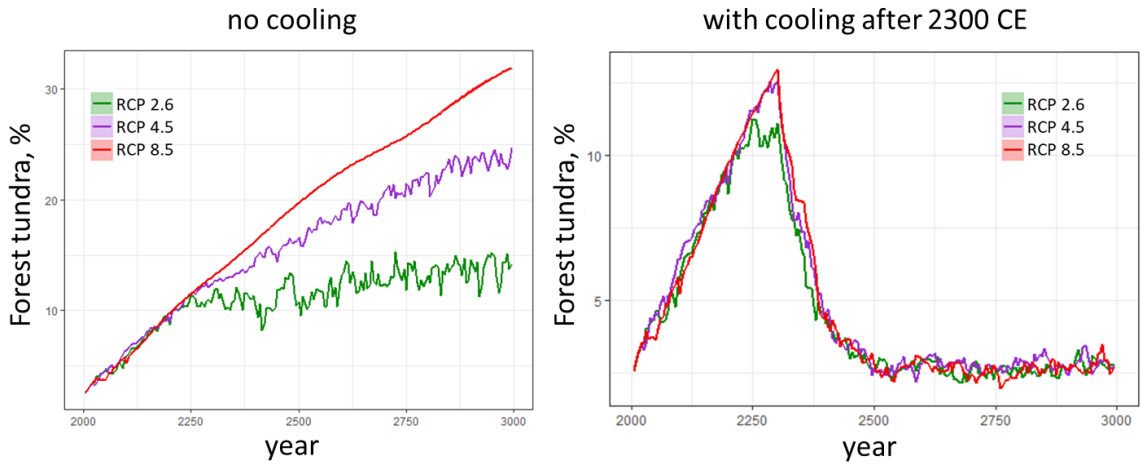

Figure 13. Potential future temporal dynamics of forest tundra (%) in the vicinity of lakes Ilirney from 2000 to 3000 CE.

Spatial changes of forest tundra in the investigated area under RCP scenarios without cooling are similar to the pattern of general tree AGB changes, also accounting for saplings and trees standing in the open tundra (Fig. 14).

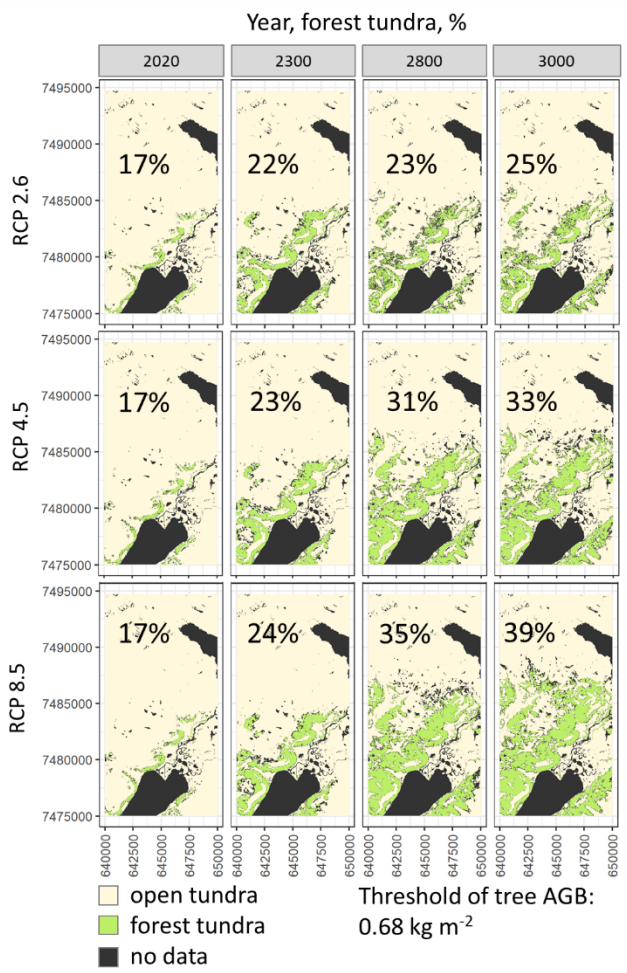

Figure 14. Spatial distribution of forest tundra through the investigated period in the vicinity of lakes Ilirney with portion of forested areas given in % for each RCP scenario and year.

3.2 Spatial and temporal validation of the contemporary larch AGB

The visual inspection of the LAVESI-simulated AGB in the quasi-true topographical landscape through the 1000 years revealed realistic spatial patterns in 2010 CE. The analysis of the simulated spatial distribution of tree stands for the year 2010 CE shows that 205 (8%) out of the 2426 sampled plots in the non-forested areas contain trees higher than 2 m and 174 (7%) - vice versa do not contain simulated trees, whereas forested in reality (Fig. 15). These falsely simulated and falsely not simulated tree stands (FSTS) are generally found at similar elevation, slope degree and TWI to the currently present estimated tree stands.

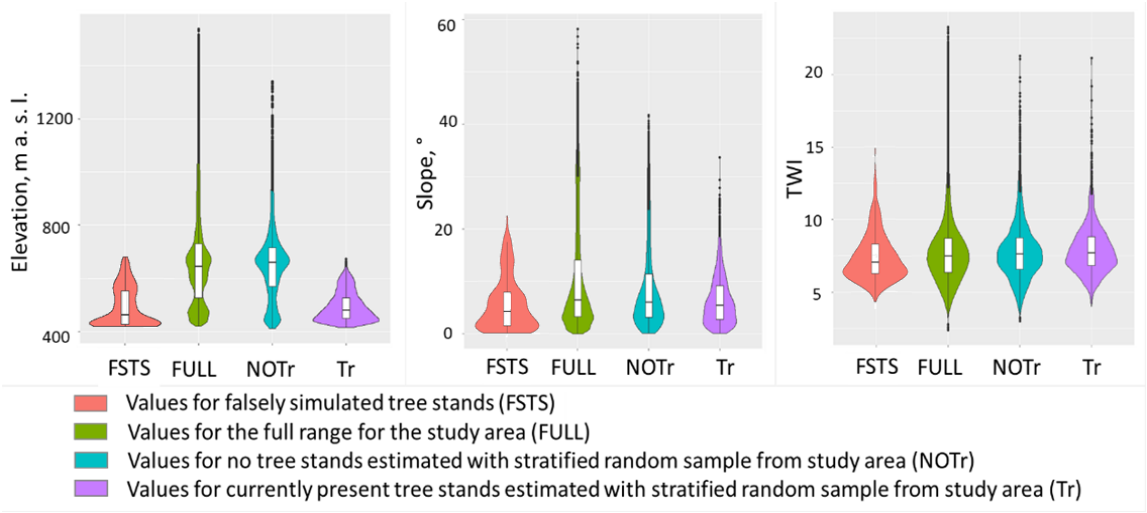

Figure 15. Distribution of values of topographical parameters in the areas of falsely simulated tree stands (FSTS) in comparison to the full range of values for the study area (FULL) and stratified random sample dataset (NOTr; Tr).

Next, we assessed simulated larch AGB values in 2018 CE at local scale with the 2018 field-based estimations (Shevtsova et al. 2020c) from 25 expedition sample plots (Fig. 16). The general magnitude of simulated larch AGB is in a similar range as the field larch AGB estimations with some exceptions. Considerably lower biomass is simulated for the extremely high AGB sites in the forest tundra, where average tree AGB is 3-5 kg m^{-2} while only 0-2 kg m^{-2} was simulated. Additionally, the simulation predicts tree presence at sites where instead of trees, high and dense *Pinus pumila* (Pall.) Regel shrubs are found (site EN18009), a species not yet considered in the model code.

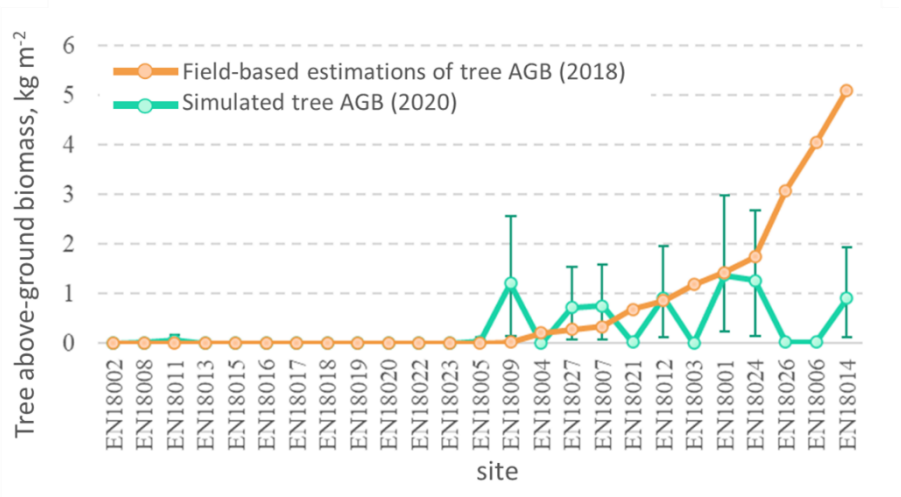

Figure 16. Larch above-ground biomass (AGB) in the field sample sites of the 2018 expedition. Comparison of field-based estimations with simulated values shows roughly the same trend, but simulation underestimates AGB for sites with the highest larch AGB and overestimates AGB for sites with a high shrub dominance (e.g., site EN18009).

The estimated temporal tree AGB change shows that observed changes in larch AGB were generally very small over the 15 years, which is well captured by the simulations (Table 3). The simulated rates of change in AGB are generally similar for all forest tundra sites (0.01–0.02 kg m^{-2} yr^{-1}) with an exception, where simulated tree AGB change is negative (EN18027). Field and Landsat-based estimations of tree AGB change are generally slightly lower or higher.

Table 3. Change in larch above-ground biomass (AGB), estimated using simulation results from the LAVESI model (RCP 2.6, 4.5 and 8.5) and by using field and Landsat data on the five forest tundra (ft) and one open tundra (ot) expedition sites, for which both field and Landsat-based AGB, as well as LAVESI simulated tree AGB are available.

Site	Larch AGB, kg m^{-2}		Change in larch AGB, kg m^{-2} (2016-2001)		Estimated rate of change in larch AGB per year, kg m^{-2} yr^{-1}	
	LAVI, 2015	LAVESI, 2000	LAVESI (2015-2000)	Field & Landsat-based (2016-2001)	LAVESI	Field & Landsat-based
EN18001 (ft)	1.274±0.233	1.037±0.247	0.237±0.680	0.133	0.016±0.045	0.009
EN18002 (ot)	0.004±0.004	0.002±0.002	0.002±0.009	0	0±0.001	0
EN18014 (ft)	0.859±0.119	0.632±0.107	0.228±0.320	0.074	0.015±0.021	0.005
EN18021 (ft	0.021±0.005	0.015±0.005	0.006±0.014	0.413	0±0.001	0.028
EN18026 (ft)	1.206±0.121	0.009±0.006	1.196±0.179	0.61	0.080±0.012	0.041
EN18027 (ft)	0.017±0.012	0.554±0.068	-0.538±0.113	0.047	-0.036±0.008	0.003

4 Discussion

4.1 Future dynamics of tree AGB at a plot level

Generally, the above-ground biomass (AGB) of *Larix cajanderi* in our simulations is predicted to increase from its current state, stabilising or increasing further until 3000 CE for all sites under the climate warming RCP scenarios without cooling. There are fluctuations in areas already forested in 2020 and sites, closer to the current treeline, revealing typical population dynamics. When comparing population dynamics in the different RCP scenarios in the beginning of the 21st century, there is clear self-thinning of the tree stands to observe (strongly prominent under the warmest climate conditions of RCP 8.5), which can be explained by the high individual tree competition (Wieczorek et al., 2017). Under climate scenarios with cooling after 2300 CE, tree AGB generally declines with the start of cooling, which indicates forest retreat. On the currently sparsely vegetated sites trees are not establishing in scenarios with cooling.

The patterns of tree establishment in this study follow the typical primary succession. On the currently forested plots (Fig. 7), we see that simulated larch individuals (as AGB) rapidly increase in number (forest densification or tree infilling) until stabilise with periodic episodes of tree-stand thinning (fluctuations in the tree AGB). On the open tundra plots with graminoid vegetation and close to the treeline, we see larch colonising new areas upslope with a time lag (steady increase in larch AGB, starting after 100-500 years depending on the position of the site), where after the arrival of seeds saplings develop and in the next stage a cohort establishes. Once trees establish under warming tree AGB develop exponentially, which characterises densification of tree stands. In case of cooling after 2300 CE tree stands show dieback, which is slower once tree stands are established, they can survive longer. For the currently forested sites exponential increase starts already in the beginning of the investigated period (2000s) and takes about 50 years to reach the stable state, whereas after cooling decrease takes about at least 500 years until the stabilisation. On the open tundra sites both processes take longer, but still tree stand establishment (300-375 years) happens quicklier as tree stand dieback (450 years and more). At the currently sparsely vegetated sites tree establishment is mostly not reaching stabilisation phase until the end of the investigated period, which leads to faster diebacks, when cooling occurs.

Simulated recent (2000–2015) larch AGB change rates (0.016-0.08 kg m^{-2} yr^{-1}) on the most forest tundra sites were faster in comparison with recent (2000–2015) larch AGB change rates (0.006 kg m^{-2} yr^{-1}) in the upper treeline zone of another Russian subarctic mountainous treeline ecotone (Polar Ural; Devi et al., 2020). Future (2020–3000) larch AGB change rates (0.0005-0.002 kg m^{-2} yr^{-1}) are much lower than recent, what can be explained by nonlinear tree AGB dynamics nature, where with the change of climate forest tundra expand fast in the first two centuries and stabilise, having phases of thinning within the rest of the investigated period until 3000 CE.

The LAVESI model is now set up to simulate at high spatial resolution landscape level, even in mountainous terrain with outputs of *Larix cajanderi,* species-specific above-ground biomass and stem density optimized on larch forest in central Chukotka. Assessing the LAVESI model predictive power was challenging. The model made a moderately good prediction of the current larch AGB state, recent temporal changes, and the general spatial distribution. However, as with many other spatially explicit models, it performs well at a general level but fails in reproducing some details (e.g., models used in Ito et al., 2020). Particularly, the representation of the height structure of the tree stands and the presence/absence of tree stands contradict real observations, and recent changes in larch AGB are underestimated in comparison to field-based estimations.

The representation of tree height structure is generally skewed in the direction of a vast production of small seedlings and trees under 2 m, with few individuals higher than 2 m. This results in a height structure, which is different from observed one during fieldwork in one year. The amounts of larch saplings can largely differ from year to year (Abaimov et al., 1998), what could also mean

that the small number of saplings observed could be much higher in the previous or next years. The model does not include such variation of high crop years so it will be overestimating in some and underestimating in other years, but the mean fits observation. However, predicted larch AGB in kg m^{-2} on 15-m radius plots is generally similar to the field estimations, although for some field sites with relatively high larch AGB from field estimations, simulated larch AGB was too low (Fig. 5). This can explain why there is a slight underestimation of larch biomass with LAVESI. Thus, in general, we can expect a higher larch AGB rate in some areas of the future landscape in the vicinity of the Ilirney lake system.

4.2 What are the future dynamics of tree AGB at the landscape level?

With the updated LAVESI model, we could predict larch AGB dynamics (general increase) and forest spreading upwards and northwards on the landscape scale. The time point when the current tree stands start widely noticeably upslope expansion is around 2200 CE. As expected, highest rates of forestation from today to 3000 CE (Fig. 8) are predicted under RCP 8.5. In every scenario, we could see a gradual increase in larch AGB with slight diebacks in currently forested areas by the end of the investigated period. These results of a first general increase (and stabilisation in the next centuries) in tree AGB in the subarctic region, even under RCP 2.6 where air temperature and precipitation changes are the smallest, and a higher increase of tree AGB under RCP 4.5 and 8.5, are in accordance with previous findings that vegetation changes were initiated during the past three decades of changing climate conditions and might be expected to be even greater with additional greenhouse gases in the atmosphere (Callagan & Carlsson, 1997).

A time required for tree stands to respond to climate changes (time lag) is hard to define based only on our results, considering that the time for tree stands to establish in the new areas is included. However, on the general graph for the investigated region (Fig. 8), we observe the lag is shortest for the RCP 8.5 scenario, which is about 500 years if considering the region of investigation as a whole area, but smaller if considering different parts of the region. It can be attributed as a clear response to the increase in July and January air temperature, as well as to the annual precipitation increase in the early 2000s. We also observe a time lag of about 200 years in case of cooling scenarios after cooling. Our results without cooling are in accordance with Chapin and Starfield (1997), who conclude that regardless of warming rate there will be substantial lags in forest expansion (150–250 years in Alaska for 5% of forest establishment) and other models, which also predict time-lagged vegetation change, highlighting migration and succession processes (Epstein et al., 2007).

A comparison of our results with existing simulation results from studies of different future vegetation changes is challenging because most of the models are global and focus on other ecosystem parameters, such as global tree cover (Gonzales et al., 2010), net ecosystem exchange of CO_2,

which includes net primary production as related to vegetation (Zhang et al., 2013), and albedo change (Zhang et al., 2013). However, predicted by our model future changes in vegetation are in the agreement with some mentioned above previously investigated ecosystem parameters. For example, Zhang et al. (2013) predict no change in albedo or latent heat flux until 2080 in central Chukotka, particularly in the Ilirney lakes area. This is in general agreement with our predictions of tree AGB, which start to exponentially increase since the beginning of the investigated period (2000s) and would probably cause differences in albedo and latent heat flux strong enough to be captured by a global model, such as Zhang et al (2013) used. Two global vegetation models in Sitch et al. (2008) show an increase in tree cover from 20 to 50% and higher in central Chukotka from 1860 to 2099, but two other global vegetation models in the same study show no or much lower (1–20%) changes in tree vegetation cover in our study area, which would be more in line with our predictions of expansion of the forest tundra (areas with tree AGB > 0.68 kg m^{-2}, less than 20 %) until 2099 CE.

Using the individual tree-based gap model University of Virginia Forest Model Enhanced (UVAFME), Shuhman et al. (2014, 2015, 2017) simulated forest response to climate change also for boreal Russia. Foster et al. (2015, 2017) have further adapted the UVAFME for use in the North American Rocky Mountains, as well as interior Alaska (Foster et al., 2019). The UVAFME model runs are set up for large regions with large parameter ranges of the input data. The simulations in terms of fitting species composition were successful in the different regions highlighting that climate change changed the species compositions. LAVESI explicitly simulates larch AGB, and we simulated tree growth at a high 30 m grid cell resolution, downscaled from a 20x20 cm environmental grid with continuous tree positions in complex mountainous terrain. By using the slope angle and TWI in the tree growth model, one efficiently introduces the complex impact of the local environment in an abstract way. Snow cover shielding in winter is important for small individuals, so steep slopes prevent snow to accumulate and are dryer in summer (Kirilenko & Solomon, 1998). Whereas flat slopes do not drain, accumulate too much water and are hence frequently waterlogged.

In case if the actual individual tree growth in a certain year is reduced, the trees' competition for resources is hampered and thus its mortality is increased. As a consequence, tree stands can only establish at favourable locations, and the impact for a study region can be tuned using different proportions of the two models, slope angle and TWI, to fit observations.

Although LAVESI simulations of the current state tree AGB are mostly in accordance with regard to tree stands shown on an ESRI high spatial resolution image, closer visual inspection reveals that several areas which currently have tree stands are not present in LAVESI and vice versa. Thus, one of the areas where forests are not simulated by LAVESI is polygonal tundra, which is one of the most challenging areas to simulate larch tree stands. The mechanism behind the simulations relies on the general presence of trees in relation to topography, derived from a DEM. However, the DEM used only had a 90-m spatial resolution and the complex structure of the polygonal tundra, with small,

elevated areas of polygonal forest tundra and occasional tree stands, could not be captured by the DEM. Moreover, assessment of larch AGB in the polygonal tundra is rather approximate since there were no field samples collected in this vegetation type in the study region.

Another common pattern of tree absence in LAVESI simulations where trees should grow can be observed in the forested areas of steep slopes in combination with high elevation on the transition from forest tundra to pine shrub tundra to graminoid tundra. It probably arises from the nature of the topography models used to restrict larch occurrence and could be improved by further parameterisation. On the other hand, it could be unrelated to the implemented parameters of LAVESI and depend on external factors. Future implementation of biotic factors such as competition between larch and pine in the model could give a better accuracy in the simulated larch distribution. A similar explanation can be attributed to the tree stands that are simulated in the areas of observed open tundra. In fact, Falkowski et al (2010) documented that diverging growth projections typically occurred for small stands with highly variable forest structure and that growth projections seem to be more influenced by errors in forest structure than by errors in species composition.

5 Conclusions

The results in this first built-up of LAVESI at landscape level in mountainous terrain, simulating larch AGB changes in central Chukotka from nowadays to 3000 CE predict an increase in tree AGB and treeline advance into the tundra (upslope and northwards) under RCP scenarios 2.6, 4.5 and 8.5 without cooling after 2300 CE. The mildest climate changes under RCP 2.6 would result in the slowest increase and less spreading of larch compared to scenarios with more pronounced warming (e.g., RCP 4.5 and 8.5). In scenarios with cooling after 2300 CE in contrast rapid treeline retreat is observed and even decrease in tree AGB in the currently forested areas to the rates, lower then present but still finally covering larger areas than in 2000.

Tree stands are predicted to develop differently in response to climate change in currently forested areas and open tundra and depending on RCP scenario. For the forested areas we predict more fluctuations in tree AGB following typical tree stand structure development with densification, stabilisation, and tree stand thinning processes. For non-forested areas we predict the same pattern of ecological development, but after tree establishment in the open areas. For open tundra tree stands, establishment is predicted to start after 100-500 years depending on the distance of the area from the current treeline. The average rates of AGB change are higher in the first 300 years of the 21st century and getting lover towards 3000 CE. Thus, for 2020-2100 CE they are 48.79±0.32 (RCP 2.6), or 62.43±0.21 (RCP 4.5), or 33.06±0.07 (RCP 8.5) t yr^{-1}; for 2100-2200 CE they are 60.68±0.41(RCP 2.6), or 47.73±0.11 (RCP 4.5), or 100.06±0.01 (RCP 8.5) t yr^{-1}; for 2200-2300 CE they are 47.68±0.44 (RCP 2.6), or 84.86±0.16 (RCP 4.5), or 80.39±0.81 (RCP 8.5) kg yr^{-1}; for 2300-

3000 CE they are 15.56±0.02 (RCP 2.6), or 39.31±0.13 (RCP 4.5), or 63.52±0.09 (RCP 8.5) t yr^{-1}; for the whole study region. In case of cooling event the highest possible forest expansion is predicted to reach not more than 10% of the investigated region and tree AGB for the whole region decrease from 2300 to 3000 CE with the rates of -18.13±0.19 (RCP 2.6), or -23.46±0.14 (RCP 4.5), -25.25±0.004 (RCP 8.5) t yr^{-1}.

LAVESI can simulate larch AGB values at the landscape level, reflecting patterns of current tree stand distribution fairly good, but slightly underestimating the observed values of tree AGB, which could be improved in the future. A comparison with other studies was challenging but revealed some agreements, as well as disagreements. However, LAVESI can reveal non-linear changes and accurately predict tree distribution, which would not be possible with a simple predictive model using climate envelopes for species presence/absence.

Data availability

The current version of LAVESI is improved and updated for the use in this study. It is publicly available on GitHub:
https://github.com/StefanKruse/LAVESI/tree/8976dfd078f9fecba624c8e2bec148006d5c0fa4.
The final version will be stored and linked with a permanent DOI on acceptance of the manuscript.

Acknowledgements

This study has been supported by the German Federal Ministry of Education and Research (BMBF), which enabled the Russian-German research programme “Kohlenstoff im Permafrost KoPf” (grant no. 03F0764A), by the Initiative and Networking Fund of the Helmholtz Association and by the ERC consolidator grant Glacial Legacy of Ulrike Herzschuh (grant no. 772852).

References

Abaimov A P, Karpel BA, Koropachinsky I Yu: On habitat borderlines of Siberian larch species. Bot Zhurn 65:118–120, 1980. [in Russian]

Abaimov AP, Lesinski JA, Martinsson O, Milyutin LI: Variability and ecology of Siberian larch species. Swedish University of Agricultural Sciences, Department of Silviculture, Reports 43, Umeå, 1998.

Abaimov, A P: Geographical distribution and genetics of Siberian larch species, in: Permafrost Ecosystems – Siberian Larch Forests, vol. 209, edited by: Osawa, A., Zyryanova, O. A., Matsuura, Y., Kajimoto, T., and Wein, R. W., Springer, Netherlands, Dordrecht, 41–58, 2010.

Arkhipov, Serguei M; Kotlyakov, Vladimir; Punning, Ya-M K; Zogorodnov, V; Nikolayev, V I; Zagorodnov, V S; Macheret, Yu Ya; Vaikmaye, R; Barkov, Nartsiss I; Korsun, S A; Korotkevich, V; Morev, V A; Evseyev, A V; Vostokova, T A; Andreev, Andrei A; Klementyev, Oleg L; Korotkevitch, Y S; Stiévenard, Michel; Sinkevich, S A; Samoylov, O Yu; Gordienko, F G; Korsun, A V; Tiugu, K R; Arkipov, S M: Deep drilling of glaciers: Russian projects in the Arctic (1975-1995). Institute of Geography, Russian Academy of Sciences, Moscow, PANGAEA, https://doi.org/10.1594/PANGAEA.707363, 2008.

Bergengren, J.C., Thompson, S.L., Pollard, D. et al.: Modeling Global Climate–Vegetation Interactions in a Doubled CO2 World. Climatic Change 50, 31–75, https://doi.org/10.1023/A:1010609620103, 2001.

Bonan, G.B., Chapin, F.S. & Thompson, S.L.: Boreal Forest and tundra ecosystems as components of the climate system. *Climatic Change* **29,** 145–167, https://doi.org/10.1007/BF01094014, 1995.

Bonan, G.B., Levis, S., Sitch, S., Vertenstein, M. and Oleson, K.W.: A dynamic global vegetation model for use with climate models: concepts and description of simulated vegetation dynamics. Global Change Biology, 9: 1543–1566, https://doi.org/10.1046/j.1365-2486.2003.00681.x, 2003.

Bonan G B: Forests and climate change: forcings, feedbacks, and the climate benefits of forests Science 320 1444–9, 2008.

Callaghan & Carlsson: Global Change and Arctic Terrestrial Ecosystems. ed. / W. C. Oechel; T. Callaghan; T. Gilmanov; J. I. Holten; B. Maxwell; U. Molau; Sveinbjörnsson (eds.). Springer, 1997. p. 201-214, 1977.

Chapin, F.S., Starfield, A.M.: Time lags and novel ecosystems in response to transient climatic change in arctic Alaska. Climatic Change 35, 449–461, https://doi.org/10.1023/A:1005337705025, 1997.

Dee, D. P., Uppala, S. M., Simmons, A. J., Berrisford, P., Poli, P., Kobayashi, S., Andrae, U., Balmaseda, M. A., Balsamo, G., Bauer, P., Bechtold, P., Beljaars, A. C. M., van de Berg, L., Bidlot, J., Bormann, N., Delsol, C., Dragani, R., Fuentes, M., Geer, A. J., Haimberger, L., Healy, S. B., Hersbach, H., Hólm, E. V., Isaksen, L., Kãllberg, P., Köhler, M., Matricardi, M., McNally, A. P., Monge-Sanz, B. M., Morcrette, J.-J., Park, B.-K., Peubey, C., de Rosnay, P., Tavolato, C., Thépaut, J.-N., and Vitart, F.: The ERA-Interim reanalysis: configuration and performance of the data assimilation system, Q. J. Roy. Meteor. Soc., 137, 553–597, https://doi.org/10.1002/qj.828, 2011.

Devi, N.M., Kukarskih, V.V., Galimova, A.A. et al. Climate change evidence in tree growth and stand productivity at the upper treeline ecotone in the Polar Ural Mountains. For. Ecosyst. 7, 7, https://doi.org/10.1186/s40663-020-0216-9, 2020.

Druel, A., C., P., Krinner, G., & Peylin, P.: Modeling the vegetation dynamics of northern shrubs and mosses in the ORCHIDEE land surface model. Journal of Advances in Modeling Earth Systems, 11, 2020–2035, https://doi.org/10.1029/2018MS001531, 2019.

Epstein, H., Yu, Q., Kaplan, J. & Lischke, H.: Simulating Future Changes in Arctic and Subarctic Vegetation. Computing in Science & Engineering, 9, 12–23, https://doi.org/10.1109/MCSE.2007.84, 2007.

Eugster, W., Rouse, W.R., Pielke Sr, R.A., Mcfadden, J.P., Baldocchi, D.D., Kittel, T.G.F., Chapin, F.S., III, Liston, G.E., Vidale, P.L., Vaganov, E. and Chambers, S.: Land–atmosphere energy exchange in Arctic tundra and boreal forest: available data and feedbacks to climate. Global Change Biology, 6: 84-115, https://doi.org/10.1046/j.1365-2486.2000.06015.x, 2000.

Falkowski M. J., Hudak A. T., Crookston N. L., Gessler, P., Uebler E. H, Smith, A., Landscape-scale parameterization of a tree-level forest growth model: A k-nearest neighbour imputation approach incorporating LiDAR data, Canadian Journal of Forest Research, 40(2):184-199, https://doi.org/10.1139/X09-183, 2010.

Foley, J.A., Levis, S., Prentice, I.C., Pollard, D. and Thompson, S.L.: Coupling dynamic models of climate and vegetation. Global Change Biology, 4: 561-579, https://doi.org/10.1046/j.1365-2486.1998.t01-1-00168.x, 1998.

Foster A. C., Armstrong, A. H., Shuman J. K., Shugart H. H., Rogers B. M., Mack, M. C, Goetz S. J, Jon Ranson, K., Importance of tree- and species-level interactions with wildfire, climate, and soils in interior Alaska: Implications for forest change under a warming climate, Ecological Modelling, 409, 108765, https://doi.org/10.1016/j.ecolmodel.2019.108765, 2019.

Foster A. C., Shugart H. H., Shuman J. K., Model-based evidence for cyclic phenomena in a high-elevation, two-species forest, Ecosystems, 19, 437-449, 2015.

Foster A. C., Shuman J. K., Shugart H. H., Dwire, K. A., Fornwalt, P. J., Sibold, J., Negron, J., Validation and application of a forest gap model to the southern Rocky Mountains, Ecol. Modell., 351, 109-128, 2017.

Gagnon M., Domine F. & Boudreau S.: The carbon sink due to shrub growth on Arctic tundra: a case study in a carbon-poor soil in eastern Canada, *Environ. Res. Commun.* 1, 091001, https://doi.org/10.1088/2515-7620/ab3cdd, 2019.

Gamache, I., Payette, S.: Height growth response of tree line black spruce to recent climate warming across the forest-tundra of eastern Canada. Journal of Ecology, 92, 835-845, https://doi.org/10.1111/j.0022-0477.2004.00913.x, 2004.

Giorgetta et al.: CMIP5 simulations of the Max Planck Institute for Meteorology (MPI-M) based on the MPI-ESM-LR model: The rcp26 experiment, served by ESGF. WDCC at DKRZ, doi:10.1594/WDCC/CMIP5.MXELr2, 2012.

Giorgetta et al.: CMIP5 simulations of the Max Planck Institute for Meteorology (MPI-M) based on the MPI-ESM-MR model: The rcp45 experiment, served by ESGF. WDCC at DKRZ, doi:10.1594/WDCC/CMIP5.MXMRr4, 2012.

Giorgetta et al.: CMIP5 simulations of the Max Planck Institute for Meteorology (MPI-M) based on the MPI-ESM-MR model: The rcp85 experiment, served by ESGF. WDCC at DKRZ, doi:10.1594/WDCC/CMIP5.MXMRr8, 2012.

Givnish T.J.: Adaptive significance of evergreen vs. deciduous leaves: solving the triple paradox *Silva Fennica* 36 (3), 703–743, https://doi.org/10.14214/sf.535, 2002.

Gonzalez, P., Neilson, R.P., Lenihan, J.M. and Drapek, R.J.: Global patterns in the vulnerability of ecosystems to vegetation shifts due to climate change. Global Ecology and Biogeography, 19, 755-768. https://doi.org/10.1111/j.1466-8238.2010.00558.x, 2010.

Harris I., Osborn T.J., Jones P. and Lister D.: Version 4 of the CRU TS Monthly High-Resolution Gridded Multivariate Climate Dataset. Scientific Data, https://doi.org/10.1038/s41597-020-0453-3, 2020.

Hijmans R J.: Raster: Geographic Data Analysis and Modeling, R package version 2.6-7, https://CRAN.R-project.org/package=raster, 2017.

Holland M.M., Bitz C.M.: Polar amplification of climate change in coupled models Climate Dynamics, 21, 221-232, 2003.

Holtmeier, F.-K.& Broll, G.: Altitudinal and polar treelines in the northern hemisphere causes and response to climate change. Polarforschung. 79,139–153, 2009.

IPCC: Climate Change 2014: Synthesis Report. Contribution of Working Groups I, II and III to the Fifth Assessment Report of the Intergovernmental Panel on Climate Change [Core Writing Team, R.K. Pachauri and L.A. Meyer (eds.)]. IPCC, Geneva, Switzerland, 151, 2014.

Ito, A., Reyer, C. P. O., Gädeke, A., Ciais, P., Chang, J., Chen, M., François, L., Forrest, M., Hickler, T., Ostberg, S., Shi, H., Thiery, W., and Tian, H.: Pronounced and unavoidable impacts of low-end global warming on northern high-latitude land ecosystems, Environ. Res. Lett., 15, 044006, https://doi.org/10.1088/1748-9326/ab702b, 2020.

Kaplan, J. O., et al.: Climate change and Arctic ecosystems: 2. Modeling, paleodata-model comparisons, and future projections, *J. Geophys. Res.*, 108, 8171, https://doi:10.1029/2002JD002559, 2003.

Kagawa, A., Naito, D., Sugimoto, A., and Maximov, T. C.: Effects of spatial and temporal variability in soil moisture on widths and $\delta^{13}C$ values of eastern Siberian tree rings, *J. Geophys. Res.*, 108, 4500, https://doi:10.1029/2002JD003019, 2003.

Kirilenko, A. P., & Solomon, A. M. Modeling dynamic vegetation response to rapid climate change using bioclimatic classification. *Climatic change*, *38*(1), 15-49, 1998.

Krieger, G., Zink, M., Bachmann, M., Bräutigam, B., Schulze, D., Martone, M., Rizzoli, P., Steinbrecher, U., Antony, J.W., De Zan, F., Hajnsek, I., Papathanassiou, K., Kugler, F., Rodriguez Cassola, M., Younis, M., Baumgartner, S., López-Dekker, P., Prats, P., Moreira, A.: TanDEM-X: a radar interferometer with two formation-flying satellites, Acta Astronaut, 89, 83–98, August-September, 2013.

Kruse, S., Wieczorek, M., Jeltsch, F., and Herzschuh, U.: Treeline dynamics in Siberia under changing climates as inferred from an individual-based model for *Larix*, Ecol. Model., 338, 101–121, https://doi.org/10.1016/j.ecolmodel.2016.08.003, 2016.

Kruse, S., Gerdes, A., Kath, N. J., and Herzschuh, U.: Implementing spatially explicit wind-driven seed and pollen dispersal in the individual-based larch simulation model: LAVESI-WIND 1.0, Geosci. Model Dev., 11, 4451–4467, https://doi.org/10.5194/gmd-11-4451-2018, 2018.

Kruse, S., Gerdes, A., Kath, N. J., Epp, L. S., Stoof-Leichsenring, K. R., Pestryakova, L. A., and Herzschuh, U.: Dispersal distances and migration rates at the arctic treeline in Siberia – a genetic and simulation-based study, Biogeosciences, 16, 1211–1224, https://doi.org/10.5194/bg-16-1211-2019, 2019.

Kruse, S., Herzschuh, U., Schulte, L., Stuenzi, S. M., Brieger, F., Zakharov, E. S. and Pestryakova, L. A.: Forest inventories on circular plots on the expedition Chukotka 2018, NE Russia, PANGAEA, doi.pangaea.de/10.1594/PANGAEA.923638, 2020.

Liang M., Sugimoto A., Tei S., Bragin I. V., Takano S., Morozumi T., Shingubara R.,. Maximov T. C., Kiyashko S. I., Velivetskaya T. A., Ignatiev A. V.: Importance of soil moisture and N availability to larch growth and distribution in the Arctic taiga-tundra boundary ecosystem, northeastern Siberia, Polar Science, 8, 4, 327–341, ISSN 1873-9652, https://doi.org/10.1016/j.polar.2014.07.008, 2014.

Mekonnen Z. A., Riley W. J. & Grant R. F.: 21st century tundra shrubification could enhance net carbon uptake of North America Arctic tundra under an RCP 8.5 climate trajectory. Environ. Res. Lett., 13, 054029, 2018

Menne M. J., Durre I., Korzeniewski B., McNeal S., Thomas K., Yin X., Anthony S., Ray R., Vose R. S., Gleason B. E. and Houston T. G.: Global Historical Climatology Network - Daily (GHCN-Daily), Version 3 NOAA National Climatic Data Center doi:10.7289/V5D21VHZ, 2012.

Miller G. H., Alley R. B., Brigham-Grette J, Fitzpatrick J. J., Polyak L., Serreze M., White J. W.C.: Arctic amplification: can the past constrain the future?, Quaternary Science Reviews,Volume 29, Issues 15–16, 1779–1790, ISSN 0277-3791, https://doi.org/10.1016/j.quascirev.2010.02.008, 2010.

Opel, T., Fritzsche, D., & Meyer, H.: Eurasian Arctic climate over the past millennium as recorded in the Akademii Nauk ice core (Severnaya Zemlya). Climate of the Past, 9 (5), 2379–2389. doi:10.5194/cp-9-2379-2013, 2013.

Osipov, S.V., Burundukova, O.L.: Characteristics of Cajander Larch (*Larix cajanderi* Mayr) on Dredging Waste Dumps in the Amur Region. *Russ J Ecol* 36, 234–238, https://doi.org/10.1007/s11184-005-0066-2, 2005.

R Core Team: R: A language and environment for statistical computing, R Foundation for Statistical Computing, Vienna, Austria, https://www.R-project.org/, 2017.

Rupp, T.S., Chapin, F.S.., III and Starfield, A.M.: Response of subarctic vegetation to transient climatic change on the Seward Peninsula in north-west Alaska. Global Change Biology, 6, 54–555. https://doi.org/10.1046/j.1365-2486.2000.00337.x, 2000.

Serreze, M.C., Walsh, J.E., Chapin, F.S. *et al.* Observational Evidence of Recent Change in the Northern High-Latitude Environment. *Climatic Change* **46,** 159–207, https://doi.org/10.1023/A:1005504031923, 2000.

Shevtsova, I., Heim, B., Kruse, S., Schröder, J., Troeva, E., Pestryakova, L., Zakharov, E. and Herzschuh, U.: Strong shrub expansion in tundra-taiga, tree infilling in taiga and stable tundra in central Chukotka (north-eastern Siberia) between 2000 and 2017, Environmental Research Letters, 15 (8), 085006, doi:10.1088/1748-9326/ab9059, 2020a.

Shevtsova, I., Herzschuh, U., Heim, B., Schulte, L., Stünzi, S., Pestryakova, L. A., Zakharov, E. S., and Kruse, S.: Recent above-ground biomass changes in central Chukotka (Russian Far East) using field sampling and Landsat satellite data, Biogeosciences Discuss. [preprint], https://doi.org/10.5194/bg-2020-416, in review, 2020b.

Shevtsova, I., Kruse, S., Herzschuh, U., Schulte, L., Brieger, F., Stuenzi, S. M., Heim, B., Troeva, E. I., Pestryakova, L. A., and Zakharov, E. S.: Total above-ground biomass of 39 vegetation sites of central Chukotka from 2018, PANGAEA, https://doi.pangaea.de/10.1594/PANGAEA.923719, 2020c.

Shevtsova, I., Kruse, S., Herzschuh, U., Schulte, L., Brieger, F., Stuenzi, S. M., Heim, B., Troe.va, E. I., Pestryakova, L. A., and Zakharov, E. S.: Individual tree and tall shrub partial above-ground biomass of central Chukotka in 2018, PANGAEA, https://doi.pangaea.de/10.1594/PANGAEA.923784, 2020d.

Shuman, J. K., Foster A. C., Shugart H. H., Hoffman-Hall A., Krylov A., Loboda T., Ershov, D., Sochilova E.: Fire disturbance and climate change: implications for Russian forests, Environ. Res. Lett., 12, 035003, 2017.

Shuman, J. K., Tchebakova, N. M., Parfenova, E. I., Soja, A. J., Shugart H. H., Ershov, D., Holcomb K.: Forest forecasting with vegetation models across Russia, Can. J. For. Res., 45, 175-184, 2015

Shuman, J. K., Shugart H. H., Krankina O. N., Testing individual-based models of forest dynamics: issues and an example from the boreal forests of Russia, Ecol. Modell., 293, 102-110, 2014.Sitch, S., Huntingford, C., Gedney, N., Levy, P.E., Lomas, M., Piao, S.L., Betts, R., Ciais, P., Cox, P., Friedlingstein, P., Jones, C.D., Prentice, I.C. And Woodward, F.I.: Evaluation of the terrestrial carbon cycle, future plant geography and climate-carbon cycle feedbacks using five Dynamic Global Vegetation Models (DGVMs). Global Change Biology, 14: 2015-2039. https://doi.org/10.1111/j.1365-2486.2008.01626.x, 2008.

Stuenzi, S. M., Boike, J., Cable, W., Herzschuh, U., Kruse, S., Pestryakova, L. A., Schneider von Deimling, T., Westermann, S., Zakharov, E. S., and Langer, M.: Variability of the surface energy balance in permafrost-underlain boreal forest, Biogeosciences, 18, 343–365, https://doi.org/10.5194/bg-18-343-2021, 2021.

Wickham, H.: ggplot2: Elegant Graphics for Data Analysis, Springer-Verlag, New York, 2016.

Wieczorek, M., Kruse, S., Epp, L. S., Kolmogorov, A., Nikolaev, A. N., Heinrich, I., Herzschuh, U.: Dissimilar responses of larch stands in northern Siberia to increasing temperatures-a field and simulation-based study. Ecology, 98(9), 2343–2355. doi:10.1002/ecy.1887, 2017.

Zevenbergen, L. W. and Thorne C. R.: Quantitative analysis of land surface topography. Earth Surface Processes and Landforms. 12: 12–56, 1987.

Zhang et al., Miller P. A., Smith B., Wania R., Koenigk T. & Döscher R.:Tundra shrubification and tree-line advance amplify arctic climate warming: results from an individual-based dynamic vegetation model, *Environ. Res. Lett.* **8** 034023, https://doi.org/10.1088/1748-9326/8/3/034023 , 2013.

Zhang, W., Miller, P. A., Jansson, C., Samuelsson, P., Mao, J., and Smith, B.: Self-amplifying feedbacks accelerate greening and warming of the Arctic. *Geophysical Research Letters*, 45, 7102-7111. https://doi.org/10.1029/2018GL077830, 2018.

Appendix A. Stratified random sampling categories

To conduct stratified random sampling, we used all possible combinations of elevation, slope and aspect with breakpoints, forming following categories:

Elevation:
- 0-400 m,
- 400-450m,
- 450-500m,
- 500-600m,
- 600-650m,
- 650-700m,
- 700-1000m,
- 1000-1500m.

Slope:
- 0-2°,
- 2-4°,
- 4-6°,
- 6-8°,
- 8-10°,
- 10-12°,
- 12-16°,
- 16-18°,
- 18-20°,
- 20-25°,
- 25-50°.

Aspect:
- 0-45°,
- 45-90°,
- 90-135°,
- 135-180°,
- 180-225°,
- 225-270°,
- 270-315°,
- 315-360°.

Appendix B. Permutation tests for tree presence versus topographical parameters

Table B1. Permutation test for the tree presence versus slope angle model with three coefficients and their significance levels.

	Estimate	Standard error	t value	Pr(>|t|)
a	12.580	1.076	11.685	<0.0001
b	12.781	1.377	9.281	<0.0001

Table B2. Permutation test for the tree presence versus topographical wetness index (TWI) model with an intercept, one coefficient, and their significance levels.

	Estimate	Standard error	t value	Pr(>|t|)
Intercept	0.980	0.045	21.879	<0.0001
c	-0.050	0.005	-9.955	<0.0001

Appendix C. Landsat-based, field, and simulated estimations of larch above-ground biomass (AGB).

Table C1. Estimations of total and exclusively larch above-ground biomass (AGB) from different sources with percentage of total AGB composed of larch AGB for each sample plot.

site	Landsat-based, kg m^2			Field estimations, kg m^2				Simulated, kg m^2		
	total AGB 2001	total AGB 2016	total AGB change 2016-2001	Larch AGB 2018	total AGB 2018	% larch AGB from total AGB	larch AGB 2001	larch AGB 2016	change larch AGB 2016-2001
EN18001	2	2.22	0.22	1.43	2.4	59.45	1.19	1.32	0.13
EN18002	0	1.74	1.74	0	0.93	0	0	0	0
EN18014	2.24	2.33	0.09	5.11	6.05	84.37	1.89	1.97	0.07
EN18021	0.94	1.64	0.69	0.68	1.15	59.56	0.56	0.97	0.41
EN18024	1.96	1.65	-0.31	1.75	6.92	25.31	0.5	0.42	-0.08
EN18025	1.56	2.27	0.71	1.03	3.88	26.58	0.41	0.6	0.19
EN18026	1.55	2.25	0.7	3.09	3.54	87.22	1.35	1.96	0.61
EN18027	1.69	1.86	0.17	0.28	1.02	27.29	0.46	0.51	0.05

7 Synthesis

This thesis is a study of the central Chukotkan vegetation, filling a knowledge gap by integrated land cover and above-ground biomass characterisation, as well as reconstruction of these parameters 15 years in the past and projecting tree above-ground biomass 980 years into the future. These investigations have clarified the origin of the recent increase in growing season NDVI (Guay et al., 2014) and gave insights on the potential future vegetation development for the first time in the area of the highly understudied central Chukotka. Land cover and AGB biomass was precisely mapped in the distinct areas of tundra, taiga-tundra and taiga for the present conditions and reconstructed 15 years back in time. These land cover and AGB data was not available in detail for this region yet. Future tree AGB simulations set up as a part of this thesis are more detailed for the study region as global models. Furthermore, generally, circumpolar, there are not many studies on the potential future AGB change, what makes my investigations more valuable for the discussions on the projections of tree AGB, specifically for mountainous tundra-taiga transition zone. The obtained results are highly relevant for understanding the future tundra-taiga/treeline dynamics, which are leading to further not well understood climate-vegetation-soil-permafrost interactions with the threat of a positive feedback to global warming considering the vast areas that could be potentially colonised by forests in Siberian high latitudes (Jobbágy and Jackson, 2000).

Circumpolar estimations (Berner et al., 2020; Guay et al., 2014) showed vegetation greening in the south-west of the investigated region. However, in depth research was needed to accurately identify what processes are behind it, as central Chukotka was not investigated in terms of vegetation change before. During my research, I investigated the land cover and associated with it compositional changes and above-ground biomass changes in terms of spatial distribution as well as in temporal context.

Invaluable insights on current vegetation of central Chukotka were obtained during expeditions in 2016 and 2018, where field data on projective cover and AGB was collected. I did not collect the 2016 vegetation data myself, but I processed all available field data to produce and publish the projective cover data from the 2016 vegetation plots and assembled the vegetation composition. On the 2018 expedition to Chukotka, I made the concept for the biomass collection in the field that was done for the first time at my institute and together with my colleagues collected all field data in 2018. In total 96 field sites were investigated with 41 taxa recorded. The sampling was done on the gradient from tundra to northern taiga, covering many vegetation communities: (1) lichen-dominated vegetation communities on the rocky ground, (2) *Dryas octopetala* and herb-dominated prostrate tundra communities, (3) *Eriophorum vaginatum* communities with inclusions of dwarf *Salix* sp., (4) *Pinus pumila* tall shrublands, (5) *Larix cajanderi* sparse tree stands with *Eriophorum vaginatum* understory, (6) *Larix cajanderi* sparse tree stands with dwarf shrub (*Vaccinium vitis-idaea, Vaccinium*

uliginosum, Betula nana, Salix sp. and other) understory, (7) *Alnus viridis* tall shrublands and (8) *Larix cajanderi* closed-canopy tree stands with inclusions of *Betula nana* medium-tall shrubs and poorly represented understory.

The field data enabled representative estimations of current composition and AGB in the study area, which coupled with Landsat data gave the possibility to access these vegetation parameters in the past. Inventories of the *Larix Cajanderi* heights and AGB in particular together with the updated LAVESI model made potential future tree AGB estimations possible.

7.1 What changes in vegetation composition have happened from 2000 to 2017 in central Chukotka?

A general increase in shrub cover and a tundra colonization by trees was expected as it is long-term development at a circum-arctic scale (see also Myers-Smith et al, 2019; Myers-Smith et al., 2011; Sturm et al., 2005; Gamache & Payette, 2005; Lloyd & Fastie, 2003), but while the first expectation could have been met (a general increase in shrub cover in central Chukotka), the latter - that trees colonize tundra in the tundra-taiga ecotone - turned out to be not the case for central Chukotka. As Wieczorek et al. (2017) noticed it is likely that larch migration to the north will be limited by seed dispersal and reproduction rates. I observed a significant increase in larch closed-canopy forest only in the northern taiga where it was previously present at the landscape scale (Shevtsova et al., 2021). That behaviour was interpreted as tree infilling. In contrast, in the tundra-taiga ecotone no evidence of significant larch forest advance was found in 2016/2017 compared to back in 2000. However, a strong increase of the forest tundra and shrub tundra was observed in tundra-taiga and northern taiga. This increase in forest and shrub tundra was attributed to shrubification. The major contributions were alder, dwarf birch and heathers. The treeless tundra stayed rather stable within the investigated period. That contrasts with the strong tundra greening on the North Slope in Alaska (Epstein et al., 2018), but is similar to Disko Island in west Greenland where no substantial greening was observed (Callaghan et al., 2011).

Overall, my findings suggest that with the current climate, tundra-taiga has already started to change in its composition gaining in woody plant cover, which subsequently can increase ecosystems carbon uptake and slow carbon losses, having lower decomposition rates than non-woody vegetation (Mekonnen *et al.,* 2018).

My short term observed changes within the 15-16 investigated years could be the start of an exponential vegetation change, which is lagging behind the warming temperatures by decades (e.g., Kruse et al. 2016). Whereas in northern taiga the vegetation composition turned out to be majorly changed since the beginning of the current century, in tundra-taiga the land-cover changes have just started with the prominent shrub cover increase, but almost no tree infilling effect. With the surface

temperature and precipitation increase we would expect these changes to be enhanced in the treeless tundra as well. However, my findings suggest that it could happen most probably with the lower rates of change and should occur predominantly in the wind-protected, nutrient-rich valleys.

7.2 How have the above-ground biomass (AGB) distribution and rates changed from 2000 to 2017 in central Chukotka?

Above-ground biomass on the investigated field sites in central Chukotka ranged from close to zero in the lichen-dominant communities in the mountains to 16 kg m^{-2} in the forested areas (Shevtsova et al., 2021). Forested sites generally had almost 4 times higher AGB (2.38 kg m^{-2}, IQR= 3.06 kg m^{-2}) than hummock tundra with dwarf or low shrubs (0.65 kg m^{-2}, IQR= 0.76 kg m^{-2}) and 7 times higher AGB, than herb-*Dryas*-dominated prostrate tundra (0.32 kg m^{-2}, IQR=0.22 kg m^{-2}). The highest AGB contributions were *Larix cajanderi* in the tree stands, *Pinus pumila* shrubs on the transitions between forest tundra and open tundra (only on the steep slopes), dwarf birch, dwarf willows and heathers in the graminoid open tundra and *Dryas octopetala* in prostrate herb tundra.

Total AGB changes from 2000/2001/2002 to 2016/2017 were the greatest in the northern taiga, what was expected giving tree infilling in larch closed-canopy forests, which resulted in 0.25 kg m^{-2} yr^{-1} AGB increase. The rates of changes in tundra-taiga AGB were 5 times lower as the highest changes in the northern taiga, i.e., 0.046 kg m^{-2} yr^{-1} (IQR= 0.046 kg $m^{-2}yr^{-1}$). In treeless tundra changes in total AGB were close to 0 kg $m^{-2}yr^{-1}$ (IQR= 0.013 kg $m^{-2}yr^{-1}$).

Rates of AGB state and change were obtained for the central Chukotka for the first time, what is valuable because differences in relief and local climate significantly influence biomass carbon stocks in different regions of the treeline ecotone (Usoltsev et al., 2014). Other remote-sensing-based estimations such as in Santoro and Cartus (2019) and Raynolds et al. (2011) have lower spatial resolution and less precise AGB estimates for central Chukotka than our mapped AGB estimates. *Larix cajanderi* AGB in western Chukotka (Berner et al., 2012) reveals similarities in the spatial patterns of AGB distribution of central Chukotka. Assessment of the carbon stocks is important under changing climate conditions since forest expansion may increase carbon sink and provide a natural mitigation of climate change (Usoltsev et al., 2014) or forest expansion can reduce albedo and enhance global warming (Bonan, 2008).

7.3 What are the spatial dynamics and rates of tree AGB change in the upcoming centuries in the northern tundra-taiga from 2020 to 3000 CE on the plot level and landscape level?

My simulations predict an increase in larch AGB and treeline advance into the tundra (upslope and northwards) for the upcoming 980 years in tundra-taiga of central Chukotka. Rates of future change in tree AGB generally the lowest for RCP 2.6 and the highest for RCP 8.5, but locally depend on the current distance to the treeline. As the Individual-based model LAVESI allows a development of individual trees in life-cycle stages and spatially explicit seed dispersal. The pattern tree AGB dynamics is following the rules of primary succession, where in the open tundra the first phase is tree establishment, which causes time-lags of 100-500 years depending on the distance to the current treeline. Second phase is followed by forest densification, which one can observe as a strong fast increase in tree AGB. Next phase is stabilisation of tree stands and episodic self-thinning, resulting in tree AGB fluctuations around a specific value, depending on the climate scenario and local site conditions. These dynamics are in concordance with fundamental ecological forest development processes. The overall average rates of AGB change are higher in the first 300 years of the 21st century and getting lower towards 3000 CE. As expected, the rates are bigger for scenario, where temperature are the highest, namely, RCP 8.5 as opposed to RCP 4.5 and RCP 2. The tree stand formation is happening faster in the currently already forested areas. In case of cooling event the highest possible forest expansion is predicted to reach not more than 10% of the investigated region and tree AGB for the whole region decrease from 2300 to 3000 CE with the rates of -18.13±0.19 (RCP 2.6), or -23.46±0.14 (RCP 4.5), -25.25±0.004 (RCP 8.5) t yr^{-1}. I case of warming without cooling event the highest possible tree AGB is predicted to reach 25% (RCP 2.6), or 33% (RCP 4.5), or 39% (RCP 8.5). Overall, simulated potential spatial distribution of the tree AGB was expected to start from tree infilling in already forested areas and then spread further across the landscape according to my findings in the recent compositional changes from 2001 to 2016. This turned out to be true for simulated tree AGB. The major limitation challenges are not fully solved in y thesis. A proper tuning of biotic and abiotic parameters and optimisation of LAVESI, as well as a lack of data for validation is required.

The specifics of the investigated region include mountains as a natural barrier, slowing down the forest expansion caused by restricting seed dispersion. That is why in other subarctic regions with plain terrain the rates of northward movement of the treeline could be much faster and not representative for mountainous regions. That makes my investigations valuable for Far East Russia, where mountainous terrain prevails.

An increase in woody vegetation is leading to higher carbon uptake. However, unlike subarctic peatland or pond-rich ecosystems it is uncertain if subarctic forests are a carbon sink

or source (Lundin et al., 2016). The tree colonisation in tundra is also decreasing the albedo and, therefore, enhancing global warming (Bonan, 2008).

Fire events, which are not explicitly accounted for in the simulations (only implicitly in the mortality rate of trees by drought), can also influence forest expansion into tundra. Thus, for instance, findings of Alexander et al. (2018) in western Chukotka suggest that larch recruitment could be even more increased because of improved seedbed conditions after increased soil burn severity, which is expected with future higher temperatures in the subarctic. Due to cold weather and low biomass fire return intervals currently taking a hundred of years (Kharuk et al., 2011). But this will change in current global warming.

7.4 Outlook: limitations and opportunities for further research

Limitations in the derivation of an 'upscaled' current state of the vegetation. The main limitation of the land-cover classification and above-ground biomass upscaling was availability of the open-source satellite cloud free data that can be used for mapping vegetation at landscape scale at a present and past (2000s) time. Vegetation classes of the central Chukotka treeline ecotone are transitional classes without strong spectral distinction. Satellite acquisitions back in time (2000s), which are from the older Landsat sensors are of much lower radiometric quality then Landsat acquisition currently available for present time (Roy et al., 2016). Band widths and positions are different. This is a challenge when also the spectral signal between the classes does not differ Although, I significantly improved comparability between acquisitions of Landsat-7 ETM+ and Landsat-8 OLI acquisitions, by developing a transformation between the two Landsat sensors for the study region, the spatial resolution of 30 m and the lower radiometric range of the older sensor Landsat-7 ETM+ are still restrictions for a good land cover classification. Therefore, spring acquisitions with snow coverage were used to provide a difference between treeless tundra and sparse tree stands. A particularly important restriction is to detect land cover change, only using the older Landsat data available before 2007 because of the failure of Landsat-7 ETM+ afterwards and few cloud-free acquisitions back in time for this region with continuous cloud cover in summer. Therefore, this limited the possibilities to map vegetation state and change interpretation from Landsat data.

The low radiometric range of the older sensor Landsat-7 ETM+ and 30-m spatial resolutions are also limitations for upscaling AGB. A comparison of our results with global and circumpolar AGB estimates (Santoro and Cartus, 2019; Raynolds et al., 2011)) showed, that our estimates captured more landscape-related spatial patterns of AGB with higher overall accuracy in the central Chukotka.

We searched for remote sensing data with higher spatial resolution in satellite archives, some were available but mostly not consistently from summer months, only for a few small parts of the focus area that needed to include the field data. Also, regrettably they did not cover the same time

windows as the Landsat acquisitions so that they could not be used for an assessment of the land cover classification and biomass. That is why we have not included high spatial resolution imagery in a multisensory approach in this study. This is a common approach for investigating vegetation, which some researchers apply, when investigating vegetation, using remote sensing data (e.g., Räsänen et al., 2019; Berner et al., 2012; Ranson et al., 2004). However, considering that nowadays with the open source Sentinel-2 satellite more data with higher spatial and temporal resolution than Landsat is available (10 m resolution, acquisitions al 2 to 3 days compared with Landsat-8 OLI with acquisitions every 11 to 12 days), and commercial spatial high-spatial resolution satellites acquire more data than in the past), my developed method and application of coupling remote sensing and field data could be beneficial for modern and future vegetation dynamics investigations.

Limitations in the past, present and future tree AGB. High-resolution imagery (ESRI World Imagery) with submeter spatial resolution was used to extract tree presence and absence in the focus area 16-KP-01 (tundra-taiga). The obtained dataset of tree presence and absence was useful for the assessment of the LAVESI simulation. Unfortunately, the ESRI World Imagery acquisition was only available for early summer 2010. Otherwise, acquisitions at least 15 years back in time could be used as validation for changes in the simulated tree AGB by derivation of changes between presence and absence of trees in the study area.

The topography is highly important for the simulation of tree stand development in the landscape. The available coarse resolution (90 m) TDX-DEM, which was used as topographical boundary condition for the larch AGB simulations also restrict vegetation modelling. The higher spatial resolution Arctic DEM (Porter et al, 2018) was not consistently available in good quality for the model domain. But even the spatial resolution of the Arctic DEM product does not have such fine scale information to realistically represent some azonal vegetation types as e.g., polygonal tundra forests, which plays a big role in tree stand formation. This type was not represented properly by our simulation results. Another example of small-scale features, which are not represented by the DEM, and thus, not in the simulations, are narrow drainage channels, where denser tree stand patches could occur in reality. However, boundaries between zonal vegetation types as open graminoid tundra and continuous forest tundra are possible to retrieve using the available DEM information. In LAVESI these boundaries between zonal vegetation types need to be calibrated with the use of topographical information for downscaling the climate input data with much lower spatial resolution. Furthermore, there are very few observational stations present near the study area and the CRU and reanalyses climate data are coarsely interpolated for the study region. That process needs thorough parameterisation, which will be continued for optimisation of the LAVESI model.

Therefore, the simulated potential future larch AGB in central Chukotka in this study still had moderate accuracy. LAVESI as a spatially explicit individual-based model has shown success in simulating changes in the tree stand development, following ecological (migrational

and successional) patterns such as seed migration, tree stand establishment, tree stand densification and thinning (as in Wieczorek et al. 2017, Kruse et al, 2019). This is very promising for simulating future tree AGB changes. The validation results are showing that the current model only has 15% of falsely simulated tree stands (present in reality, but not present in simulation or vice versa). Absolute values of larch AGB were compared to the field estimations, where sites, which had significantly lower simulated tree AGB, than field-estimated tree AGB are either associated with high field estimations or the fact that LAVESI is not yet fully optimised to meet the current treeline highest border. Tree AGB change was validated with the help of field and Landsat-based data. The validation showed similar rates of change for 3 out of 6 sites, for two more sites simulated values were lower and for one more site simulated value was higher, than field- and Landsat based estimations. Thus, generally the LAVESI was close to realistically predict changes in tree AGB in the study area. However, further parametrisation is required to achieve optimal results. One of the directions for improvement would be the tuning of biological and topographical parameters of the LAVESI to come to the similar current forest distribution as it is to observe on the high-resolution map.

A temporal validation of the simulated larch AGB is one of the biggest challenges since the limitation of available cloud free satellite much data, which can be used for validation. However, it can be improved in the future, using measurements of tree parameters and sampled tree discs, which were made during two expeditions in 2016 and 2018. Such validation can be found successfully applied e.g., in Devi et al. (2020) and Wieczorek et al (2017a), where tree rings were used to assess the current state and reconstruct the stand structure in different periods of time in the past. In my project it would help to validate tree presence back in time, where no other data are available.

Fastest changes in vegetation of central Chukotka are predicted in the next 300 years. Their rates depend on the climate scenario and location of a particular area along the tundra-taiga gradient. In the forested areas tree stands are going to become denser in northern taiga and in the tundra-taiga ecotone, whereas forest expansion is happening much faster in the northern taiga. Open tundra will have a time lag, because of tree establishment phase. Overall, changes in vegetation would be also important for assessment of wildlife habitats loss and for development of conservational measures in the region of interest.

References

Abaimov, A. P.: Geographical distribution and genetics of Siberian larch species, in: Permafrost Ecosystems – Siberian Larch Forests, 209, (Eds) Osawa, A., Zyryanova, O. A., Matsuura, Y., Kajimoto, T., and Wein, R. W., Springer, Netherlands, Dordrecht, 41-58, 2010.

Heather, D. A.r, Natali, S. M., Loranty, M. M., Ludwig, S. M., Spektor, V. V., Davydov, S., Zimov, N., Trujillo, I. and Mack, M. C.: Impacts of increased soil burn severity on larch forest regeneration on permafrost soils of far northeastern Siberia, Forest Ecology and Management, 417, 144-153, https://doi.org/10.1016/j.foreco.2018.03.008, 2018.

Bergengren, J. C., Thompson, S. L., Pollard, D. et al.: Modeling Global Climate–Vegetation Interactions in a Doubled CO2 World. Climatic Change, 50, 31-75. https://doi.org/10.1023/A:1010609620103, 2001.

Berner, L. T., Beck, P. S. A., Loranty, M. M., Alexander, H. D., Mack, M. C., and Goetz, S. J.: Cajander larch (Larix cajanderi) biomass distribution, fire regime and post-fire recovery in northeastern Siberia, Biogeosciences, 9, 3943-3959. https://doi.org/10.5194/bg-9-3943-2012, 2012.

Berner, L. T., Beck, P. S. A., Bunn, A. G. and Goetz, S. J. Plant response to climate change along the forest-tundra ecotone in northeastern Siberia. Glob Change Biol, 19, 3449-3462. https://doi.org/10.1111/gcb.12304, 2013.

Berner, L. T.., Heather, D. A., Loranty, M. M., Ganzlin, P., Mack, M. C. Davydov, S. P., Goetz, S. J.: Biomass allometry for alder, dwarf birch, and willow in boreal forest and tundra ecosystems of far northeastern Siberia and north-central Alaska, Forest Ecology and Management, 337, 110-118. https://doi.org/10.1016/j.foreco.2014.10.027, 2015.

Berner, L. T., Jantz, P., Tape, K. and Goetz, S. J.: Tundra plant above-ground biomass and shrub dominance mapped across the North Slope of Alaska, Environmental Research Letters, 13(3), 035002, https://doi:10.1088/1748-9326/aaaa9a, 2018.

Berner, L.T., Massey, R., Jantz, P. et al.: Summer warming explains widespread but not uniform greening in the Arctic tundra biome. Nat Commun 11, 4621, https://doi.org/10.1038/s41467-020-18479-5, 2020.

Billings, W. D., Luken, J. O., Mortensen, D. A. et al.: Arctic tundra: A source or sink for atmospheric carbon dioxide in a changing environment? Oecologia, 53, 7-11. https://doi.org/10.1007/BF00377129, 1982.

Bokhorst, S.F., Bjerke, J.W., Tømmervik, H., Callaghan, T.V. and Phoenix, G.K.: Winter warming events damage sub-Arctic vegetation: consistent evidence from an experimental manipulation and a natural event. Journal of Ecology, 97, 1408-1415. https://doi.org/10.1111/j.1365-2745.2009.01554.x, 2009.

Blok et al.: The response of Arctic vegetation to the summer climate: relation between shrub cover, NDVI, surface albedo and temperature, Environ. Res. Lett., 6, 035502, 2011.

Bonan, G. B., Levis, S., Sitch, S., Vertenstein, M. and Oleson, K.W.: A dynamic global vegetation model for use with climate models: concepts and description of simulated vegetation dynamics. Global Change Biology, 9, 1543-1566. https://doi.org/10.1046/j.1365-2486.2003.00681.x, 2003.

Bonan, G. B.: Forests and climate change: forcings, feedbacks, and the climate benefits of forests, Science, 320, 1444–1449, https://doi.org/10.1126/science.1155121, 2008.

Callaghan, T.V., Johansson, M., Brown, R.D. et al.: The Changing Face of Arctic Snow Cover: A Synthesis of Observed and Projected Changes. AMBIO 40, 17-31, https://doi.org/10.1007/s13280-011-0212-y, 2011.

Campbell, J. B.: Introduction to remote sensing, (Eds) Campbell, J. B., Wynne, R. H., 5th ed, 1944.

Campioli, M., Michelsen, A., Demey, A. et al.: Net Primary Production and Carbon Stocks for Subarctic Mesic–Dry Tundras with Contrasting Microtopography, Altitude, and Dominant Species. Ecosystems 12, 760-776. https://doi.org/10.1007/s10021-009-9255-3, 2009.

Danby, R.K. and Hik, D.S.: Variability, contingency and rapid change in recent subarctic alpine tree line dynamics. Journal of Ecology, 9, 52-363. https://doi.org/10.1111/j.1365-2745.2006.01200.x, 2007.

Devi, N.M., Kukarskih, V.V., Galimova, A.A. et al.: Climate change evidence in tree growth and stand productivity at the upper treeline ecotone in the Polar Ural Mountains, For. Ecosyst. 7, 7. https://doi.org/10.1186/s40663-020-0216-9, 2020.

Dial, R. J., Berg, E. E., Timm, K., McMahon, A., and Geck, J.: Changes in the alpine forest-tundra ecotone commensurate with recent warming in southcentral Alaska: Evidence from orthophotos and field plots, J. Geophys. Res., 112, G04015, doi:10.1029/2007JG000453, 2007.

Druel, A., C., P., Krinner, G., and Peylin, P.: Modeling the vegetation dynamics of northern shrubs and mosses in the ORCHIDEE land surface model. Journal of Advances in Modeling Earth Systems, 11, 2020-2035. https://doi.org/10.1029/2018MS001531, 2019.

Egorova A. A, Vasileva I. I., Stepanova H. A., Fesko N.N.: Flora of tundra zone of Yakutia [Flora tundrovoy zona Yakutii], Russian Akademie of Seinces, Yakutsk. [in Russian], 1991.

Epstein, H., Yu, Q., Kaplan, J. and Lischke, H.: Simulating Future Changes in Arctic and Subarctic Vegetation, Computing in Science & Engineering, 9, 12-23. https://doi: 10.1109/MCSE.2007.84, 2007.

Epstein, H. et al., Dynamics of aboveground phytomass of the circumpolar Arctic tundra during the past three decades, Environ. Res. Lett., 7, 015506, 2012.

Epstein H, Bhatt U, Raynolds M, Walker D, Forbes B C, Horstkotte T, Macias-Fauria M, Martin A, Phoenix G, Bjerke J, Tømmervik H, Fauchald P, Vickers H, Myneni R and Dickerson C: Tundra Greenness Arctic Report Card 2018, URL: https://www.arctic.noaa.gov/Report-Card, 2018.

Frost, G. V. and Epstein, H. E.: Tall shrub and tree expansion in Siberian low Arctic ecotones since the 1960s, Global Change Biology, 20, 1264-77, https://doi: 10.1111/gcb.12406, 2013.

Frost, G. V., Epstein, H. E. and Walker, D. A.: Regional and landscape-scale variability of Landsat-observed vegetation dynamics in northwest Siberian tundra Environmental Research Letters, 9, 025004, https://doi: 10.1088/1748-9326/9/2/025004, 2014.

Gamache, I. and Payette, S.: Latitudinal Response of Subarctic Tree Lines to Recent Climate Change in Eastern Canada. Journal of Biogeography, 32(5), 849-862, 2005.

Greenwood, S. and Jump, A. S.: Consequences of Treeline Shifts for the Diversity and Function of High Altitude Ecosystems, Arctic, Antarctic, and Alpine Research, 46 (4), 829-840, https://10.1657/1938-4246-46.4.829, 2014.

Guay, K. C., Beck, P. S. A., Berner, L. T., Goetz, S. J., Baccini, A. and Buermann, W.: Vegetation productivity patterns at high northern latitudes: a multi-sensor satellite data assessment Global Change Biology, 20, 3147–58, https://doi: 10.1111/gcb.12647, 2014.

Hudson, J. M. G. and Henry, G. H .R.: Increased plant biomass in a High Arctic heath community from 1981 to 2008. Ecology, 90, 2657-2663. https://doi.org/10.1890/09-0102.1, 2009.

Jobbagy, E.G., Jackson, R.B.: The vertical distribution of soil organic carbon and its relation to climate and vegetation. Ecol. Appl. 10, 423–436, https://doi.org/ 10.2307/2641104, 2000.

Karavaev, M.N. Notes on flora of Yakutia. Moscow: Publishing House of the Academy of Sciences of the USSR. [in Russian], 1958.

Kharuk, V. I., Ranson, K. J., Dvinskaya, M. L., and Im, S. T.: Wildfires in northern Siberian larch dominated communities, Environ. Res. Lett., 6, 045208, https://doi.org/10.1088/1748-9326/6/4/045208, 2011.

Krasnoborov I. N. Flora Sibiriae, Nauka, Novosibirsk, 1988-2003. [in Russian]

Krestov P.V.: Forest Vegetation of Easternmost Russia (Russian Far East). In: Kolbek J., Šrůtek M., Box E.O. (eds) Forest Vegetation of Northeast Asia. Geobotany, vol 28, Springer, Dordrecht, https://doi.org/10.1007/978-94-017-0143-3_5, 2003.

Kruse S., Gerdes A., Kath N. J., Epp L. S., Stoof-Leichsenring, K. R., Pestryakova L. A. and Herzschuh U.: Dispersal distances and migration rates at the arctic treeline in Siberia – a genetic and simulation-based study Biogeosciences 16, 1211-1224 doi: 10.5194/bg-16-1211-2019, 2019.

Kruse, S., Wieczorek, M., Jeltsch, F., and Herzschuh, U.: Treeline dynamics in Siberia under changing climates as inferred from an individual-based model for *Larix*, Ecol. Model., 338, 101–121, https://doi.org/10.1016/j.ecolmodel.2016.08.003, 2016.

Lloyd, A. H. and Fastie, C. F.: Recent changes in treeline forest distribution and structure in interior Alaska, Écoscience, 10 (2), 176-185, https://10.1080/11956860.2003.11682765, 2003.

Lantz, T. C., Gergel, S. E. and Henry, G. H. R.: Response of green alder (Alnus viridis subsp. fruticosa) patch dynamics and plant community composition to fire and regional temperature in north-western Canada, Journal of Biogeography, 37(8),1597–1610, https://doi:10.1111/j.1365-2699.2010. 02317.x, 2010.

Lloyd, A. H. and Fastie, C. L: Recent changes in treeline forest distribution and structure in interior Alaska, Écoscience, 10:2, 176-185, https://doi:10.1080/11956860.2003.11682765, 2003.

Lundin, E. J., Klaminder, J., Giesler, R., Persson, A., Olefeldt, D., Heliasz, M., Christensen, T. R., and Karlsson, J.: Is the subarctic landscape still a carbon sink? Evidence from a detailed catchment balance, Geophys. Res. Lett., 43, 1988-1995, https://doi:10.1002/2015GL066970, 2016.

Maslov, M.N., Kopeina, E.I., Zudkin, A.G., Koroleva N.E., Shulakov A.A., Onipchenko V.G., Makarov, M.I.: Stocks of phytomass and organic carbon in tundra ecosystems of northern Fennoscandia, Moscow Univ. Soil Sci. Bull, 71, 113–119, https://doi.org/10.3103/S0147687416030042, 2016.

Mekonnen, Z. A., Riley, W. J., and Grant, R. F.: 21st century tundra shrubification could enhance net carbon uptake of North America Arctic tundra under an RCP 8. 5 climate trajectories. Environmental Research Letters, 13 (5), 054029, 2018.

Michelsen, A., Rinnan, R. and Jonasson, S.: Two Decades of Experimental Manipulations of Heaths and Forest Understory in the Subarctic, AMBIO, 41, 218–230, https://doi.org/10.1007/s13280-012-0303-4, 2012.

Mulder, C.P.H., Iles, D.T. and Rockwell, R.F.: Increased variance in temperature and lag effects alter phenological responses to rapid warming in a subarctic plant community, Glob Change Biol, 23, 801-814. https://doi.org/10.1111/gcb.13386, 2017.

Myers-Smith .I H., Kerby J. T., Phoenix G. K., Bjerke J.W., Epstein H. E., Assmann J.J., John C., Andreu-Hayles L., Angers-Blondin S., Beck P. S. A., Berner L.T., Bhatt U. S., Bjorkman A. D., Blok D., Bryn A., Christiansen C. T., Cornelissen J. H. C., Cunliffe A.M., Elmendorf S.C., Forbes B.C., Goetz S.J., Hollister R. D., de Jong R., Loranty M. M., Macias-Fauria M., Maseyk K., Normand S., Olofsson J., Parker T.C., Parmentier F.-J. W., Post E., Schaepman-Strub G., Stordal F., Sullivan P. F., Thomas H. J. D., Tømmervik H., Treharne R., Tweedie C. E., Walker D. A., Wilmking M. and Wipf S.: Complexity revealed in the greening of the Arctic. Nature Climate Change, 10, 106–117, https://doi: 10.1038/s41558-019-0688-1, 2020.

Myers-Smith, I. H., Grabowski, M. M., Thomas, H. J. D., Angers-Blondin, S., Daskalova, G. N., Bjorkman, A. D., Cunliffe, A. M., Assmann, J. J., Boyle, J., McLeod, E., McLeod, S., Joe, R., Lennie, P., Arey, D., Gordon, R., and Eckert, C.: Eighteen years of ecological monitoring reveals multiple lines of evidence for tundra vegetation change. Ecological Monographs 89 (2): e01351. 10.1002/ecm.1351, 2019.

Myers-Smith I H, Forbes B C, Wilmking M et al.: Shrub expansion in tundra ecosystems: dynamics, impacts and research priorities. Environmental Research Letters, 6, 045509, https://doi: 10.1088/1748-9326/6/4/045509, 2011.

Payette, S., Fortin, M.-J. and Gamache, I: The Subarctic Forest–Tundra: The Structure of a Biome in a Changing Climate: The shifting of local subarctic tree lines throughout the forest–tundra biome, which is linked to ecological processes at different spatiotemporal scales, will reflect future global changes in climate, BioScience, 51(9), 709–718, https://doi.org/10.1641/0006-3568(2001)051[0709: TSFTTS]2.0.CO;2, 2001.

Porter, C., Morin, P.; Howat, I., Noh, M.-J., Bates, B.,Peterman, K., Keesey, S., Schlenk, M., Gardiner, J., Tomko, K., Willis, M., Kelleher, C., Cloutier, M., Husby, E., Foga, S., Nakamura, H., Platson, M., Wethington, M. Jr., Williamson, C., Bauer, G., Enos, J., Arnold, G., Kramer, W., Becker, P., Doshi, A. D., C., Cummens, P. Laurier, F., Bojesen, M.: "ArcticDEM", Harvard Dataverse, V1, https://doi.org/10.7910/DVN/OHHUKH, 2018.

Post, E., Forchhammer, M. C., Bret-Harte, M. S., Callaghan, T. V., Christensen, T., Elberling, B., Fox, A. D., Gilg, O., Hik, D. S., Hoye, T. T., Ims, R. A., Jeppesen, E., Klein, D. R., Madsen, J., McGuire, A. D., Rysgaard, S., Schindler, D. E., Stirling, I., Tamstorf, M. P., and Aastrup, P.: Ecological Dynamics Across the Arctic Associated with Recent Climate Change. Science, 325(5946), 1355-1358. https://doi.org/10.1126/science.1173113, 2009.

Ranson, K.J., Sun, G., Kharuk, V.I., and Kovacs, K.: Assessing tundra–taiga boundary with multi-sensor satellite data, Remote Sensing of Environment, 93(3), 283-295. https://doi.org/10.1016/j.rse.2004.06.019, 2004.

Räsänen, S. J., Aurela, M. and Virtanen, T.: Predicting aboveground biomass in Arctic landscapes using very high spatial resolution satellite imagery and field sampling, International Journal of Remote Sensing, 40(3), 1175-1199. https://doi.org/10.1080/01431161.2018.1524176, 2019.

Raynolds, M., Walker, D., Epstein, H., Pinzon, J. and Tucker, C.: A new estimate of tundra-biome phytomass from trans-Arctic field data and AVHRR NDVI, Remote Sensing Letters, 3(5), 403-411, doi:10.1080/01431161.2011.609188, 2011.

Shaver, G. and Chapin, F.: Production: Biomass Relationships and Element Cycling in Contrasting Arctic Vegetation Types, Ecological Monographs, 61(1), 1-31, https://doi:10.2307/1942997, 1991.

Shevtsova, I., Herzschuh, U., Heim, B., Kruse, S., Schröder, J., Troeva, E. I., Pestryakova, L. A., and Zakharov, E. S.: Foliage projective cover of 57 vegetation sites of central Chukotka from 2016, PANGAEA, https://doi.org/10.1594/PANGAEA.908570, 2019.

Shevtsova, I., Heim, B., Kruse, S., Schröder, J., Troeva, E., Pestryakova, L., Zakharov, E. and Herzschuh, U.: Strong shrub expansion in tundra-taiga, tree infilling in taiga and stable tundra in central Chukotka (north-eastern Siberia) between 2000 and 2017, Environmental Research Letters, 15(8), 085006, https://doi:10.1088/1748-9326/ab9059, 2020a.

Shevtsova, I., Kruse, S., Herzschuh, U., Schulte, L., Brieger, F., Stuenzi, S. M., Heim, B., Troeva, E. I., Pestryakova, L. A., and Zakharov, E. S.: Foliage projective cover of 40 vegetation sites of central Chukotka from 2018, PANGAEA, https://doi.pangaea.de/10.1594/PANGAEA.923664, 2020b.

Shevtsova, I., Kruse, S., Herzschuh, U., Schulte, L., Brieger, F., Stuenzi, S. M., Heim, B., Troeva, E. I., Pestryakova, L. A., and Zakharov, E. S.: Total above-ground biomass of 39 vegetation sites of central Chukotka from 2018, PANGAEA, https://doi.pangaea.de/10.1594/PANGAEA.923719, 2020c.

Shevtsova, I., Kruse, S., Herzschuh, U., Schulte, L., Brieger, F., Stuenzi, S. M., Heim, B., Troeva, E. I., Pestryakova, L. A., and Zakharov, E. S.: Individual tree and tall shrub partial above-ground biomass of central Chukotka in 2018, PANGAEA, https://doi.pangaea.de/10.1594/PANGAEA.923784, 2020d.

Shevtsova, I., Herzschuh, U., Heim, B., Schulte, L., Stünzi, S., Pestryakova, L. A., Zakharov, E. S., and Kruse, S.:, Recent above-ground biomass changes in central Chukotka (Russian Far East) using field sampling and Landsat satellite data, Biogeosciences, 18, 3343–3366, https://doi.org/10.5194/bg-2020-416, 2021.

Sitch, S., Huntingford, C., Gedney, N., Levy, P.E., Lomas, M., Piao, S.L., Betts, R., Ciais, P., Cox, P., Friedlingstein, P., Jones, C.D., Prentice, I.C. and Woodward, F.I.: Evaluation of the terrestrial carbon cycle, future plant geography and climate-carbon cycle feedbacks using five Dynamic Global Vegetation Models (DGVMs). Global Change Biology, 14, 2015-2039. https://doi.org/10.1111/j.1365-2486.2008.01626.x, 2008.

Sturm M., Racine C. H. and Tape K. D.: Increasing shrub abundance in the Arctic Nature 411 546–7, https://doi: 10.1038/35079180, 2001.

Sturm, M., Schimel, J., Michaelson, G., Welker, J.M., Oberbauer, S. F. Liston, G.E., Fahnestock, J., and Romanovsky, V.E.: Winter Biological Processes Could Help Convert Arctic Tundra to Shrubland, BioScience, 55 (1), 17-26, https://doi.org/10.1641/0006-3568(2005)055[0017:WBPCHC]2.0.CO;2, 2005.

Sullivan, P.F., Arens, S.J.T., Chimner, R.A. and Welker J. M.: Temperature and Microtopography Interact to Control Carbon Cycling in a High Arctic, Fen. Ecosystems 11, 61–76, https://doi.org/10.1007/s10021-007-9107-y, 2008.

Tape, K., Sturm, M. and Racine, C.: The evidence for shrub expansion in Northern Alaska and the Pan-Arctic Global Change Biology 12 686–702 doi: 10.1111/j.1365-2486.2006.01128.x, 2006.

Tolmatchev A. I.: Flora Arctica, Academia Scientarum USSR, Moskov-Leningrad, 1970-1987. [in Russian]

Usoltsev, V., Somogyi, Z., Chasovskikh, V. and Noritsina, Y.V.: Aboveground Biomass Carbon in the Alpine and Arctic Treeline Ecotones in the Ural Region. Environment and Natural Resources Research, 4(1), 2014.

Vankoughnett, M.R. and Grogan, P.: Plant production and nitrogen accumulation above- and belowground in low and tall birch tundra communities: the influence of snow and litter. Plant Soil 408, 195–210. https://doi.org/10.1007/s11104-016-2921-2, 2016.

Villarreal S, Hollister R.D., Johnson, D. R., Lara M. J., Webber P. J. and Tweedie C. E.: Tundra vegetation change near Barrow, Alaska (1972–2010), *Environ. Res. Lett.,* 7, 015508, https://doi.org/10.1088/1748-9326/7/1/015508, 2012.

Walker, D.A., Raynolds, M.K., Daniëls, F.J., Einarsson, E., Elvebakk, A., Gould, W.A., Katenin, A.E., Kholod, S.S., Markon, C.J., Melnikov, E.S., Moskalenko, N.G., Talbot, S.S., Yurtsev, B.A. and the other members of the CAVM Team: The Circumpolar Arctic vegetation map. Journal of Vegetation Science, 16: 267-282. https://doi.org/10.1111/j.1654-1103.2005.tb02365.x, 2005.

Walker, D.A., Kuss, P., Epstein, H.E., Kade, A.N., Vonlanthen, C.M., Raynolds, M.K. and Daniëls, F.J.: Vegetation of zonal patterned-ground ecosystems along the North America Arctic bioclimate gradient. Applied Vegetation Science, 14, 440-463, https://doi.org/10.1111/j.1654-109X.2011.01149.x, 2011.

Wallén, B.: Above and below Ground Dry Mass of the Three Main Vascular Plants on Hummocks on a Subarctic Peat Bog. Oikos, 46(1), 51-56, https://doi:10.2307/3565379, 1986.

Walsh, J. E., Chapman, W. L., and Shy, T. L.: Recent decrease of sea level pressure in the central Arctic. Journal of Climate, 9(2), 480-486, https://doi.org/10.1175/1520-0442(1996)009<0480:RDOSLP>2.0.CO;2 , 1996.

Webb, E. E., Heard, K., Natali, S. M., Bunn, A. G., Alexander, H. D., Berner, L. T., Kholodov, A., Loranty, M. M., Schade, J. D., Spektor, V., and Zimov, N.: Variability in above- and belowground carbon stocks in a Siberian larch watershed, Biogeosciences, 14, 4279–4294, https://doi.org/10.5194/bg-14-4279-2017, 2017.

Wieczorek M, Kolmogorov A, Kruse S, Jacobsen I, Nitze I, Nikolaev A, Heinrich I, Pestryakova L and Herzschuh U.: Disturbance-effects on treeline larch-stands in the lower Kolyma River area (NE Siberia), Silva Fennica 51(3) 1666 doi: 10.14214/sf.1666, 2017.

Wipf, S., Rixen, C. and Mulder, C.P.H.: Advanced snowmelt causes shift towards positive neighbour interactions in a subarctic tundra community. Global Change Biology, 12: 1496-1506, https://doi.org/10.1111/j.1365-2486.2006.01185.x, 2006.

Ylänne, H., Stark, S. and Tolvanen, A.: Vegetation shift from deciduous to evergreen dwarf shrubs in response to selective herbivory offsets carbon losses: evidence from 19 years of warming and simulated herbivory in the subarctic tundra. Glob Change Biol, 21: 3696-3711, https://doi.org/10.1111/gcb.12964, 2015.

Yu, Z., Beilman, D. W., Frolking, S., MacDonald, G. M., Roulet, N. T., Camill, P. and Charman, D. J.: Peatlands and Their Role in the Global Carbon Cycle, Eos Trans. AGU, 92(12), 97, 2011.

Zeng, H. Q., and Jia, G. S.: Impacts of snow cover on vegetation phenology in the Arctic from satellite data. Adv. Atmos. Sci., 30(5), 1421–1432, https://doi: 10.1007/s00376-012-2173-x, 2013.

Zhang W, Miller P. A., Smith B., Wania R., Koenigk T. and Döscher R.: Tundra shrubification and tree-line advance amplify arctic climate warming: results from an individual-based dynamic vegetation model, Environ. Res. Lett. 8, 034023, https://doi.org/10.1088/1748-9326/8/3/034023, 2013.

Acknowledgements

I want to thank German Federal Ministry of Education and Research (BMBF) for financial support, which enabled the Russian-German research program "Kohlenstoff im Permafrost KoPf" (grant no. 03F0764A), as well as, Initiative and Networking Fund of the Helmholtz Association and by the ERC consolidator grant Glacial Legacy of Ulrike Herzschuh (grant no. 772852), Russian Foundation for Basic Research (grant no. 18-45-140053 r_a), Ministry of Science and Higher Education of the Russian Federation (grant no. FSRG-2020-0019). I also want to acknowledge all participants of the joint German-Russian expeditions "Keperveem 2016" and "Chukotka 2018" for making contribution to collecting valuable vegetation data, used in this study. Special thanks to my main supervisor Prof Dr Ulrike Herzschuh, who guided me through my scientific work and provided me with constructive and quick feedbacks, Dr Birgit Heim for providing me with invaluable insights to remote sensing, also guiding me throughout my PhD studies and giving me constructive feedbacks, Dr Stefan Kruse for extensive help with the LAVESI simulations, guiding me and giving constructive comments on my research, Lena Popova for providing technical support with Landsat data preparation and Luca Farkas for assisting in the laboratory work with drying and weighting AGB samples.